CONFORMANCE IMPROVEMENT USING GELS

Second Annual Technical Progress Report,
Reporting Period: September 1, 2002 through August 31, 2003

Principal Author: Randall S. Seright
(505) 835-5571

Report Date: September 2003

DOE Award Number: DE-FC26-01BC15316

Name and Address of Submitting Organization:
New Mexico Petroleum Recovery Research Center
New Mexico Institute of Mining and Technology
Socorro, New Mexico 87801

NM PRRC Contributors: Robert Sydansk, Richard Schrader, John Hagstrom II, Kathryn Wavrik, Ying Wang, Abdullah Al-Dhafeeri, Yin Xiong, Kristin Herlugson, Merrie Michelle Huskey, Joe Sammur
SUNY Contributor: Brent Lindquist

PRRC Report 03-15

DISCLAIMER

DEDICATION

This report is dedicated to the memory of Tom Reid. During his time with the National Petroleum Technology Office, Tom played a very constructive part in overseeing our research. We will miss his insights, his vision, his dedication to advancing petroleum engineering, and his friendship.

ABSTRACT

This report describes work performed during the second year of the project, "Conformance Improvement Using Gels." The project has two objectives. The first objective is to identify gel compositions and conditions that substantially reduce flow through fractures that allow direct channeling between wells, while leaving secondary fractures open so that high fluid injection and production rates can be maintained. The second objective is to optimize treatments in fractured production wells, where the gel must reduce permeability to water much more than that to oil.

Pore-level images from X-ray computed microtomography were re-examined for Berea sandstone and porous polyethylene. This analysis suggests that oil penetration through gel-filled pores occurs by a gel-dehydration mechanism, rather than a gel-ripping mechanism. This finding helps to explain why aqueous gels can reduce permeability to water more than to oil.

We analyzed a Cr(III)-acetate-HPAM gel treatment in a production well in the Arbuckle formation. The availability of accurate pressure data before, during, and after the treatment was critical for the analysis. After the gel treatment, water productivity was fairly constant at about 20% of the pre-treatment value. However, oil productivity was stimulated by a factor of 18 immediately after the treatment. During the six months after the treatment, oil productivity gradually decreased to approach the pre-treatment value. To explain this behavior, we proposed that the fracture area open to oil flow was increased substantially by the gel treatment, followed by a gradual closing of the fractures during subsequent production.

For a conventional Cr(III)-acetate-HPAM gel, the delay between gelant preparation and injection into a fracture impacts the placement, leakoff, and permeability reduction behavior. Formulations placed as partially formed gels showed relatively low pressure gradients during placement, and yet substantially reduced the flow capacity of fractures (with widths from 1 to 4 mm) during brine and oil flow after placement. Regardless of gel age before placement, very little gel washed out from the fractures during brine or oil flow. However, increased brine or oil flow rate and cyclic injection of oil and water significantly decreased the level of permeability reduction.

A particular need exists for gels that can plug large apertures (e.g., wide fractures and vugs). Improved mechanical strength and stability were demonstrated (in 1- to 4-mm-wide fractures) for a gel that contained a combination of high- and low-molecular weight polymers. This gel reduced the flow capacity of 2- and 4-mm-wide fractures by 260,000. In a 1-mm-wide fracture, it withstood 26 psi/ft without allowing any brine flow through the fracture.

Cr(III)-acetate-HPAM gels exhibited disproportionate permeability reduction in fractures. The effect was most pronounced when the gel was placed as gelant or partially formed gels. The effect occurred to a modest extent with concentrated gels and with gels that were "fully formed" when placed. The effect was not evident in tubes.

We explored swelling polymers for plugging fractures. Polymer suspensions were quickly prepared and injected. In concept, the partially dissolved polymer would lodge and swell to plug the fracture. For three types of swelling polymers, behavior was promising. However, additional development is needed before their performance will be superior to that of conventional gels.

TABLE OF CONTENTS

TABLE OF FIGURES

LIST OF TABLES

ACKNOWLEDGMENTS

Financial support for this work is gratefully acknowledged from the United States Department of Energy (NETL/National Petroleum Technology Office), the State of New Mexico, ConocoPhillips, Marathon, PDVSA/Intevep, Shell, and the Ufa branch of YuganskNIPIneft. I greatly appreciate the efforts of those individuals who contributed to this project. Brent Lindquist (State University of New York at Stony Brook) was instrumental during the analyses described in Chapter 2. John Hagstrom conducted the experimental work described in Chapter 3 and part of Chapter 5. The field data for Chapter 4 was provided by Gel-Tec (Dan Pender and John Gould) and Vess Oil. Richard Schrader performed the experimental work described in Chapters 5, 6, and 7, with help from Kate Wavrik, Ying "Annie" Wang, and Joe Sammur. Bob Sydansk played the major role in Chapters 8 and 9, with help from Abdullah Al-Dhafeeri, Yin "Kiki" Xiong, Merrie Michelle Huskey, and Ying "Annie" Wang. I especially appreciate the thorough review of this manuscript by Julie Ruff and Bob Sydansk. Both Bob and Julie provided helpful technical comments for all chapters.

EXECUTIVE SUMMARY

This report describes work performed during the second year of the project, "Conformance Improvement Using Gels." This three-year research project has two objectives. The first objective is to identify gel compositions and conditions that substantially reduce flow through fractures that allow direct channeling between wells, while leaving secondary fractures open so that high fluid injection and production rates can be maintained. This goal will be reached by (1) characterizing gel propagation through fractures as a function of fracture width, length, and height, injection rate, gel composition, and temperature, (2) correlating rheology in fractures with that in a viscometer, and (3) using the experimental results to develop an appropriate model for gel placement and treatment sizing.

The second objective is to optimize treatments in fractured production wells, where the gel must reduce permeability to water much more than that to oil. Within this objective, the specific goals are to (1) determine the correct mechanism(s) for the disproportionate permeability reduction, (2) identify conditions that maximize the phenomenon, (3) find materials and methods that make the phenomenon predictable and controllable, and (4) establish a methodology to determine how much gelant should be injected in a given fractured production well.

Re-Examination of X-Ray Computed Microtomography
In previous work, we used X-ray computed microtomography to determine why gels reduce permeability to water more than that to oil in strongly water-wet Berea sandstone and strongly oil-wet porous polyethylene cores. At a recent Gordon Conference, attendees questioned a few of our findings. Therefore, to double check our results, our X-ray images were re-analyzed using a different method for segmenting the fluids (i.e., differentiating between water and oil). In the first analysis, fluid phase identification was made by subtracting an image having both fluid phases present (one phase of which was doped with a strong X-ray attenuating compound) from the corresponding image in which only the wetting phase was present in the pore space. In the second method, this subtraction process was not performed. Instead, a method called "indicator kriging" was used to distinguish between oil and water in a given image.

Comparison of the First and Second Analyses. Compared with the first analysis, the second analysis revealed larger pores in polyethylene (because a larger population was sampled). This finding validated one of our critics, who pointed out that Berea and polyethylene should have different pore size distributions. The second analysis also showed lower S_{wr} and S_{or} in Berea, which was more consistent with floods in larger cores. The second analysis showed many more pores at high and low saturations in Berea than the first analysis. In the transition from S_{wr} to S_{or}, many Berea pores gained oil in the first analysis but not the second. Both analyses confirmed that S_{wr} averaged about 60% in the smallest detected Berea pores and that a wide range of saturations could be found for any pore size. The average S_{or} was 80% in the smallest detected polyethylene pores (which were the same size as the smallest detected pores in Berea). The behavior in polyethylene followed conventional expectations for a strongly oil-wet porous medium. Other qualitative trends were the same for both analyses.

Important Findings from the Combined Analysis. During the transition from S_{wr} to S_{or} in Berea before gel placement, pores in all detected size ranges experienced significant gains in

water saturation. Pore size did not significantly influence the extent of the transition. In contrast, in polyethylene before gel placement, oil was largely immobile in smaller pores. Injection of our 20-cp gelant mobilized oil in both porous media even though the pressure gradients during gelant placement were less than those during previous oil or water floods. Immediately after gel placement, an extremely high resistance (F_{rrw}>10,000) to water flow occurs (in either Berea or polyethylene), presumably because impermeable gel occupies nearly all of the aqueous pore space. During oil flow after gel placement in Berea, a 55% reduction (on average) in gel volume occurred in pores of all detected size ranges, thus leading to a relatively high permeability to oil (F_{rro}=15). This reduction occurred even though the pressure gradients were less than during previous floods. Gel volume was most often reduced in pores that experienced the greatest saturation changes during floods before gel placement. After gel placement, 86.1% of the pores had higher S_{wr} values than before gel. Presumably, gel accounted for this increase. The gel that remained was widely distributed with respect to pore size. At S_{or} after gel placement in Berea, 93.3% of the pores had higher oil saturations than at S_{or} before gel placement. The overall S_{or} in Berea jumped from 18.4% before gel placement to 51% after. The greater level of trapped oil greatly restricted water flow (F_{rrw}=1,220). A wide range of saturation changes occurred for all pore sizes, and the average saturation change was insensitive to pore size.

In polyethylene, reduction in gel volume (caused by oil flow) occurred mainly in small pores. Overall, oil injection reduced gel volume by only 16.3%. However, in pores smaller than 10^{-4} mm^3, gel volume was reduced by 63.5%. A reduction of only 10.2% occurred in pores that were larger than 10^{-3} mm^3. In contrast to Berea, the overall S_{or} in polyethylene was significantly lower after gel placement than before gel placement (0.3% versus 17.0%). Thus, oil trapping could not explain the large disproportionate permeability reduction seen in porous polyethylene (F_{rrw}/F_{rro}=2,130/24=89).

Because the first oil injection after gel placement did not reduce gel volume to a greater extent in large pores than in small pores, gel destruction or reduction in gel volume was probably caused by a dehydration mechanism rather than a gel-ripping mechanism. This observation applies to both strongly water-wet Berea sandstone and strongly oil-wet porous polyethylene.

Conclusions from a Study of Phase Connectivity. Before gel placement (in either Berea or polyethylene), at least 97.9% of the injected phase (oil or water) was contained within a single blob. In contrast before gel placement, most residual non-wetting blobs were probably "singlets"—i.e., isolated within individual pores. We suspect that most of the residual wetting phase was contained within a single blob. However, we could not prove this because our resolution was not sufficient to detect thin film connections smaller than 4.1 μm. Changes in blob connectivity qualitatively followed the trends expected from the saturation changes. The largest oil blob always grew when the oil saturation increased and shrank when the oil saturation decreased. Similarly, the largest water blob always grew when the water saturation increased and shrank when the water saturation decreased. In Berea at S_{or} after gel placement, 77.6% of the residual oil was contained within the largest blob. This blob was 122 times larger than the largest oil blob at S_{or} before gel placement.

Remaining Issues. A number of issues and questions were raised during this work. First, why were S_{wr} values not greater (i.e., near 100%) in Berea's small pores? Since S_{or} values were ~80%

in strongly oil-wet porous polyethylene before gel, S_{wr} values in strongly water-wet Berea were expected to be at least as great. The pore and throat sizes in polyethylene were no smaller than those in Berea. Second, why was oil mobilized during gelant injection even though the pressure gradients were less than those before gel placement? Third, why did oil injection cause reductions in gel volume averaging 55% in Berea and 16% in polyethylene even though the pressure gradients were less than those before gel placement? Fourth, why was reduction of gel volume (during oil injection) insensitive to pore size in Berea? Fifth, why was the residual oil phase in Berea after gel so highly connected? What pores participated in the largest residual oil blob? How did the blob throat, blob body, and blob aspect ratios compare with the participating pore throat, body, and aspect ratios? Additional work is needed to answer these questions. Of course, our ultimate goal in these studies is to identify ways to maximize disproportionate permeability reduction in a predictable and controllable manner.

Disproportionate Permeability Reduction in Fused Silica

We examined the ability of gels to reduce permeability to water more than that to oil in clay-free fused silica cores. For an adsorption-based polymer, oil and water residual resistance factors were both very low (not surprisingly, since limited adsorption sites were available). For a pore-filling gel [Cr(III)-acetate-HPAM], water residual resistance factors were over 1,000 times greater than the oil residual resistance factors. Silica cores may be useful during future mechanistic studies.

Gel Treatment in an Arbuckle Production Well

We analyzed results from a Cr(III)-acetate-HPAM gel treatment that was applied by Gel-Tec and Vess Oil Company in the Jennie Johansen #8 production well in the Arbuckle formation. The availability of accurate pressure data before, during, and after the treatment was critical for the analysis. Productivity values before the treatment were 90 times greater than those expected from the Darcy equation for radial flow—indicating the presence of a very conductive feature, such as a fracture. The productivity data was used to estimate an effective average fracture width between 0.2 and 0.4 cm. Based on injectivity data during gelant injection, the fracture area that was contacted by gelant or gel increased significantly with increased volume of gelant injection. This fracture area was probably over 166,000 ft^2 by the end of the 3,000-bbl treatment. Some doubt exists whether any significant gelant leakoff occurred into the 5-md dolomite matrix. If it did occur, the distance of gelant leakoff from the fracture faces was fairly constant with additional injection. The gelant leakoff distance was less than 2 ft and may have been significantly less than 1 ft. After the gel treatment, water productivity was fairly constant at about 20% of the pre-treatment value. However, oil productivity was stimulated by a factor of 18 immediately after the treatment. During the six months after the treatment, oil productivity gradually decreased to approach the pre-treatment value. Two mechanisms were considered to explain why the gel treatment increased oil productivity. Consistent with the observations during gelant injection, one mechanism suggested that the fracture area open to oil flow was increased substantially by the gel treatment, followed by a gradual closing of the fractures during subsequent production. If this mechanism is correct, the longevity of these gel treatments may be increased by including a proppant during gelant placement.

Disproportionate Permeability Reduction in Fractures

We investigated whether Cr(III)-acetate-HPAM gels show disproportionate permeability reduction in open fractures. After extrusion of formed gels into fractures, the pressure gradients for first gel failure were similar for either brine or oil flow, which in turn, were similar to the pressure gradient observed during gel placement. In contrast, during steady state flow after first breaching the gel, the permeability to water (within the fracture) was reduced moderately more than that to oil. For these measurements, disproportionate permeability reduction was most evident at low flow rates. However, additional experiments that employed sequential injection of oil and water banks into the same fractured core did not show a rate dependence for the effect. Experiments where gels were placed as gelants (rather than extruded into place as formed gels) in short fractures exhibited reductions in water permeability that were significantly greater than those to oil. However, these results showed substantial variability that did not definitively correlate with fracture width, gel concentration, or core material.

Gel failure in tubes was also studied (using gel placed as gelant). Consistent with predictions from a force balance, the failure pressure gradient was inversely proportional to tube diameter; however, significant data scatter was noted. Within this scatter, it was not evident that the pressure gradient for gel failure depended on the tube material. Disproportionate permeability reduction was not clearly demonstrated.

Effect of Injection Delay on Gel Properties in Fractures

For our 1X Cr(III)-acetate-HPAM gel (with 0.5% Alcoflood 935, 0.0417% Cr(III) acetate at 41°C), the following conclusions were reached during a study of the effects of gelant/gel aging (i.e., delay between gelant preparation and subsequent injection into a fractured core) on the extrusion, leakoff, and washout properties in 1-mm-wide fractures. First, leakoff rates and pressure gradients during gel extrusion increased most significantly between 5 hours (i.e., the gelation time) and 16 hours after gelant preparation. For gelant injection delays less than 5 hours and for gel injection delays greater than 16 hours, leakoff rates and pressure gradients were relatively insensitive to the aging time. During first brine injection after gel placement, the pressure gradient where brine first breached the gel was greatest (~8 psi/ft) for the gel that was aged from 12 to 24 hours before injection. Significantly lower breaching pressure gradients were seen at either longer or shorter injection delays. After breaching the gel during brine injection at 206 ft/d, the pressure gradient declined to a final stabilized value around 2.5 psi/ft for gels aged from 16 to 24 hours. As brine injection rate increased to 33,000 ft/d, the stabilized pressure gradient increased in proportion to rate raised to the 0.3 power. This behavior was not sensitive to injection delay. For a given brine injection rate, the stabilized pressure gradient was generally greatest for gels aged from 16 to 24 hours before injection. However, when comparing behavior for gel aging times between 12 minutes and 10 days at a given rate, the largest stabilized pressure gradient was no more than 6 times greater than the smallest pressure gradient. Gels aged from 16 to 24 hours showed the maximum diversion of brine into the matrix (i.e., minimized brine flow through the fracture). Regardless of injection delay, the diversion provided by the gels deteriorated substantially as the brine rate increased to 33,000 ft/d.

Use of Swelling Polymers to Plug Fractures

We explored swelling polymers for plugging fractures. Suspensions of granular or powder-form polymers were quickly prepared and injected before they dissolved fully. In concept, the partially

dissolved polymer would lodge and swell to plug the fracture. We compared the behavior of three types of swelling polymers with that of our standard 1-day-old 1X Cr(III)-acetate-HPAM gel (that was prepared using Alcoflood 935). The three swelling polymers included (1) undissolved Alcoflood 935 [with or without Cr(III) crosslinking], (2) Alcosorb polymers with $CrCl_3$, and (3) Diamond Seal. The undissolved Alcoflood 935 and the Alcosorb polymers showed significant problems with gravity segregation. Although the Diamond Seal used five times the concentration of the Alcoflood 935 and Alcosorb polymers, it did not exhibit a problem with gravity segregation. During first brine injection after polymer or gel placement, all three types of swelling polymers showed promise in requiring significant pressure gradients for the brine to first breach the polymer or gel. In 1-mm-wide fractures, the breaching pressure gradients were 8.2 psi/ft for the 1X Alcoflood 935 gel and 9.7 psi/ft for an undissolved Alcoflood 935 polymer that was mixed with $CrCl_3$. In 2-mm-wide fractures, the breaching pressure gradients were 1.2 psi/ft for the 1X Alcoflood 935 gel and 18.2 psi/ft for the Diamond Seal. In 4-mm-wide fractures, the breaching pressure gradients were 2.8 psi/ft for the 1X Alcoflood 935 gel, 3.7 psi/ft for the Diamond Seal, and 11.4 psi/ft for Alcosorb AB3C with $CrCl_3$. After breaching the gel, the Alcosorb and Diamond Seal formulations tended to be more effective than the 1X Alcoflood 935 gel in reducing fracture conductivity at low brine injection rates, but less effective at high brine rates.

In several field applications, the addition of particulates to injected gelants reportedly increased the gel's resistance to washout from fractures or voids. In continuing our search for effective particulates that will not experience severe gravity segregation, we investigated four new materials: (1) strand fibers, (2) milled glass fibers (bag form), (3) milled glass fibers (canister form), and (4) acrylic deck dust. The milled glass fibers (supplied in bag form) had the best suspension qualities. However, gravity segregation was significant with all of the materials.

Partially Formed Gels in Fractured Production Wells

A study was conducted to characterize water-shutoff polymer gels that are injected in the partially formed (partially matured) state into fractures. The study involved placement of chromium(III)-carboxylate/acrylamide-polymer gels in 1-mm- (0.04 in.-) wide, by 2-ft-long, by 1.5-in.-high fractures in 700-md unfired Berea sandstone. The three aqueous chromium(III)-carboxylate/acrylamide-polymer [CC/AP or Cr(III)-acetate-HPAM] gels in this study used chromic triacetate as the chemical crosslinker. They were formulated with a high-Mw ($5x10^6$ daltons) acrylamide polymer and were designated 1X, 2X, and 3X, containing 0.5, 1.0, and 1.5 wt% polymer, respectively.

A partially formed (7-hr-old) 1X CC/AP gel propagated more readily through a 1-mm-wide fracture than a "fully formed" (1-day-old) gel with the same chemical composition. The effective viscosity of the "fully formed" gel in the fracture was nearly an order of magnitude greater than the effective viscosity of the partially formed gel. During first brine injection after gel placement in 1-mm-wide fractures, the pressure gradient required to first breach the gel ranged from 5 to 99 psi/ft for gels containing from 0.5% to 1.5% polymer. The stabilized residual resistance factors (permeability reduction factors) for the first brine floods ranged from 6,400 to 12,000, increasing with increased polymer concentration and gel strength. For the 1X gel, these stabilized permeability reduction factors were comparable for formulations injected in the gelant state, the partially formed state, and the "fully formed" state. During brine flow after gel placement, most (>90%) of the gel remained in the fracture and did not washout.

The CC/AP gels exhibited disproportionate permeability reduction during brine and oil flow through fractures. During one experiment with the 1X gel, brine permeability in the fracture was reduced 166 times more than that for oil. For the 1X and 3X gels, the permeability reduction factor for oil flow remained constant through four cycles of brine and oil injection. In contrast, the permeability reduction factor for brine decreased more than a factor of 10 during these cycles.

Gels Containing High- and Low-Molecular Weight Polymers in Fractures

Water-shutoff polymer gels, when formulated with a combination of high- and low-molecular weight (Mw) polymers, provided improved performance (mechanical strength and stability) in 1- to 4-mm-wide fractures. These gels were injected in a *partially formed* (partially matured) state. The CC/AP or Cr(III)-acetate-HPAM gel formulation contained 1.5 wt% high-Mw ($5x10^6$ daltons) acrylamide polymer and 2.0 wt% low-Mw (~500,000 daltons) acrylamide polymer, crosslinked with chromic triacetate. The CC/AP gel formulation exhibited an effective viscosity of roughly 500 cp during placement at 16,600 ft/d superficial velocity in a 1-mm-wide fracture. After placement, it provided exceptionally good fracture plugging characteristics. The gel withstood 52 psi differential pressure (26 psi/ft pressure gradient) for 24 hrs, while permitting no detectable brine flow through the fracture. Subsequently, when the differential pressure was increased to 175 psi (88 psi/ft pressure gradient), the gel imparted a brine residual resistance factor (permeability reduction factor) of 30,000.

When placed in a 2-mm-wide fracture, the same gel required 37 psi/ft pressure gradient for brine to breach the gel. After exceeding this critical pressure gradient, the stabilized brine residual resistance factor was 260,000. When placed in a 4-mm-wide fracture, the same gel required 25 psi/ft pressure gradient for brine to breach the gel. After exceeding this critical pressure gradient, the stabilized brine residual resistance factor in the fracture was again 260,000. At a fixed injection rate, the effective viscosity of the gel solution within the fracture increased with fracture width. The shear-thinning nature of the formulation explains this behavior.

After placement of the gel in a 4-mm-wide fracture, stabilized residual resistance factors decreased by a factor of 2.6 when the brine superficial velocity was increased by a factor of 16 (i.e., from 259 to 4,140 ft/d in the fracture). Similar results were obtained during an analogous experiment in a 2-mm fracture. After placement of the gel in a fracture, the magnitude of the disproportionate permeability reduction decreased with increasing cycles of water/oil flooding. In a 4-mm-wide fracture, the high- and low-Mw CC/AP gel exhibited modest disproportionate permeability reduction (factors from 2 to 6).

Technology Transfer

Technology transfer efforts for the project are listed in Appendix A.

1. INTRODUCTION

Fractures (either natural or artificially induced) often cause excess water production and reduced oil recovery efficiency, especially during waterfloods and improved oil recovery projects. Fractures constitute a channeling and water-production problem that has a high potential for successful treatment by gels and certain other chemical blocking agents. Especially in fractured production wells, gels can substantially diminish water production if the gel can reduce permeability to water much more than that to oil.

This report describes work performed during the second year of the project, "Conformance Improvement Using Gels." Results from the first year are described in Ref. 1.

Objectives

This research project has two objectives. The first objective is to identify gel compositions and conditions that substantially reduce flow through fractures that allow direct channeling between wells, while leaving secondary fractures open so that high fluid injection and production rates can be maintained. This goal will be reached by (1) characterizing gel propagation through fractures as a function of fracture width, length, and height, injection rate, gel composition, and temperature, (2) correlating rheology in fractures with that in a viscometer, and (3) using the experimental results to develop an appropriate model for gel placement and treatment sizing.

The second objective is to optimize treatments in fractured production wells, where the gel must reduce permeability to water much more than that to oil. Within this objective, the specific goals are to (1) determine the correct mechanism(s) for the disproportionate permeability reduction, (2) identify conditions that maximize the phenomenon, (3) find materials and methods that make the phenomenon predictable and controllable, and (4) establish a methodology to determine how much gelant should be injected in a given fractured production well.

Report Content

This report describes work performed during the second year of the project. Chapter 2 re-examines the use of X-ray computed microtomography to identify the mechanism responsible for gels reducing the permeability to water more than that to oil. Chapter 3 describes coreflood studies of disproportionate permeability reduction. Chapter 4 analyzes a field gel treatment that was applied in an Arbuckle production well. Chapter 5 investigates disproportionate permeability reduction by gels in fractures and tubes. Chapter 6 describes the effects of gel injection delay on extrusion, leakoff, and washout behavior for gels in a 1-mm-wide fracture. Chapter 7 considers the use of swelling polymers to plug fractures. In Chapter 8, the use of partially formed gels in fractures is examined. Chapter 9 describes a gel prepared from both high- and low-molecular weight polymers and its application in fractures. Finally, technology transfer activities are described in Appendix A.

2. RE-EXAMINATION OF X-RAY COMPUTED MICROTOMOGRAPHY

Previous Conclusions

In previous work, we used X-ray computed microtomography to determine why gels reduce permeability to water more than that to oil in strongly water-wet Berea sandstone and strongly oil-wet porous polyethylene cores.[1-4] The aqueous Cr(III)-acetate-HPAM gel used in this work contained 0.5% Alcoflood 935 HPAM (~$5x10^6$ daltons, 5-10% degree of hydrolysis), 0.0417% Cr(III) acetate, 1% NaCl, and 0.1% $CaCl_2$. The brine contained 1% NaCl and 0.1% $CaCl_2$. The oil was hexadecane that was doped with either 10% iodohexadecane (used in Berea) or 15% bromohexadecane (used in polyethylene). All experiments were performed at room temperature except gelation, which occurred at ~60°C. Important conclusions drawn from the work include:

1. Although Berea sandstone and porous polyethylene had very different porosities (22% versus 40%) and permeability (0.47 versus 8.8 darcys), the distributions of pore sizes and aspect ratios were similar.
2. For Berea sandstone, the water saturation in the smallest detected pores averaged 60%.
3. The Cr(III)-acetate-HPAM gel caused comparable oil and water permeability reductions in both porous media. Gel reduced permeability to water by 80 to 90 times more than that to oil.
4. The distributions of water and oil saturations (versus pore size) in the two porous media were substantially different before, during, and after gel placement.
5. Disproportionate permeability reduction occurred by different mechanisms in the two porous media. In Berea, gel caused trapping of substantial volumes of oil that remained immobile during water flooding. With this high trapped oil saturation, water was forced to flow through narrow films, through the smallest pores, and through the gel itself. In contrast, during oil flooding, oil pathways remained relatively free from constriction by the gel.
6. In the polyethylene core, oil-trapping did not contribute significantly. Instead, oil films and a relatively small number of pore pathways provided conduits for the oil.

At a recent Gordon Conference (Andover, NH, August 8, 2002), attendees were surprised at some of the above findings. Some felt that water saturation in the smallest pores of strongly water-wet Berea should average near 100% instead of 60%. Others questioned that two porous media with such different porosities and permeabilities could have similar pore size distributions.

Differences between the 1st and 2nd Analyses

Procedural Differences. To double check our results, our X-ray images were re-analyzed (with Brent Lindquist's 3DMA software) using a different method for segmenting the fluids. In our first analysis, assignment of the locations of rock, water, and oil voxels were accomplished as follows. First, the rock locations were identified from X-ray images of cores that were saturated only with the wetting phase. These rock locations were used in subsequent images to pin down the liquid-filled pore space. Second, fluid phase identification was made by subtracting an image having both fluid phases present (one phase of which was doped with a strong X-ray attenuating compound) from the corresponding image in which only the wetting phase was present in the pore space. A histogram of the subtracted X-ray attenuation coefficients showed a bimodal distribution—the peaks in the distribution corresponding to water- and oil-filled voxels. The subtracted image contains significantly greater overlap between the peaks than an unsubtracted image. There are several reasons for overlap between the peaks in the histogram:

i) The finite size of a voxel means that any X-ray attenuation coefficient measured is an average over the voxel volume.
ii) Variations in X-ray counting statistics result in variations in attenuation coefficients.
iii) Minor alignment errors, on the order of 1/2-1 voxel width, occur.

While i) and ii) influence peak overlap in non-subtracted images, in subtracted images their influence is exacerbated. Item iii) contributes for subtracted images, but not unsubtracted ones.

In the first analysis, simple thresholding was used to distinguished water-and oil-filled voxels. The threshold was determined from the bimodal subtraction histogram, with the threshold value picked to lie in the "valley'" between the two peaks. Simple thresholding is well known to result in speculated images (i.e. apparent blobs of one phase trapped in the other). The extent of the speculation is proportional to the overlap between the two peaks in the difference histogram.

In the newer analysis, rock locations determined from single-phase flooded core images were still used in subsequent images of the two-phase flooded core to identify the liquid-filled space. However the subtraction procedure was not used. Rather, a segmentation procedure based upon indicator kriging was used to segment the phases in the pore space only. This avoided any artificial spreading induced by a subtraction procedure. Additionally, the indicator kriging method does not rely on global thresholding, but performs local segmentation based upon maximum likelihood decisions. The result is a cleaner resolution of the fluid phases.

The basic idea of kriging is to estimate an unknown random variable (e.g., the “true” X-ray attenuation value of a voxel) by a linear combination of known random variables (i.e., measured attenuation values) plus a possible systematic shift. The data values, however, are not assumed to be independent (as in classical linear regression analysis) but are correlated spatially. The estimate is required to be unbiased, and the variance of the error in the estimate is required to be minimized. This leads to a constrained minimization problem, whose solution follows from a “constrained normal” system of linear equations known as the ordinary kriging system. While ordinary kriging estimates the value of the random variable at a point, indicator kriging gives the probability that the value at the point is greater than some threshold value. This probability then “indicates” the possible state (0 or 1, air or rock) at the point. Indicator kriging does so by capitalizing on the proportion of neighboring data valued above the same threshold, and accounts for the proximity of each datum to the unsampled location.

2nd Analysis Revealed Larger Pores in Polyethylene. Figs. 1 and 2 compare the number and volume distributions for Berea sandstone using the first and second analyses. The second analysis included 25% more pores (2,176 pores) than the first analysis (1,736 pores). Results from the two analyses were quite similar, although the second analysis indicated a significant peak in the volume distribution at 0.006 mm^3 that was not detected in the first analysis (Fig. 2). This secondary peak resulted from a relatively small number of large pores that were included in the second analysis but not the first.

Figs. 3 and 4 compare the number and volume distributions for porous polyethylene using the first and second analyses. The second analysis indicated significantly larger pores than the first

analysis. Also, consistent with one issue raised at the Gordon Conference, the second analysis revealed that the porous polyethylene generally had larger pores than Berea sandstone. Why was this conclusion not reached during the first analysis? The apparent explanation is that the second analysis included about five times more pores (1,879 pores) than the first analysis (386 pores). Evidently, 386 pores were not sufficient to represent the porous polyethylene sample.

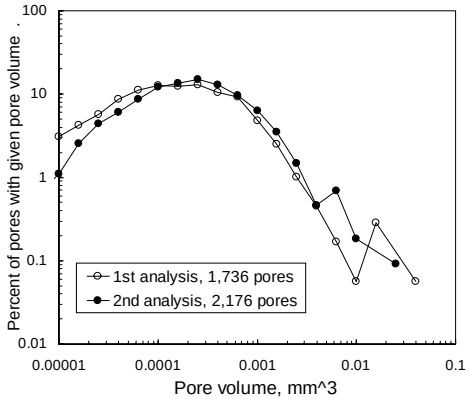

Fig. 1—Number distributions of pores for Berea sandstone.

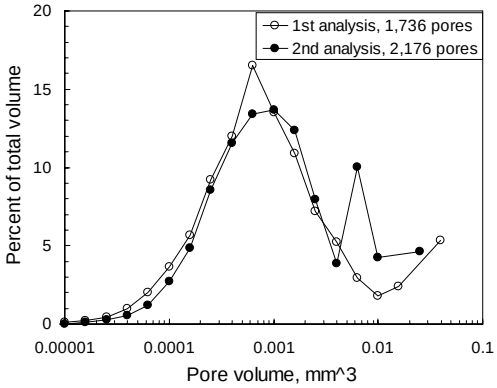

Fig. 2—Volume distributions of pores for Berea sandstone.

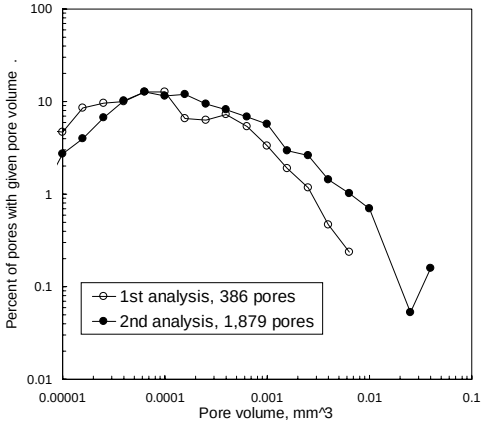

Fig. 3—Number distributions of pores for porous polyethylene.

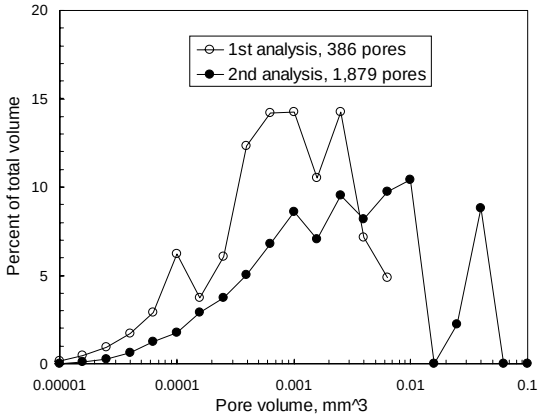

Fig. 4—Volume distributions of pores for porous polyethylene.

2nd Analysis Showed Lower S_{wr} and S_{or} in Berea. For each flooding stage before and after gel placement, the average water saturation versus pore size was compared for the first and second analyses in Fig. 5 for Berea sandstone and in Fig. 6 for porous polyethylene. Table 1 also summarizes the overall water saturations after each flooding step. In Berea before gel placement, the second analysis showed significantly lower water saturations at S_{wr} (overall average: 16.0% versus 24.7%) and significantly higher water saturations at S_{or} (overall average: 81.6% versus 56.5%) than the first analysis. Results from the second analysis were more consistent with saturations determined from other flooding experiments in Berea using larger cores.

Table 1—Average water saturations after various flooding stages.

	Berea		Polyethylene	
Condition	1st analysis	2nd analysis	1st analysis	2nd analysis
@ S_{or1} before gel			77.7%	86.0%
@ S_{wr} before gel	24.7%	16.0%	15.2%	16.5%
@ S_{or} or S_{or2}	56.5%	81.6%	75.0%	83.0%
@ Gel placement	47.7%	63.7%	94.4%	99.8%
@ S_{wr} after gel	29.0%	28.7%	75.7%	83.5%
@ S_{or} after gel	21.3%	49.0%	92.4%	99.7%

Both Analyses Showed 60% Average S_w in the Smallest Detected Berea Pores. At S_{wr} (Fig. 5a), note that the average water saturation in the smallest detected pores was roughly 60% for both analyses. On first consideration, this finding appears to contradict those who expect the water saturation to approach 100% in the smallest pores of a strongly water-wet porous medium. In reconciliation, pores may be present (especially in clays) that were smaller than we can detect with X-ray computed microtomography. (Our voxel size was 4.1 μm.) At any rate, the smallest detected pores ($\sim 5 \times 10^{-6}$ mm^3) in our analysis were confirmed to average roughly 60% water saturation at S_{wr}. However, the reader should recognize that saturation data were scattered over the entire range from 0 to 100% (as will be shown in Fig. 8a).

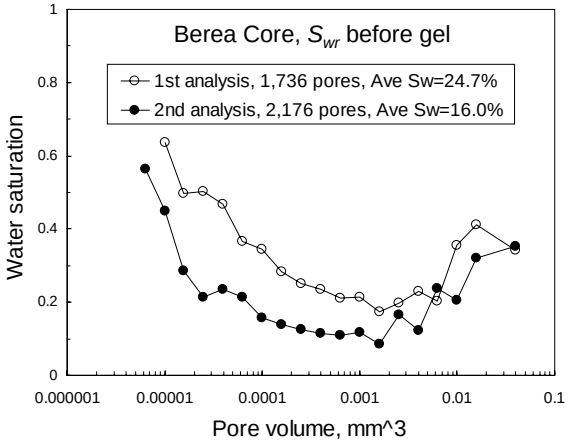

Fig. 5a—At S_{wr} before gel.

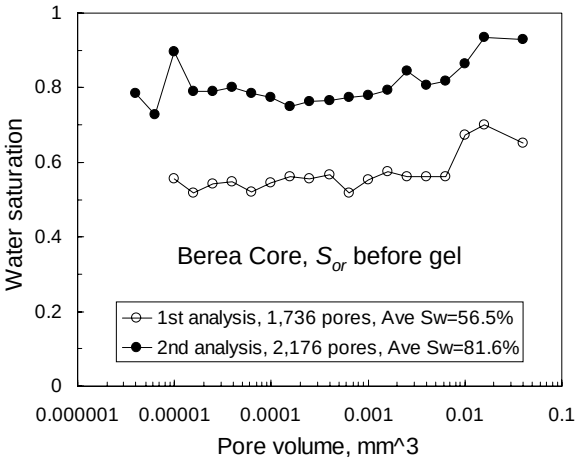

Fig. 5b—At S_{or} before gel.

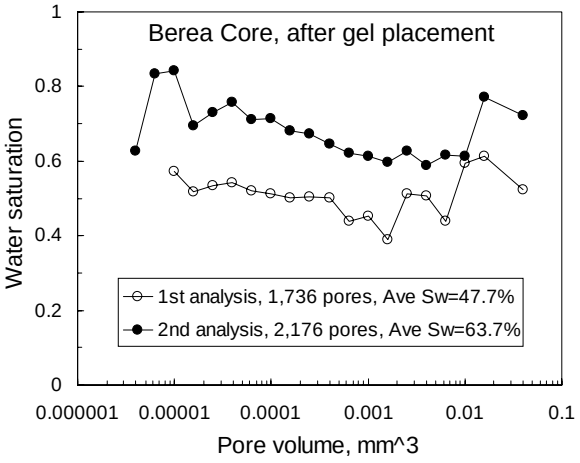

Fig. 5c—After gel placement.

Fig. 5—Average S_w versus pore size, Berea.

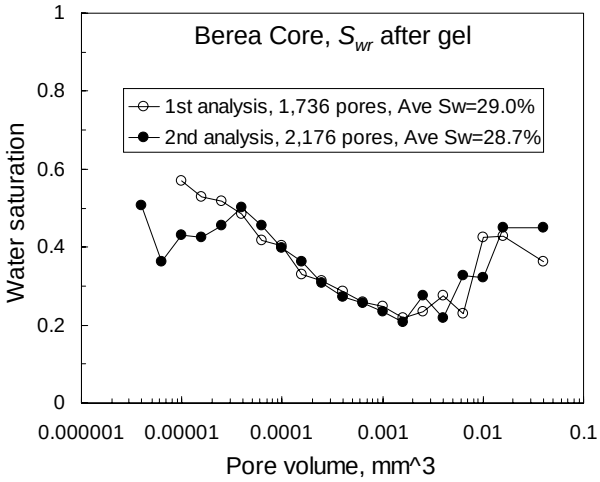

Fig. 5d—At S_{wr} after gel.

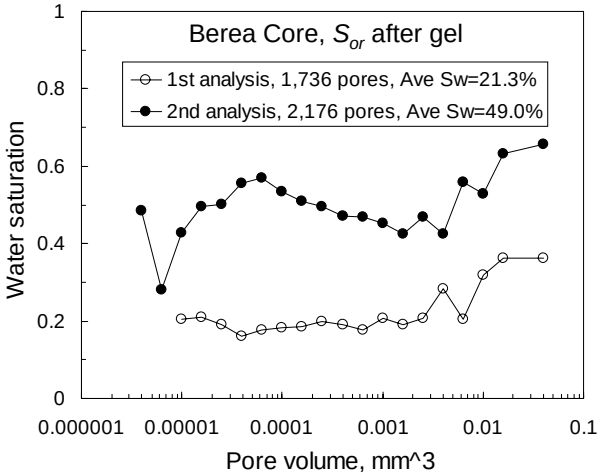

Fig. 5e—At S_{or} after gel.

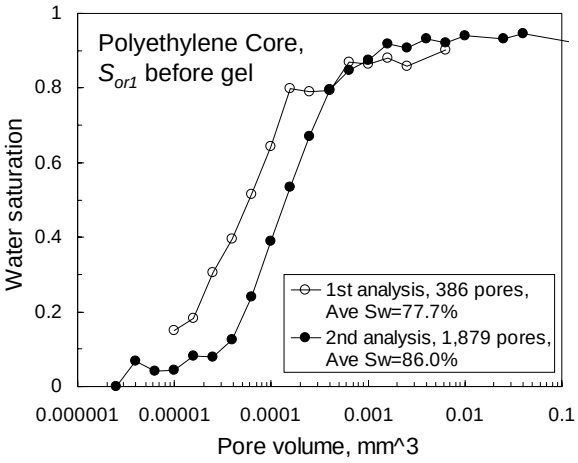

Fig. 6a—At S_{or1} before gel.

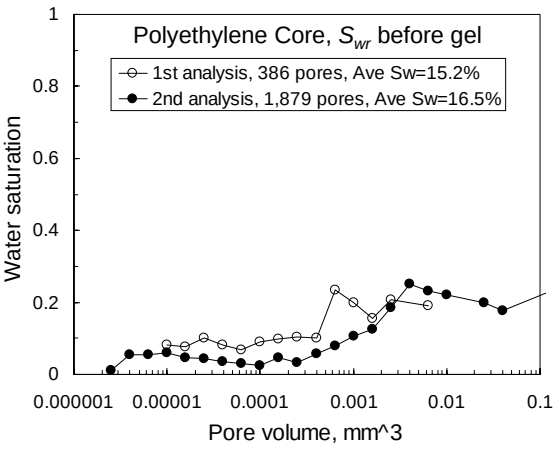

Fig. 6b—At S_{wr} before gel.

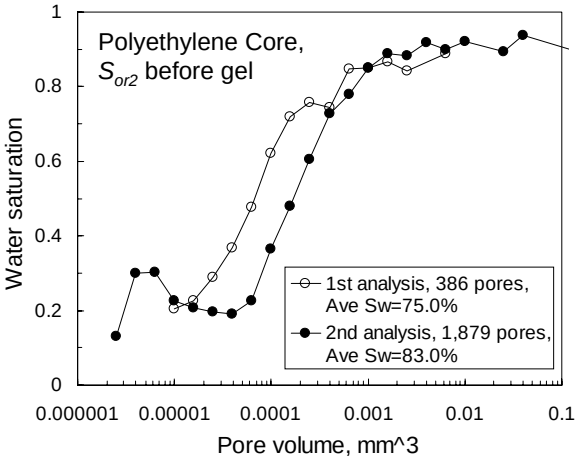

Fig. 6c—At S_{or2} before gel.

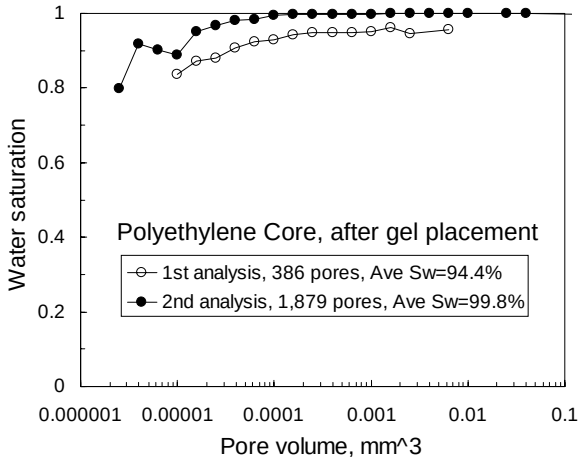

Fig. 6d—After gel placement.

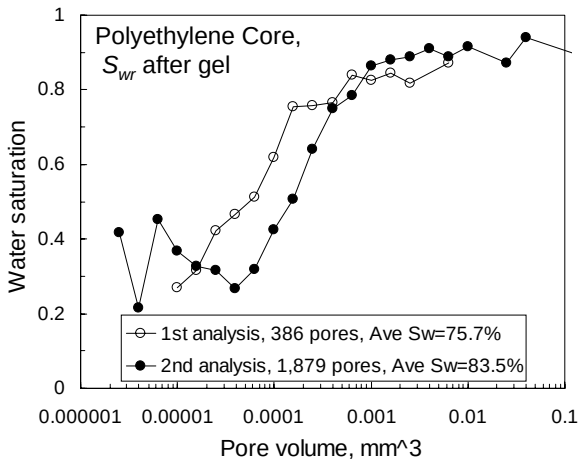

Fig. 6e—At S_{wr} after gel.

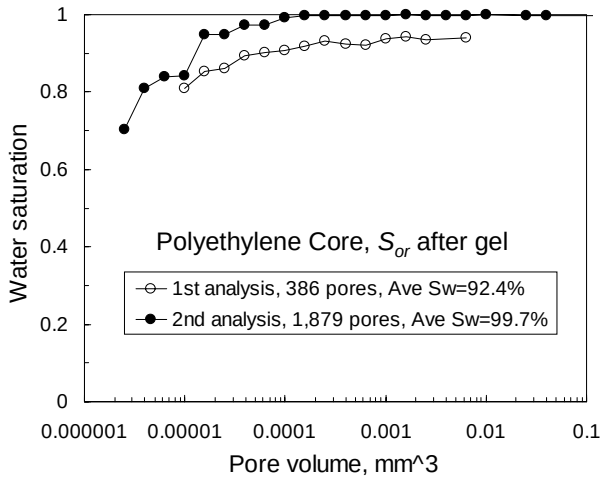

Fig. 6f—At S_{or} after gel.

Fig. 6—Average S_w versus pore size, polyethylene.

Average S_w Was 20% in the Smallest Detected Polyethylene Pores. At S_{or2} (Fig. 6c), the average water saturation in the smallest detected pores was roughly 20% for both analyses. In other words, the wetting phase (oil) saturation averaged around 80% in the smallest detected polyethylene pores. Recall that the wetting phase (water) saturation averaged only 60% in the smallest detected Berea pores. For both porous media, the smallest detected pores were about the same size (~$5x10^{-6}$ mm^3). One might explain these observations by suggesting that the affinity of polyethylene for oil was stronger than the affinity of sandstone for water. However, this suggestion is counter-intuitive since polar interactions between Berea minerals and water should be stronger than the non-polar interactions between polyethylene and hexadecane.

Qualitative Trends Were the Same for Both Analyses. Examination of Fig. 5 reveals differences between the first and second analyses of Berea. In particular for three of the five images (Figs. 5b, 5c, and 5e), the second analysis showed significantly greater water saturations than in the first analysis. However, most of the key trends remain unchanged. The basic shapes of the curves were similar for the two analyses. At S_{or}, significantly more residual oil was trapped after gel placement than before the gel was placed (compare Figs. 5b and 5e). This observation led to a key mechanistic conclusion for disproportionate permeability reduction in Berea. Both the analyses indicated that gel trapped at least 32 saturation percentage points more oil than when gel was not present. By creating a higher S_{or}, the water pathways became greatly constricted, leading to a very high water residual resistance factor (F_{rrw}=1,220).

In the porous polyethylene core, smaller differences were noted between the results from the first and second analyses (Fig. 6). For 5 of the 6 images, the overall average water saturation from the second analysis was 5 to 8 saturation percentage points higher than that from the first analysis. Also, for 3 of the 6 images (Figs. 6a, 6c, and 6e), water saturations in 10^{-5} to 10^{-4} mm^3 pores were noticeably higher from the first analysis than the second. Beyond that, results from the two analyses were quite similar for the polyethylene core. The basic shapes of the curves and the conclusions drawn were the same for both analyses.

2nd Analysis Showed Many More Pores at High/Low Saturations in Berea. Figs. 7a and 7b show the distributions of saturations for individual pores at S_{wr} (Fig. 7a) and at S_{or} (Fig. 7b) from the first analysis. The solid curves in these figures plot the average water saturations for a given pore size. These curves show the same data plotted by the open symbols in Figs. 5a and 5b. Note that very few pores have water saturations below 5% in Fig. 7a (at S_{wr}) and very few pores have water saturations above 95% in Fig. 7b (at S_{or}). Figs. 8a and 8b provide analogous results from the second analysis. Whereas in the first analysis, only 0.2% of the pores had S_w < 5% at S_{wr} (Fig. 7a), 54.5% of the pores had S_w < 5% at S_{wr} for the second analysis (Fig. 8a). In the first analysis, only 0.6% of the pores had S_w > 95% at S_{or} (Fig. 7b), while 39.4% of the pores had S_w > 95% at S_{or} for the second analysis (Fig. 8b). Figs. 8c to 8e show the distributions of saturations for individual pores for other flooding steps for Berea, using the second analysis. Consistent with the results from the first analysis, a wide range of saturations were found for any given pore size at any given flooding step.

For the porous polyethylene core, the distributions of saturations for individual pores are shown in Fig. 9 for the second analysis. These distributions were not noticeably different from those from the first analysis.[1]

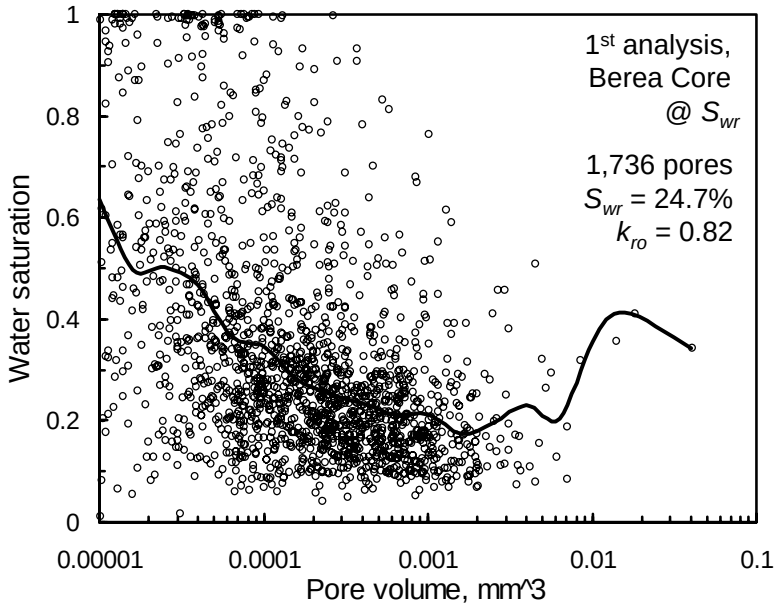

Fig. 7a—At S_{wr} before gel.

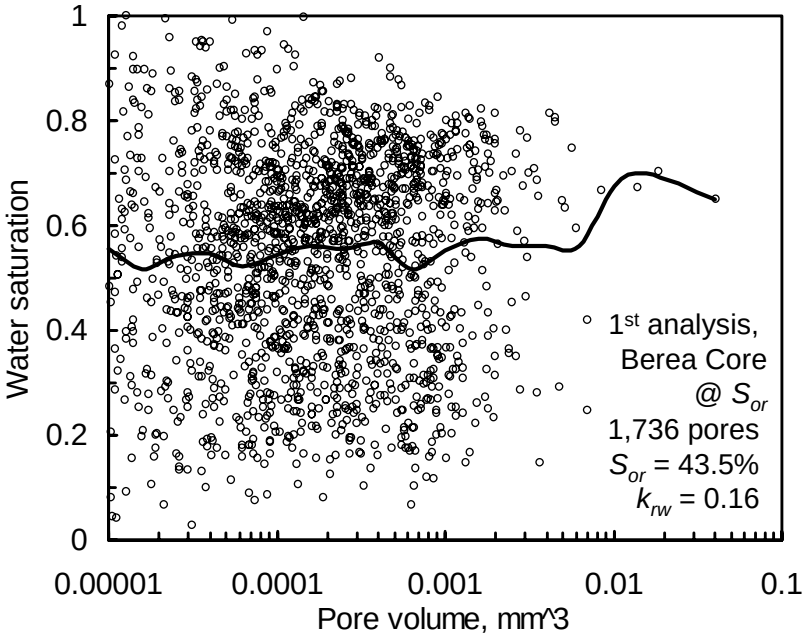

Fig. 7b—At S_{or} before gel.

Fig. 7—1st Berea analysis, 1,736 pores.

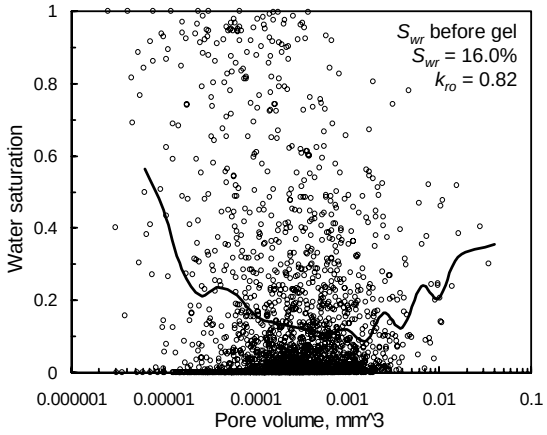

Fig. 8a—At S_{wr} before gel.

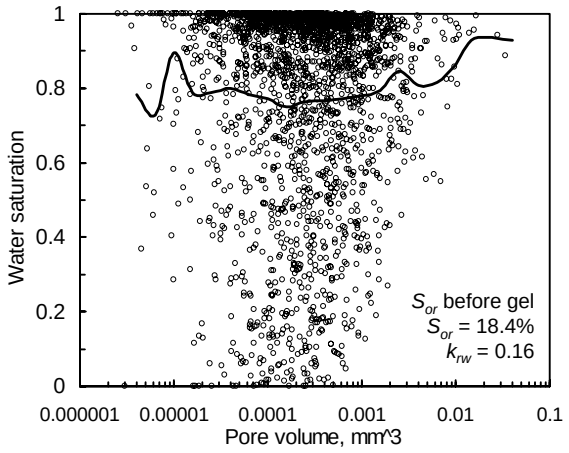

Fig. 8b—At S_{or} before gel.

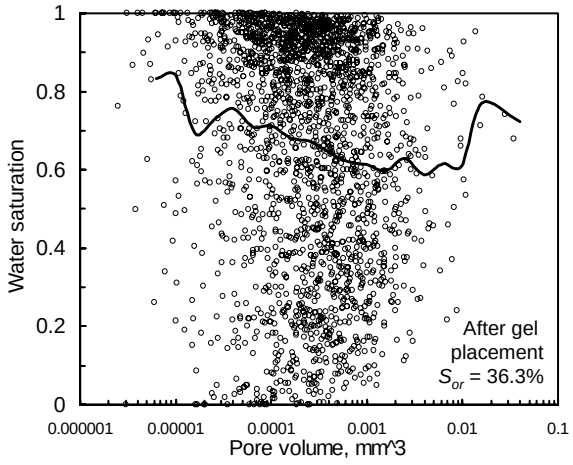

Fig. 8c—After gel placement.

Fig. 8—2nd Berea analysis, 2,176 pores.

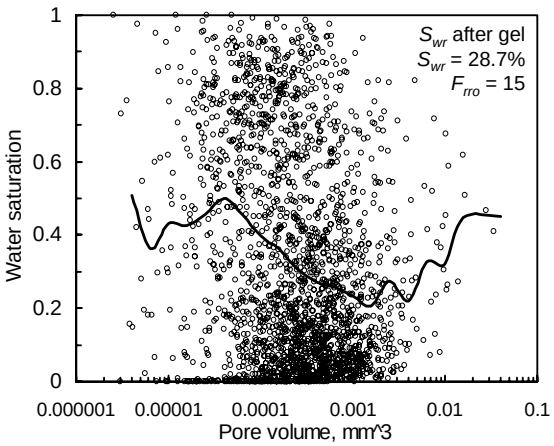

Fig. 8d—At S_{wr} after gel.

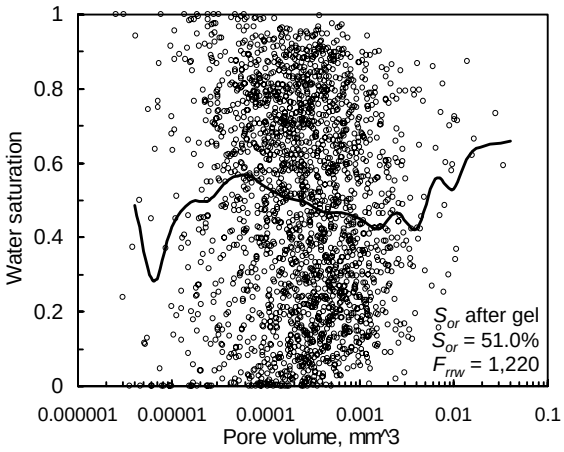

Fig. 8e—At S_{or} after gel.

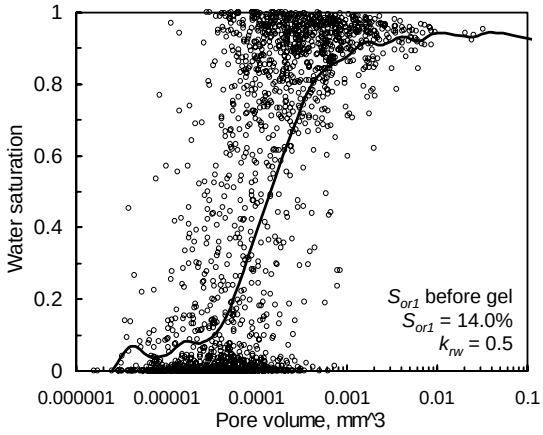

Fig. 9a—At S_{or1} before gel.

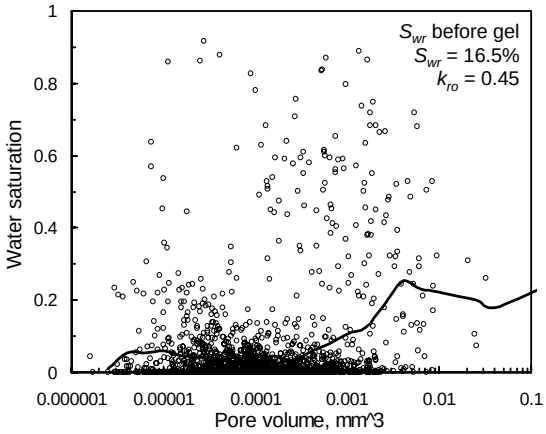

Fig. 9b—At S_{wr} before gel.

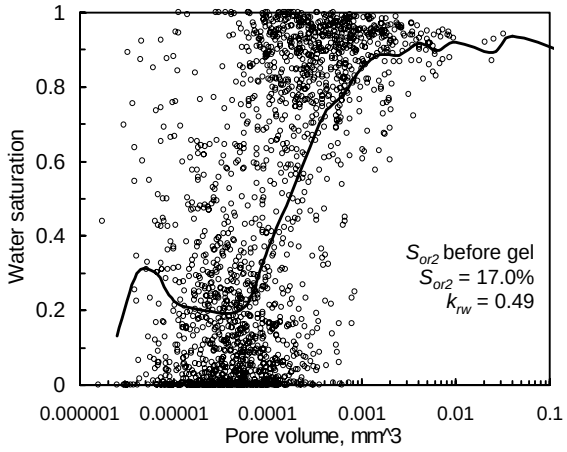

Fig. 9c—At S_{or2} before gel.

Fig. 9—2nd Polyethylene analysis, 1,879 pores.

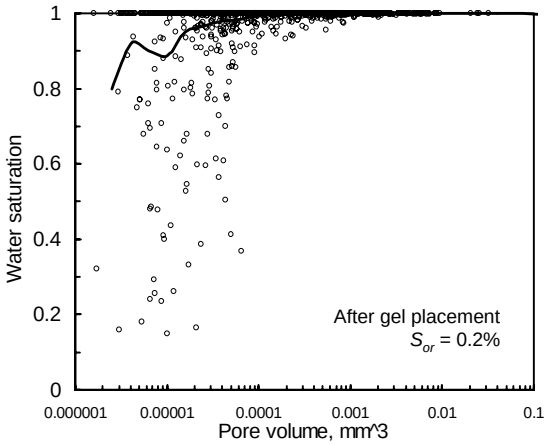

Fig. 9d—After gel placement.

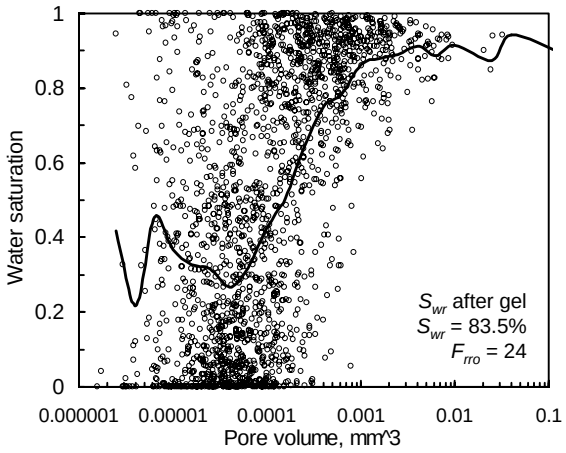

Fig. 9e—At S_{wr} after gel.

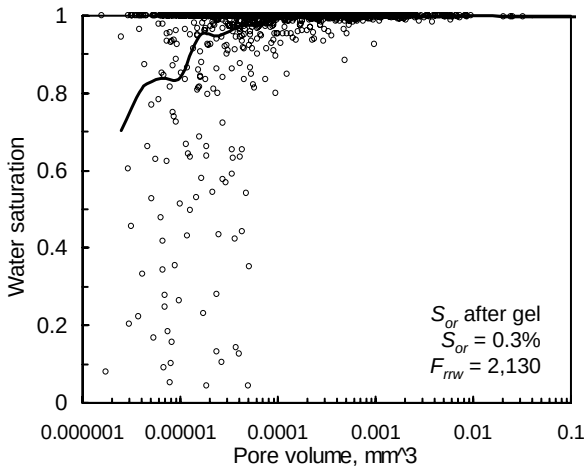

Fig. 9f—At S_{or} after gel.

In Transition from S_{wr} to S_{or}, Many Berea Pores Gained Oil in 1st Analysis but Not in 2nd. The analysis can provide saturation changes for individual pores throughout the flooding sequence. Using the first analysis, Fig. 10 plots these changes in water saturation in Berea for the transition from S_{wr} to S_{or} before gel placement. The solid line plots the average change in water saturation for a given pore size. This figure suggests that the average behavior results from a large variety of S_w changes that occur in individual pores. Especially for the smaller pores, many pores (21.5% of the total from Table 2) appeared to lose water even though water was injected.

In contrast, when the second analysis was applied to the same data (Fig. 11a), very few pores (1.1% from Table 2) experienced an increase in oil saturation during the transition from S_{wr} to S_{or}. In fact, for three of four flooding stages, the number of pores that gained oil during water injection or that gained water during oil injection was less during the second analysis than during the first analysis (Table 2). Figs. 11 and 12 show saturation changes for individual pores for various transitions using the second analysis. Tables 2 and 3 summarize counter-intuitive saturation changes for the various flooding stages in Berea and polyethylene. Most of the counter-intuitive changes that were noted during the first analysis but not during the second were associated with the smaller pores (compare Figs. 10 and 11a). We suspect that the second analysis more effectively distinguished between oil and water in the smaller pores.

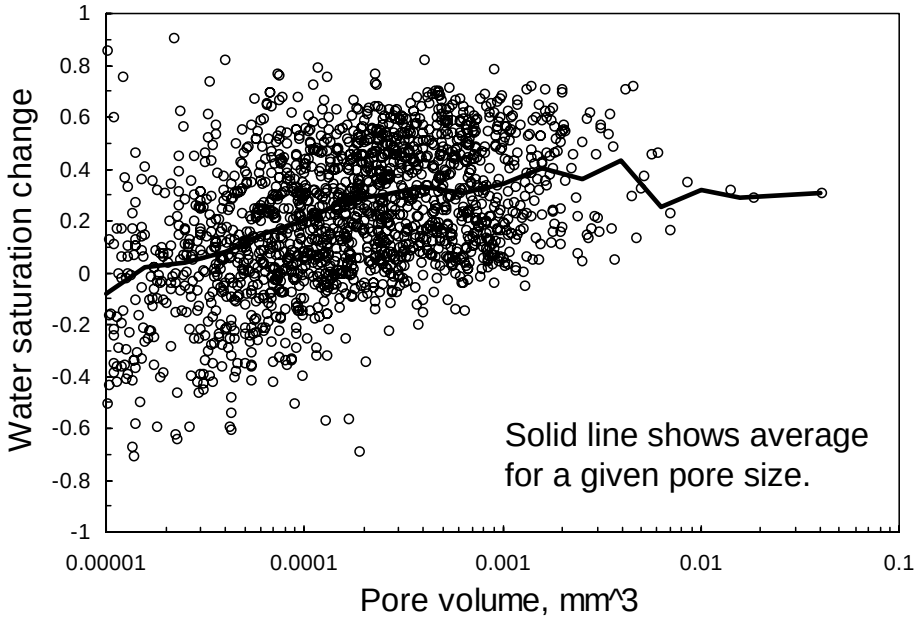

Fig. 10—S_w changes from S_{wr} to S_{or} in Berea, 1st analysis.

Table 2—Counter-intuitive saturation changes, Berea.

	% of pores that gained oil when water was injected		% of pores that gained water when oil was injected	
Transition	1st analysis	2nd analysis	1st analysis	2nd analysis
S_{wr} to S_{or} before gel	21.5	1.1		
S_{or} before gel to gel	57.9	78.2		
Gel to S_{wr} after gel			27.5	4.0
S_{wr} to S_{or} after gel	80.7	22.6		

Table 3—Counter-intuitive saturation changes, polyethylene.

	% of pores that gained oil when water was injected		% of pores that gained water when oil was injected	
Transition	1st analysis	2nd analysis	1st analysis	2nd analysis
S_{or1} to S_{wr} before gel			24.6	13.7
S_{wr} to S_{or2} before gel	3.6	0.6		
S_{or2} before gel to gel	1.0	0.5		
Gel to S_{wr} after gel			0.8	0.1
S_{wr} to S_{or} after gel	0.5	0.5		

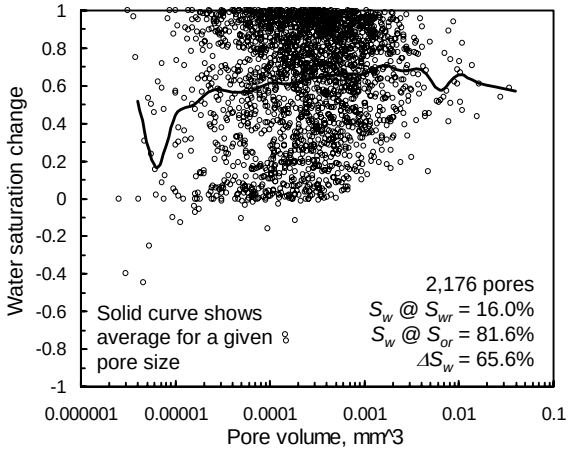

Fig. 11a—S_{wr} to S_{or}.

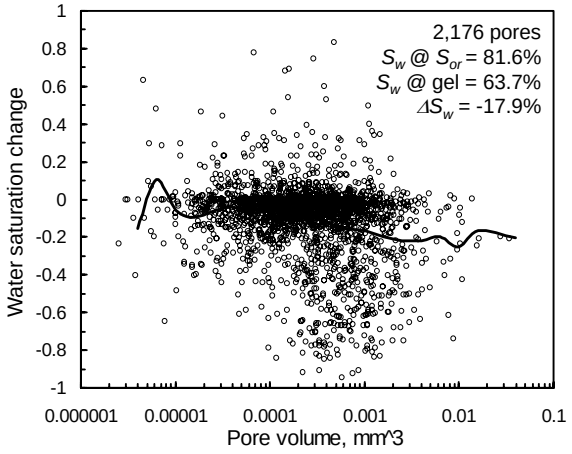

Fig. 11b—S_{or} to gel placement.

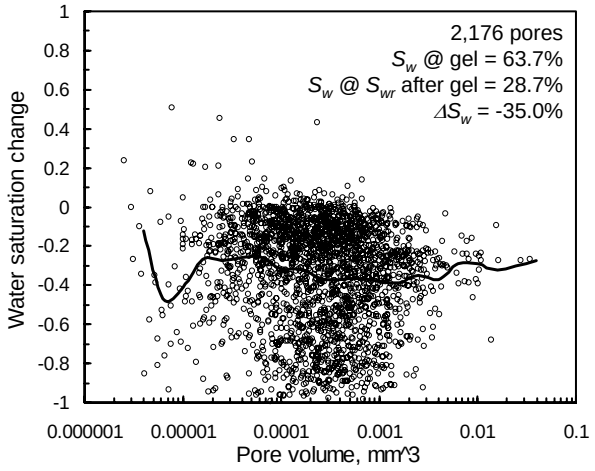

Fig. 11c—Gel placement to S_{wr} after gel.

Fig. 11—S_w changes in Berea, 2nd analysis.

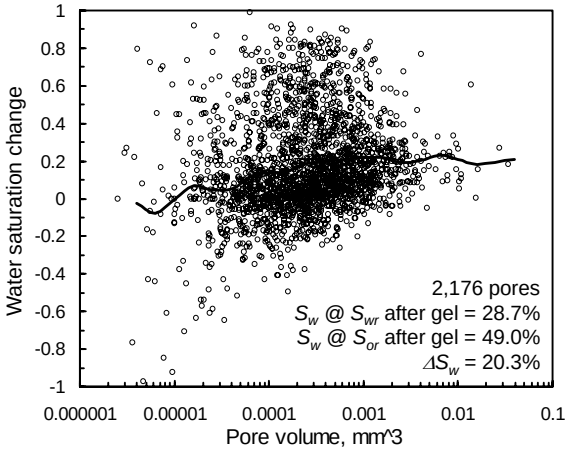

Fig. 11d—S_{wr} after gel to S_{or} after gel.

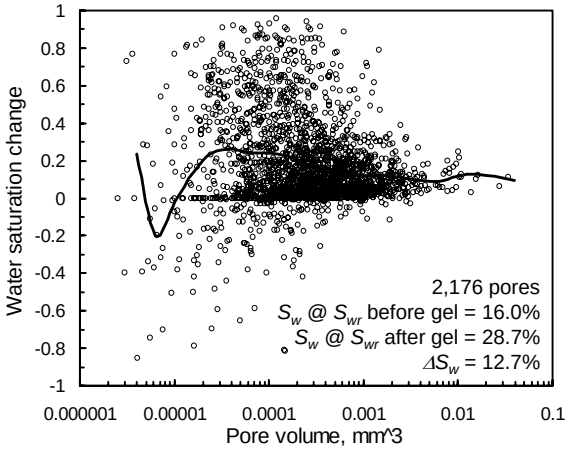

Fig. 11e—S_{wr} before gel to S_{wr} after gel.

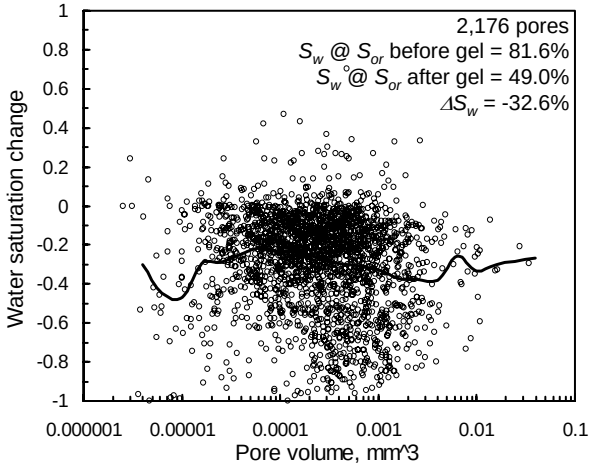

Fig. 11f—S_{or} before gel to S_{or} after gel.

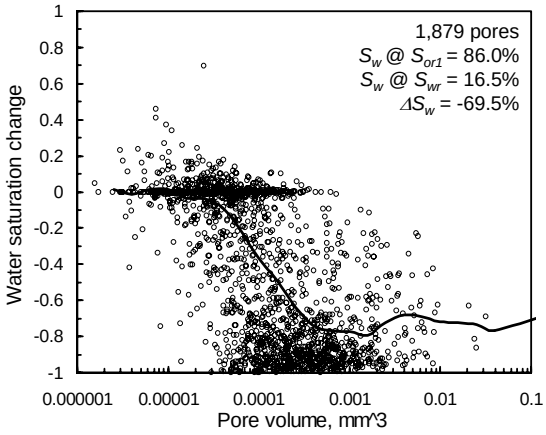

Fig. 12a—S_{or1} to S_{wr}.

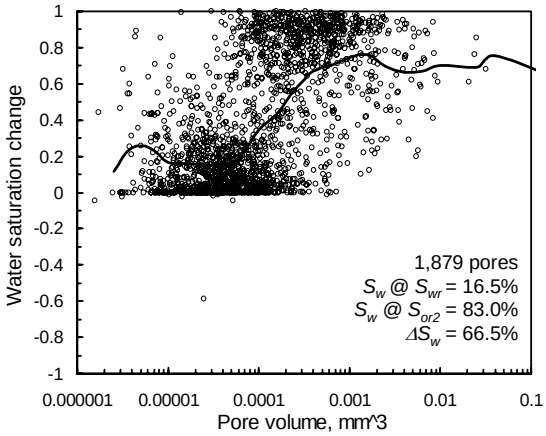

Fig. 12b—S_{wr} to S_{or2}.

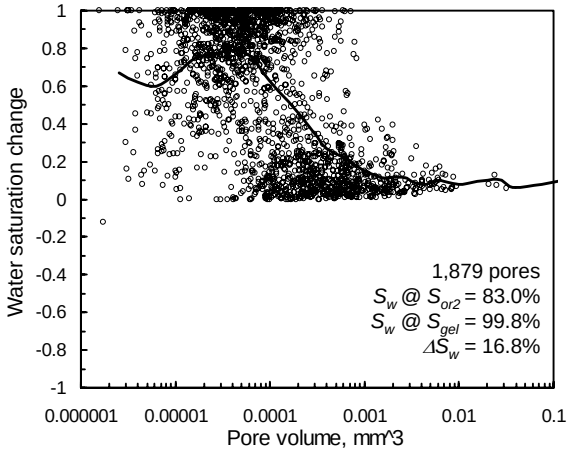

Fig. 12c—S_{or2} to gel placement.

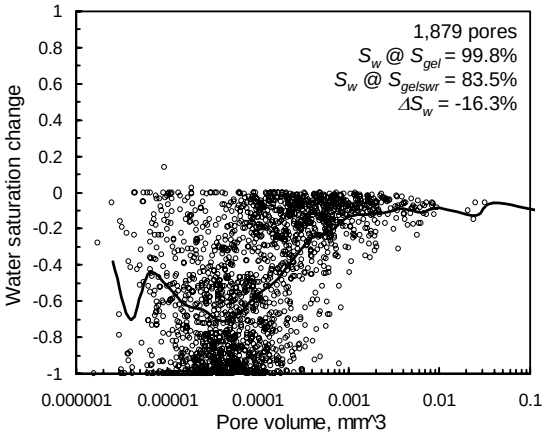

Fig. 12d—Gel placement to S_{wr} after gel.

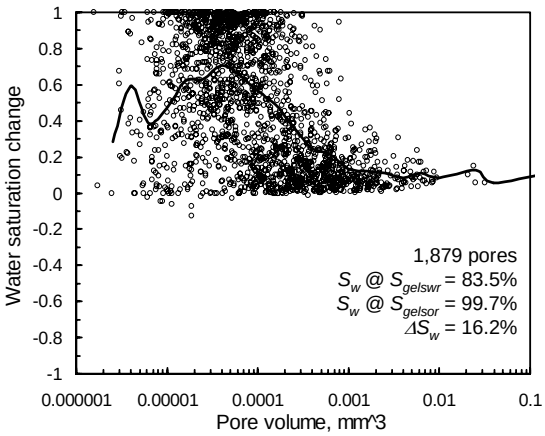

Fig. 12e—S_{wr} after gel to S_{or} after gel.

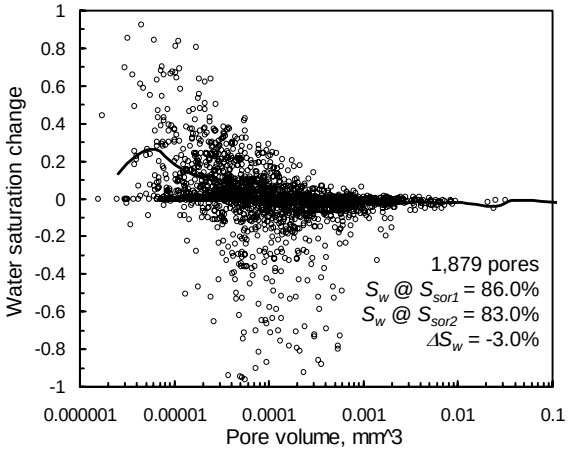

Fig. 12f—S_{or1} before gel to S_{or2} before gel.

Fig. 12—S_w changes in polyethylene, 2nd analysis.

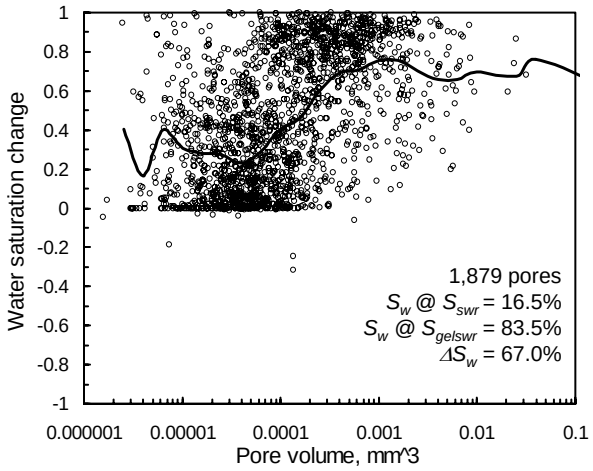

Fig. 12g—S_{wr} before gel to S_{wr} after gel.

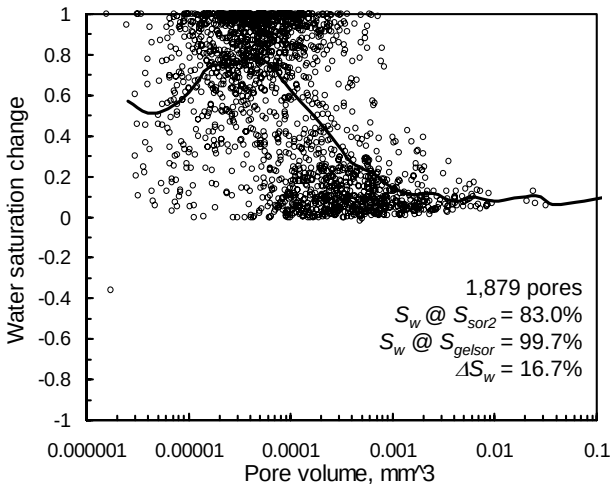

Fig. 12h—S_{or} before gel to S_{or} after gel.

Other Comparisons of Saturation Distributions. The saturation distributions can be compared in another useful way by plotting the cumulative fraction of the pore volume as a function of increasing water saturation. Figs. 13 and 14 provide these plots (using the second analysis) for the Berea and polyethylene cores, respectively. Fig. 13 shows that a substantial difference existed between the S_{wr} and S_{or} distributions before gel placement, but these differences were diminished considerably after gel placement. Nonetheless, the curves were noticeably different for each flooding stage.

In contrast for polyethylene, the six curves followed one of three distinct trends (Fig. 14). The two curves for S_{or} before gel placement and the curve for S_{wr} after gel placement were very similar. Also, the curve immediately after gel placement and the final S_{or} curve after gel placement were very similar. The S_{wr} curve before gel placement was distinct from the other

curves. As with Berea, a substantial difference existed between the S_{wr} and S_{or} distributions before gel placement, but these differences were diminished considerably after gel placement.

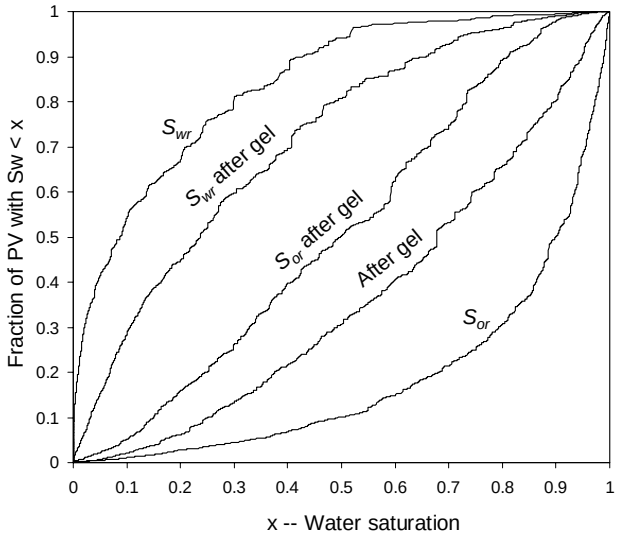

Fig. 13—S_w distributions in Berea.

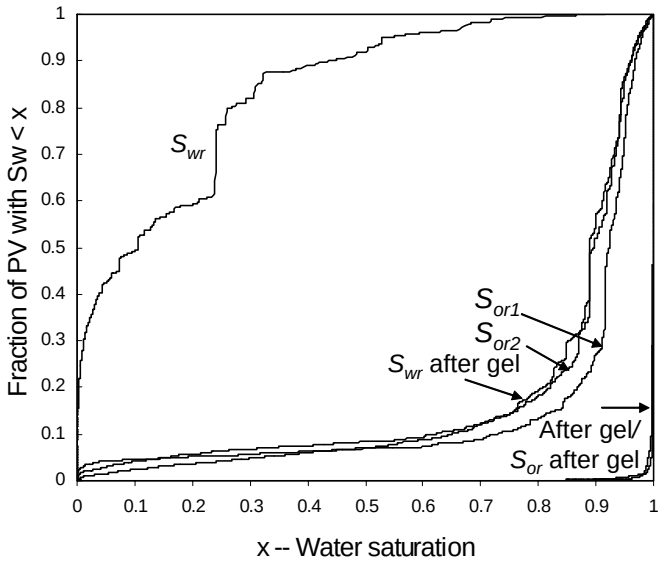

Fig. 14—S_w distributions in polyethylene.

The saturation data can also be viewed by the fraction of pores that possess some minimum saturation value. Figs. 15 and 16 provide these plots as a function of pore size for Berea and polyethylene, respectively. On the *x*-axis, the pore sizes are grouped by decade. In each plot, five saturation levels are shown: <10%, <25%, <50%, <75%, and <90%. These plots help to further quantify the relationships in Figs. 8, 11, and 12.

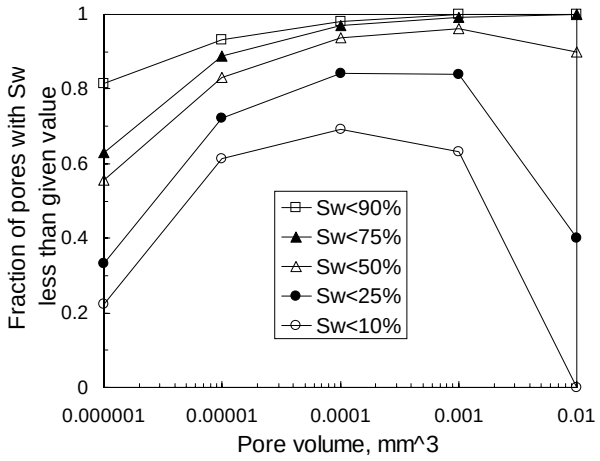

Fig. 15a—At S_{wr} before gel.

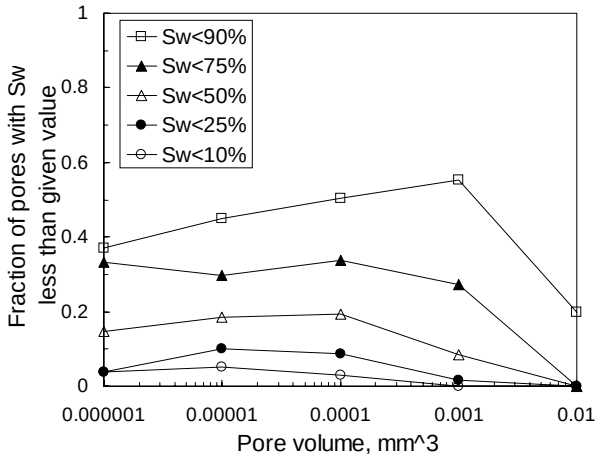

Fig. 15b—At S_{or} before gel.

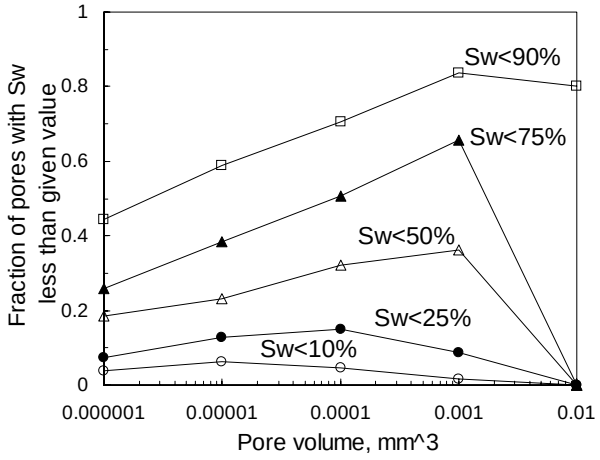

Fig. 15c—After gel placement.

Fig. 15—S_w levels in Berea.

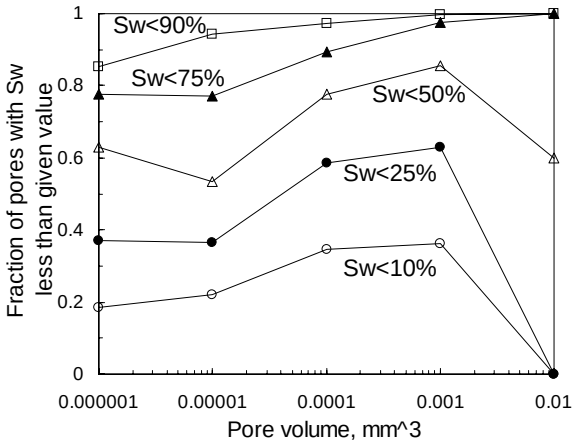

Fig. 15d—At S_{wr} after gel.

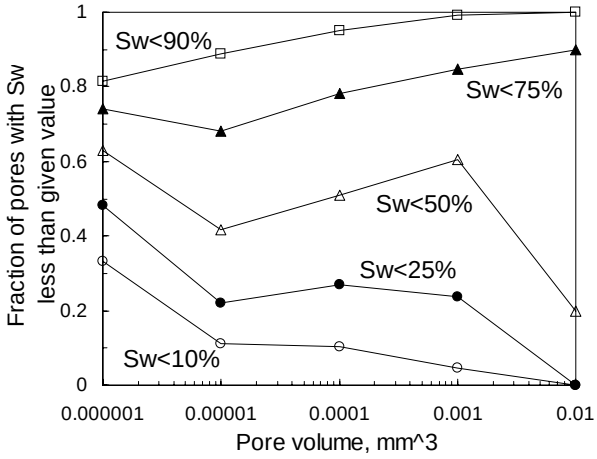

Fig. 15e—At S_{or} after gel.

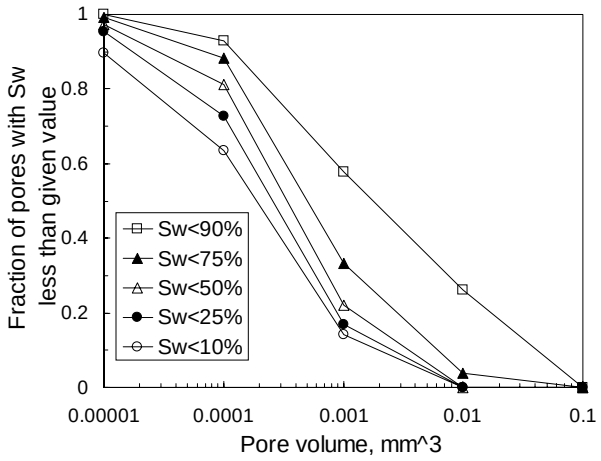

Fig. 16a—At S_{or1} before gel.

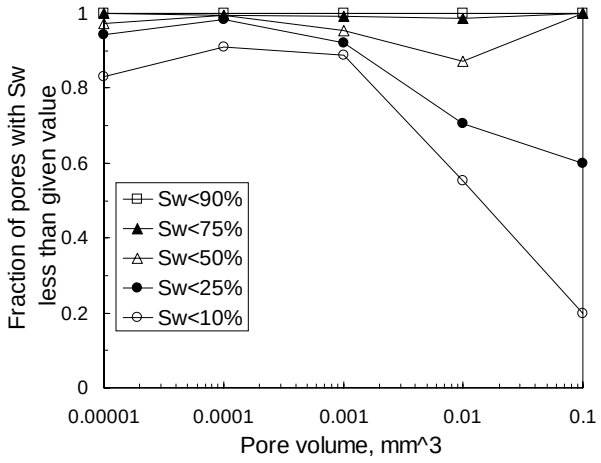

Fig. 16b—At S_{wr} before gel.

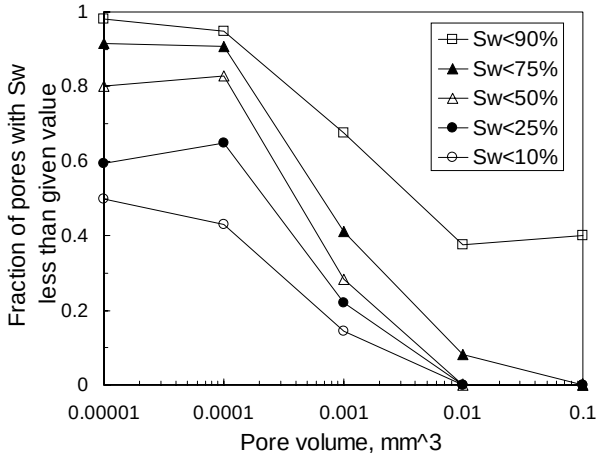

Fig. 16c—At S_{or2} before gel.

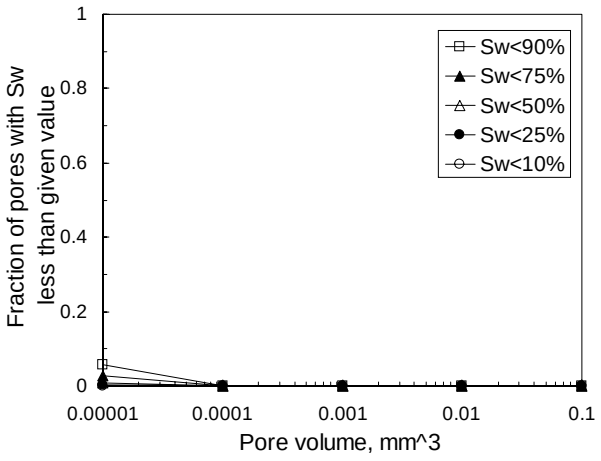

Fig. 16d—After gel placement.

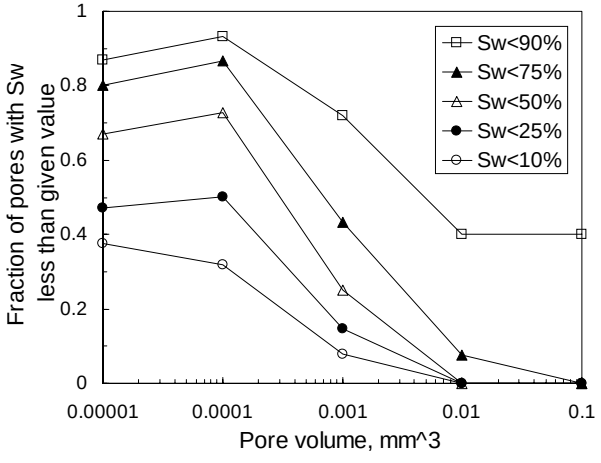

Fig. 16e—At S_{wr} after gel.

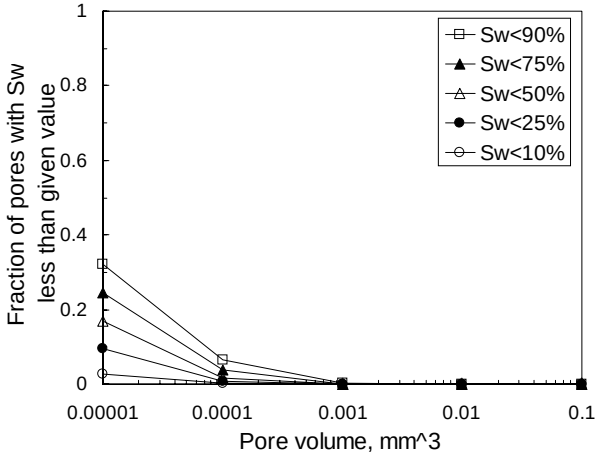

Fig. 16f—At S_{or} after gel.

Fig. 16—S_w levels in polyethylene.

Important Findings from the Combined Analysis

In Berea before Gel, Saturation Changes Were Insensitive to Pore Size. During the transition from S_{wr} to S_{or} in Berea (Fig. 11a and compare Figs. 8a and 8b), pores in all detected size ranges experienced significant gains in water saturation. Pore size did not appear to significantly influence the extent of the transition.

In Polyethylene before Gel, Oil Was Largely Immobile in the Smaller Pores. At S_{or1} in polyethylene, most small pores had nearly 100% oil saturation, while most large pores had nearly 100% water saturation (Fig. 9a). When oil was injected to drive the core to S_{wr} (Figs. 9b and 12a), water was displaced from most medium to large pores so that most pores ended with nearly 100% oil saturation. When water was re-injected to drive the core to S_{o2}, most large pores again filled almost completely with water while most small pores retained high oil saturations (Figs. 9c and 12b). Interestingly, a complementary behavior was not seen in Berea. We have no explanation for the differences.

20-cp Gelant Mobilized Oil in Both Porous Media. During gelant placement in Berea, the image volume surprisingly increased in oil saturation (from 18.4% to 36.3%). To rationalize this result, recall that the image volume was located in the center of the core and was small compared to the total pore volume of the core. Oil from upstream of the image volume probably was mobilized by flow of the 20-cp gelant, and that oil coincidentally lodged in the image volume. The overall oil saturation in the core did not increase during gelant placement. Within the image volume, medium to large pores (10^{-4} to 10^{-2} mm^3) were most likely to gain in oil saturation (Fig. 11b). Interestingly, the pressure gradient during gelant injection was always less than that during the previous brine or oil flows. This constraint was intentionally part of our experimental design to minimize oil mobilization. Since oil was mobilized, factors other than high pressure gradients were responsible for this mobilization.

During gelant placement in polyethylene, most oil that was trapped in small pores was displaced, so that all pores ended with high gelant saturations (Fig. 9d and 12c). As in Berea, the pressure gradient during gelant injection was always less than that during the previous brine or oil flows. Why was oil mobilized from the small pores during gelant injection but not during the previous water injection—especially since the pressure gradient (35 psi/ft) during water injection was higher than during gelant injection? Could polymer or Cr(III) adsorption have altered the wettability (oil-wet to water-wet) of the polyethylene? This suggestion seems unlikely considering the hydrophobic nature of the surface and the hydrophilic nature of the polymer and crosslinker. Wang[8] suggested that viscoelastic forces associated with flow of polymer solutions may re-distribute forces on a microscopic scale so that oil may be mobilized. This explanation may also help explain oil mobilization during our Berea experiments. More work is needed to determine if this explanation is applicable for our polyethylene and Berea experiments.

Oil Injection Reduced Gel Volume in Berea. Perhaps the most important conclusion from the first analysis was that oil injection effectively reduced gel volume in many Berea pathways that were utilized by oil before gel placement. This conclusion was confirmed by the second analysis. (The exact mechanism of destruction or reduction in volume is unknown at this point. It could occur by oil (a) ripping through the gel, (b) concentrating or dehydrating the gel, (c) mobilizing the gel, or (d) chemically destroying the gel.) When gelant was placed, it effectively displaced all

brine so that gel formed in all aqueous pore spaces. This observation was confirmed many times in previous work by noting that the Cr(III)-acetate-HPAM gel reduced Berea's permeability to water to levels associated with the permeability of the gel itself to water (i.e., water residual resistance factors of 10,000 or greater and final permeability in the microdarcy range).[5,6] When oil was injected after gel formation, the oil saturation increased (by 18.7 saturation percentage points from the first analysis and by 35 saturation percentage points from the second analysis—see Table 1). Fig. 11c shows that most (95.2% of the total) pores gained oil (lost water) when oil was injected after gel placement. The effect of oil on the gel did not appear sensitive to pore size, since the average water saturation (solid curve in Fig. 11c) decreased by about 35% regardless of pore size. Considering that the water saturation was 63.7% immediately before oil injection and 28.7% after oil injection, and assuming that gel occupied all of the aqueous pore space, the oil apparently destroyed (or reduced in volume) 55% of the gel. The pressure gradients during these experiments were limited so that they never exceeded those applied before the gel was placed. Therefore, it seems unlikely that the reduction in gel volume occurred because of exposure to excessive pressure gradients.

Fig. 17 provides additional insight into the process of reducing gel volume during oil injection. This plot shows the 300 pores (1/7 of total) that experienced the greatest increase in oil saturation during the process of oil injection after gel placement. Before gel placement, these pores were nearly full of oil at S_{wr} and were nearly full of water at S_{or}. Thus, oil and water both flowed freely into and filled these pores before gel placement. They were also easily accessible to oil after gel.

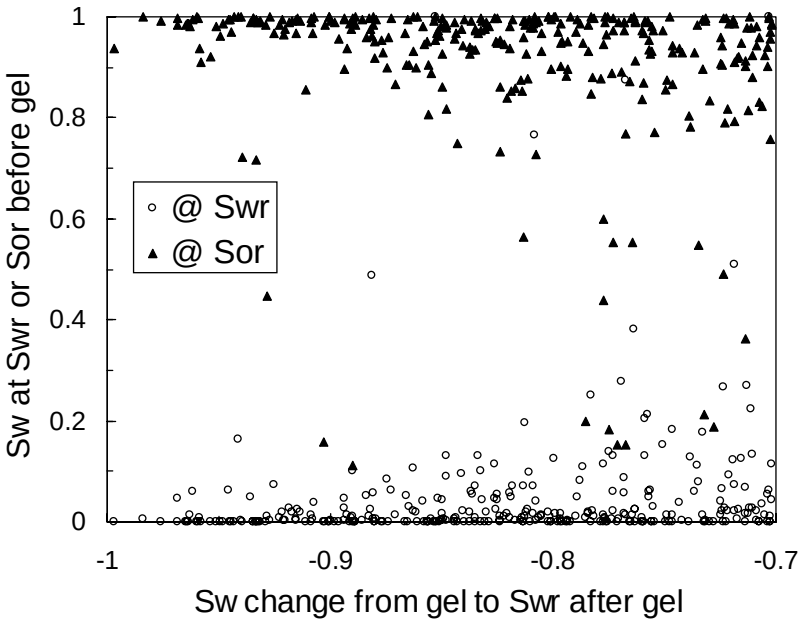

Fig. 17—Oil damaged gel most in pores that were easily filled by oil or water before gel.

In Polyethylene, Reduction of Gel Volume Occurred Mainly in Small Pores. As in Berea, gel appeared to form in all aqueous pore spaces (because permeability to water was in the μd range immediately after gel formation). When oil was injected after gel formation, oil saturation increased on average by 63 saturation percentage points for pores that were smaller than 10^{-4}

mm^3 but only by 11 saturation percentage points for pores that were larger than 10^{-3} mm^3 (see Fig. 12d). If gel occupied all aqueous pore space, oil injection apparently reduced the overall gel volume by only 16.3%. However, in pores smaller than 10^{-4} mm^3, gel volume was reduced by 63.5%, while only a 10.2% reduction occurred in pores that were larger than 10^{-3} mm^3. Recall in Berea that oil injection reduced gel volume on average by 55%, and this reduction was not sensitive to pore size. Thus, compared to Berea, reduction of gel volume during oil injection into gel-filled porous polyethylene was more likely in small pores but less likely in large pores. As with our Berea experiments, the pressure gradients were not allowed to exceed 35 psi/ft during any stage of the polyethylene experiments. So again, it seems unlikely that reduction of gel volume occurred because of exposure to excessive pressure gradients. If high-pressure gradients were responsible, gel damage should have been greater in larger pores than in smaller pores.

During Oil Flow in Berea, Many Paths Were the Same before and after Gel Placement. In the first analysis, the water saturation at S_{wr} before gel placement (24.7%) was fairly close to the water saturation at S_{wr} after gel placement (29.0%). Also, the distributions of water saturations versus pore size were very similar before and after gel placement. These observations suggested that many of the oil paths after gel placement were the same as those before gel placement.

In the second analysis, an increase in overall water saturation at S_{wr} was noted before versus after gel placement—16.0% versus 28.7%. The left side of Fig. 18 shows that many pores that had low S_{wr} values before gel placement experienced a significant increase in water saturation after gel. 86.1% of the pores had higher S_{wr} values after gel placement than before gel. Presumably, gel accounted for this increase. In the previous section, we estimated that oil injection reduced gel volume by 55%. Fig. 18 suggests that the remaining gel was widely distributed. Fig. 18 also shows that few pores had lower S_{wr} values after gel placement than before gel.

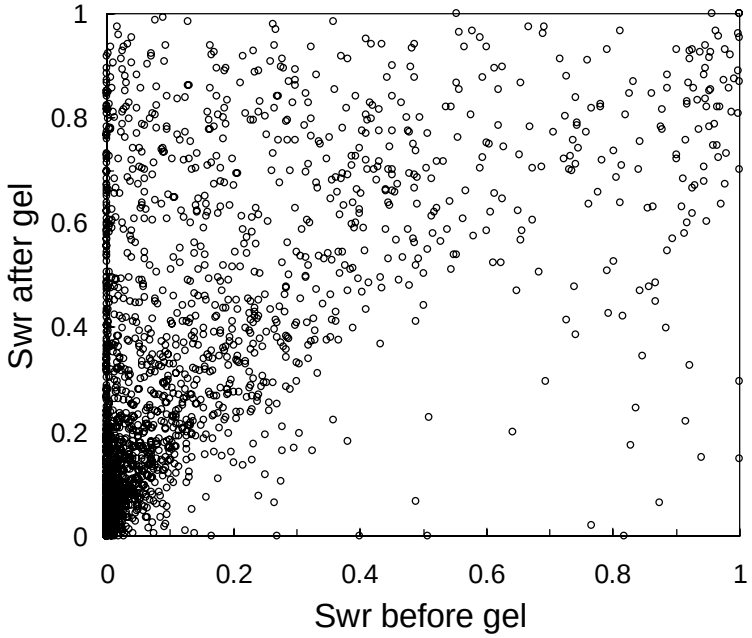

Fig. 18—Crossplot of S_{wr} before versus after gel placement in Berea.

On the other hand, the analysis confirmed that many pores had nearly the same water saturation before and after gel placement (see Fig. 11e and the cluster of data points in the bottom left of Fig. 18). In particular, 46% of the pores changed less than 10 saturation percentage points for the transition from S_{wr} before gel placement to S_{wr} after gel placement.

Water Flow after Oil Flow after Gel Placement in Berea. During oil injection after gel placement, the oil residual resistance factor (permeability reduction) was 15. During subsequent water injection, the water residual resistance factor was 1,220. Thus, the gel reduced permeability to water 81 times more than to oil. As mentioned earlier, much of the gel was destroyed or reduced in volume during oil injection after gel placement. Why was the final permeability to water so much lower than that to oil? Previous analysis[1-4] indicated that the gel trapped significantly more residual oil. The second analysis confirmed this conclusion, which indicated that S_{or} jumped from 18.4% before gel placement to 51% after gel placement. With many pores permanently occupied by oil, water was forced to flow through narrow films and through the gel itself—explaining the large water residual resistance factor (i.e., 1,220). In contrast, oil pathways remained relatively free from constriction by the gel, so the oil residual resistance factor was much less (i.e., 15).

During the transition from S_{wr} after gel placement to S_{or} after gel placement, the average increase in water saturation was 20.3%. Fig. 11e reveals that a wide range of saturation changes occurred for all pore sizes and that the average saturation change was not particularly sensitive to pore size. Interestingly, 22.6% of the pores gained oil even though water was injected (Table 2).

At S_{or} after gel placement, 93.3% of the pores had higher oil saturations than at S_{or} before gel placement. Fig. 11f reveals that a wide range of saturation changes occurred for all pore sizes and that the average saturation change was insensitive to pore size. Fig. 19 provides further information comparing oil saturations before versus after gel placement. It confirms that most pores had higher S_{or} values after gel than before gel.

In Polyethylene, S_{wr} after Gel Placement Looked Like S_{or} before Placement. A comparison of Figs. 9a, 9c, and 9e suggests that the saturation distributions at S_{wr} after gel placement in polyethylene were very similar to those at S_{or} before gel placement. Fig. 14 confirms this observation. Why should this similarity occur? Two factors contribute. First as mentioned earlier, injected oil entered and destroyed (or reduced the volume of) gel preferentially in the small pores where residual oil was located before gel placement. Second, subsequently injected water displaced most oil from the smaller pores. (Since the larger pores were permanently filled with gel, no displacement apparently occurred in the larger pores.) It is interesting that water could displace oil from the small pores after gel placement but not before gel placement. As mentioned earlier, the pressure gradients for the post-gel floods were less than those for the pre-gel floods. Therefore, at present, we have no explanation for this behavior.

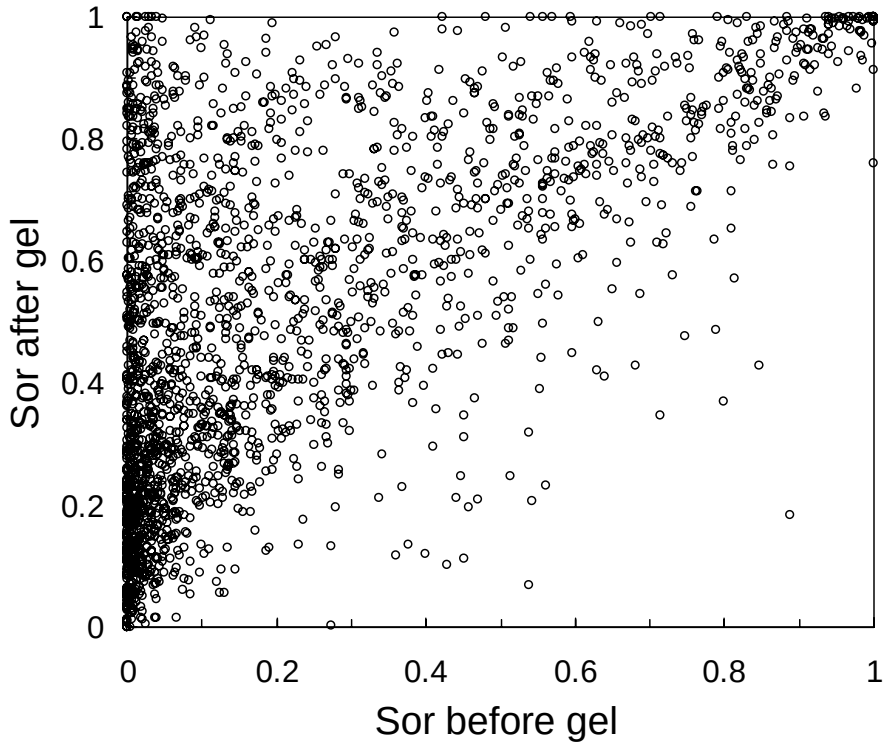

Fig. 19—Crossplot of S_{or} before versus after gel placement in Berea.

Connectivity of Phases

Before Gel Placement, the Injected Phase Was Highly Connected. Brent Lindquist at SUNY determined the connectivity of the fluid phases in porous media. Table 4 lists these values for the injected phases before gel placement (in both Berea and polyethylene). The table lists the percent of the total phase volume that was contained within the largest continuously connected volume. Not surprisingly, for all five cases listed, nearly 100% of the injected phase was continuous or contained by the largest phase volume. This observation held regardless of the fluid that wetted the porous medium.

Table 4—% of total phase volume that was connected for the injected phase (before gel).

Condition	% of total phase volume connected
Oil injected into Berea (S_{wr})	98.9
Water injected into Berea (S_{or})	97.9
1st water injected into polyethylene (1st S_{or})	99.9
Oil injected into polyethylene (S_{wr})	99.9
2nd water injected into polyethylene (2nd S_{or})	99.8

Fig. 20 plots the distribution of sizes for the small blobs that were not connected to the main body (or "blob") of the injected phase. The figure plots the percent of the total phase volume in separate blobs as a function of blob size. The *x*-axis plots blob sizes on a per decade basis. For

any size decade, the minor blobs accounted for considerably less than 1% of the total phase volume. Also, no obvious correlation existed between blob size and fractional phase volume in a given size range. It is possible that many or all of the small blobs represented in Fig. 20 were actually connected to the largest blob. We may not have detected very small connections—especially for thin films associated with the wetting phase.

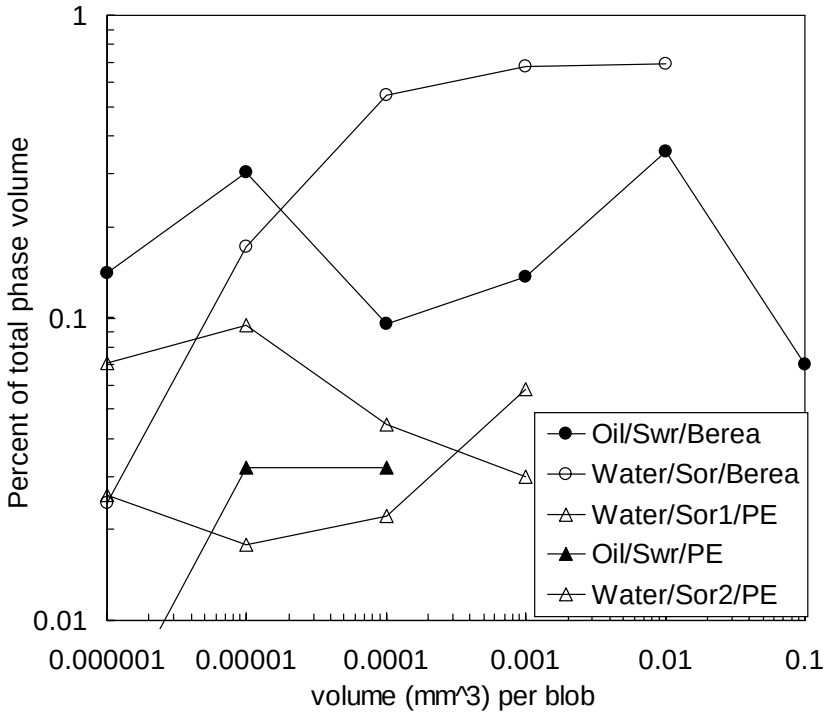

Fig. 20—Distribution of small blobs for the injected phase (before gel).

Before Gel Placement, the Residual Phase Was Widely Distributed. The previous discussion focused on the injected phase. Table 5 lists the percent of the total residual phase (before gel) that was contained within the largest blob. In Berea, the largest oil blob accounted for 1.76% of the total residual oil phase. Thus, the non-wetting phase was present in many small disconnected blobs. The solid circles in Fig. 21 show the distribution of blob sizes for residual oil in Berea.

Table 5—% of total phase volume that was connected for the residual phase (before gel).

Condition	% of total phase volume connected (largest blob)
Water in Berea at S_{wr}	5.04
Oil in Berea at S_{or}	1.76
Oil in polyethylene at 1st S_{or}	36.2
Water in polyethylene at S_{wr}	4.15
Oil in polyethylene at 2nd S_{or}	46.1

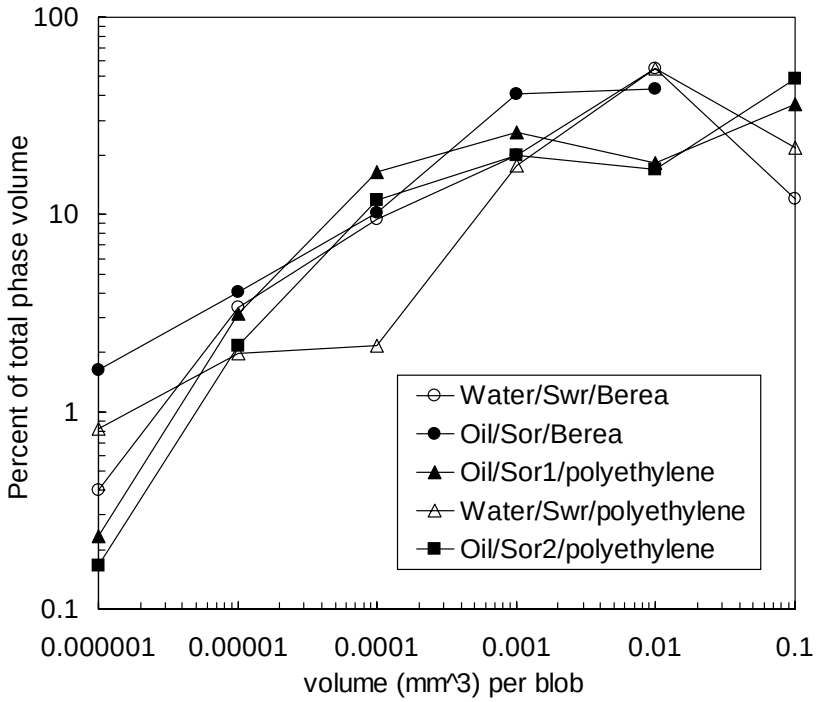

Fig. 21—Distribution of small blobs for the residual phase (before gel).

In polyethylene, the largest water blob accounted for 4.15% of the total residual water phase. The larger pore sizes in polyethylene might explain why this blob was larger than the largest residual oil blob in Berea. For the residual water blobs in polyethylene (open triangles in Fig. 21), the distribution was weighted to larger blob sizes compared to the distribution of oil blobs in Berea.

Most Residual Non-Wetting Blobs Were Probably "Singlets". In Berea, 50% of the residual non-wetting phase was contained in blobs larger than 0.000767 mm^3. In polyethylene, 50% of the residual non-wetting phase was contained in blobs larger than 0.00368 mm^3. For comparison, in Berea, 50% of the pore space was contained in pores larger than 0.000764 mm^3. In polyethylene, 50% of the pore space was contained in pores larger than 0.00263 mm^3. Fig. 22 compares the blob size distributions for the residual non-wetting phases with the pore size distributions in Berea and polyethylene. For both porous media, the blob size distribution roughly paralleled the pore size distribution. The distributions were normalized so the total oil volume at S_{or} in Berea was only 18.4% of the total pore volume, and the total water volume at S_{wr} in polyethylene was only 16.5% of the total pore volume. Thus, for any given size decade in Fig. 22, the actual phase volume was typically only one-fifth or one-sixth of the pore volume.

In Berea at S_{or}, 51% of the pores had oil saturations below 10% (Fig. 8b). Considering that Berea was strongly water wet, most blobs probably existed as "singlets"—i.e., most residual oil blobs were isolated within individual pores. "Multiplet" blobs were probably less common—i.e., few non-wetting residual blobs resided in more than one pore. This conclusion is consistent with that reported by Chatzis *et al.*[7] A similar conclusion was reached for polyethylene at S_{wr}, where 87% of the pores had water saturations below 10% (Fig. 9b).

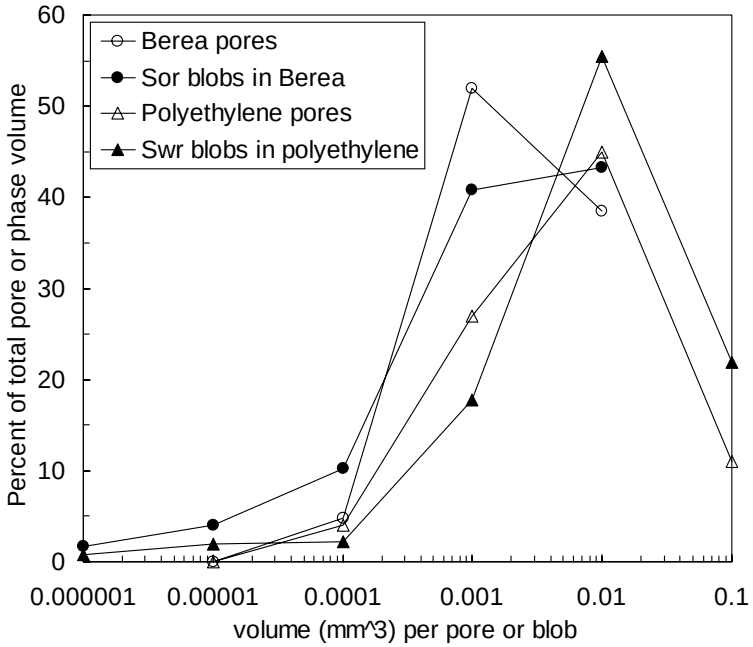

Fig. 22—Blob versus pore size distribution for the residual phase (before gel).

Were Residual Wetting Blobs Connected by Thin Films? For a strongly wetted porous medium, the residual wetting phase was expected to be nearly all connected. In other words, we expected a single water blob to exist at S_{wr} in strongly water-wet Berea or a single oil blob to exist in strongly oil-wet polyethylene at S_{or}. In polyethylene, Table 5 indicates that the largest oil blob contained 36.2% of the total oil volume at S_{or1} and 46.1% of the total oil volume at S_{or2}. Fig. 23 shows the relative sizes for other oil blobs, as a function of blob size decade. Since the oil films were extremely thin (nanometer thicknesses) and our voxel size was 4.1 μm, we probably did not detect many of the connections between the residual oil blobs. The same logic likely applies to residual water blobs in Berea. The largest detected water blob accounted for 5.04% of the residual water in Berea at S_{wr}. Fig. 23 shows the relative sizes for other water blobs, as a function of blob size decade. Presumably, thin undetected water films connect most of the residual water blobs in Berea. However, we cannot prove this.

After Gel, the Injected Phase Appeared Highly Connected. The largest detected blobs for the injected phases after gel placement are listed in Table 6. In all cases, the largest blob contained a substantial portion of the total phase volume. In Berea at S_{wr} after gel, the oil saturation was 71.3%, and 96.1% of the injected oil was connected. This value emphasizes the widespread reduction of gel volume by oil throughout the image volume. Assuming that gel occupied all of the aqueous pore space when placed (63.7% from Table 1), oil injection destroyed 55% of the gel (35 saturation point increase in oil saturation). Fig. 11e suggests some resistance to gel destruction in the small- to moderate-sized pores (because many of these pores had post-gel water saturations that were greater than before gel). However, the figure also shows that for all size ranges, many pores had nearly the same saturations after gel as before gel. Since gel presumably formed in the aqueous pore space in most (if not all) pores (Fig. 8c), oil injection caused widespread reduction in gel volume in most pores in order to reach S_{wr} after gel (Fig. 8d).

The solid circles in Fig. 23 show the distribution of other (smaller) oil blobs in Berea at S_{wr} after gel. For all size decades, the blobs (i.e., oil blobs in Berea) contributed less than 1% of the total phase volume. Some of these oil blobs could have been encapsulated by gel.

Table 6—% of total phase volume that was connected for the injected phase (after gel).

Condition	% of total phase volume connected
Oil injected into Berea (S_{wr})	96.1
Water injected into Berea (S_{or})	80.5
Oil injected into polyethylene (S_{wr})	45.5
Water injected into polyethylene (S_{or})	99.98

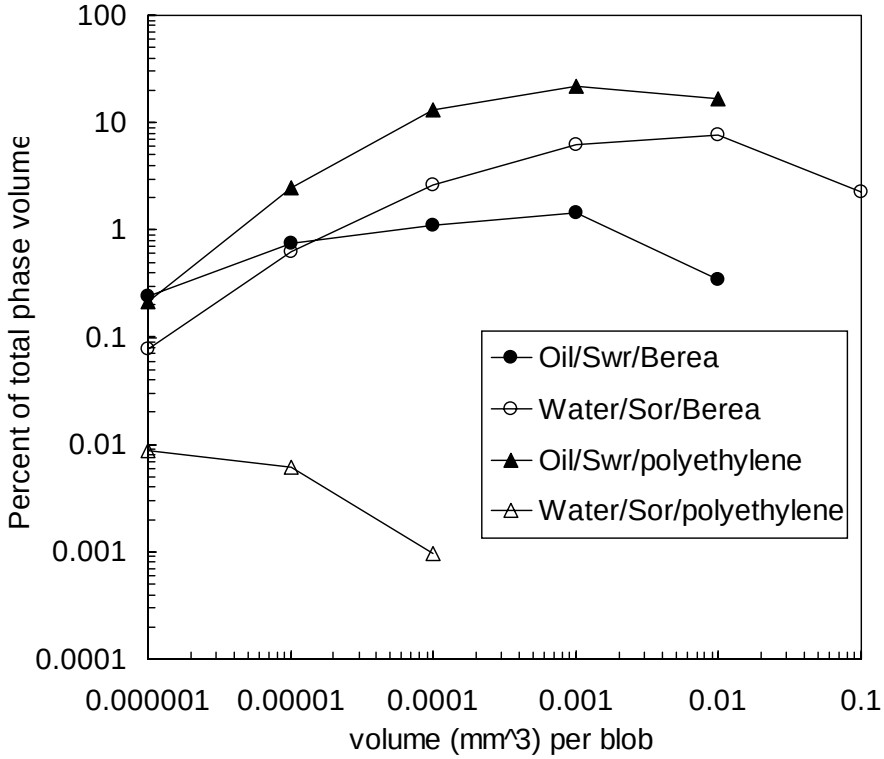

Fig. 23—Distribution of small blobs for the injected phase (after gel).

During water injection after gel placement in Berea, the final water saturation was 49.0%, and 80.5% of the aqueous phase was connected within the largest blob. Although significant water volume was contained in blobs within the smaller size decades (open circles in Fig. 23), we cannot discount the possibility that these blobs may be connected through thin undetected water films that follow pore walls. Also, our use of XMT cannot distinguish between free water and gel. Since the water saturation at S_{wr} was 28.7% after gel placement, the final gel saturation may have been as high as 28.7%. Assuming that the gel did not swell during final water injection, the free water saturation at S_{or} after gel was at least 20.3% (i.e., 49.0%-28.7%).

During oil injection after gel placement in polyethylene, the final oil saturation was 16.5%, and 45.5% of the hexadecane oil was contained by the largest blob. Fig. 23 indicates that the oil volume in blobs within the smaller size decades (solid triangles) was noticeably more than that for water at S_{or} in Berea after gel. Nevertheless, we suspect that most of these blobs were connected by thin undetected oil films.

During water injection after gel placement in polyethylene, the final water saturation was 99.7%, and 99.98% of that water was connected. Since S_{wr} during the prior oil injection was 83.5%, the final gel saturation may have been as much as 83.5% and the free water saturation may have been 16.2% (i.e., 99.7%-83.5%).

After Gel, the Residual Phases Were Highly Connected. The most interesting observation during water injection after gel placement in Berea was that the residual oil was highly connected. In particular, S_{or} after gel placement was 51.0%, and 77.6% of that oil was contained within the largest oil blob (Table 7). This blob was 122 times larger than the largest oil blob at S_{or} before gel placement (i.e., 77.6/1.76x51.0/18.4). This high degree of connection helps explain the relatively high permeability to oil after gel placement. The solid circles in Fig. 24 show the relative volume contributions for the smaller residual oil blobs as a function of blob size decade.

Table 7—% of total phase volume that was connected for the residual phase (after gel).

Condition	% of total phase volume connected (largest blob)
Water in Berea at S_{wr}	25.7
Oil in Berea at S_{or}	77.6
Water in polyethylene at S_{wr}	99.8
Oil in polyethylene at S_{or}	32.3

For water at S_{wr} in Berea after gel placement, the water saturation was 28.7%, and 25.7% of this water was included in the largest residual water blob. As discussed previously, since water was the wetting phase, we suspect that most (if not all) of the aqueous phase was actually connected, but that our XMT technique was simply not able to detect the thin film connections along the pore walls. Even so, it is interesting that the connected volume (25.7% of the total 28.7% S_{wr}) was substantially larger than the connected volume noted at S_{wr} before gel placement (5.04% of the total 16.0% S_{wr}). Perhaps with the higher S_{wr} after gel placement, the connecting water film was thicker and easier to detect than before gel placement.

For oil at S_{or} in polyethylene after gel placement, the oil saturation was only 0.3%, and 32.3% of this oil was included in the largest residual oil blob. Since oil was the wetting phase, we suspect that most (if not all) of the oil phase was actually connected, but that our XMT technique was simply not able to detect the thin film connections along the pore walls. In view of the low oil saturation and the difficulty in seeing the connecting water films in Berea, it is somewhat surprising that we could detect a relatively large residual oil blob in polyethylene.

For water at S_{wr} in polyethylene after gel placement, the water saturation was 83.5%, and 99.8% of this water was connected. We suspect that this was probably one large gel blob.

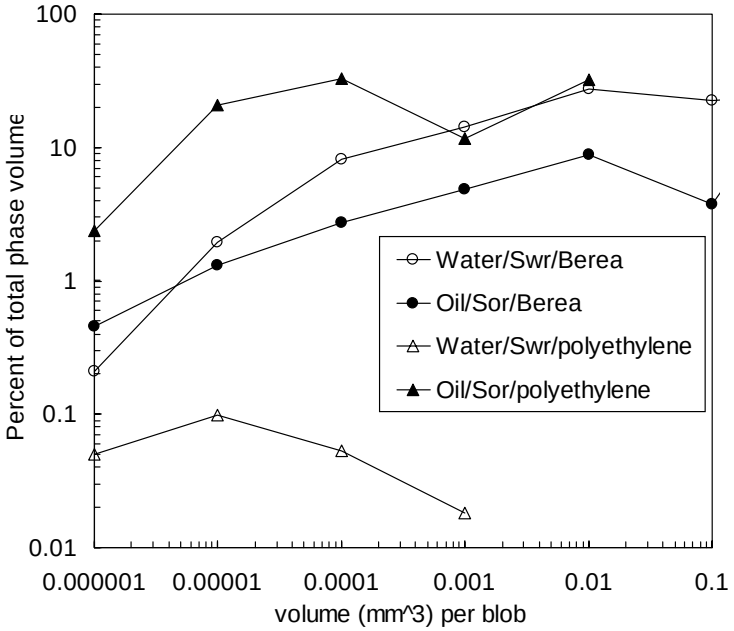

Fig. 24—Distribution of small blobs for the residual phase (after gel).

Connectivity Changes from Gelant Injection. As mentioned earlier, injection of the 20-cp gelant mobilized oil—decreasing the oil saturation for polyethylene and actually increasing the oil saturation for the image volume for Berea. The changes in connectivity qualitatively followed the trends expected from the saturation changes (Table 8). In Berea, gelant injection caused oil saturation in the image volume to increase from 18.4% to 36.3% (Table 1), the largest oil blob grew from 1.76% (Table 5) to 11.8% (Table 8) of the total oil phase volume, and the largest water blob shrank from 97.9% (Table 4) to 95.0% (Table 8) of the total water phase volume. In polyethylene, gelant injection decreased oil saturation from 17% to 0.2% (Table 1), the largest oil blob shrank from 46.1% (Table 5) to 4.23% (Table 8), and the largest water blob grew from 99.8% (Table 4) to 99.985% (Table 8).

Table 8—% of total phase volume that was connected after gelant injection.

Condition	% of total phase volume connected (largest blob)
Water in Berea	95.0
Oil in Berea	11.8
Water in polyethylene	99.985
Oil in polyethylene	4.23

The correlation between oil saturation and blob connectivity continued to hold during oil injection after gel formation. In Berea, oil injection after gel placement caused oil saturation in the image volume to increase from 36.3% to 71.3% (Table 1), the largest oil blob grew from 11.8% to 96.1% (Table 9) of the total oil phase volume, and the largest water blob shrank from 95.0% to 25.7% (Table 9) of the total water phase volume. In polyethylene, oil injection after gel placement increased oil saturation from 0.2% to 16.5% (Table 1), the largest oil blob grew from 4.23% to 45.5% (Table 9), and the largest water blob contracted slightly from 99.985% to 99.78% (Table 9). Close examination of Table 9 (in conjunction with Table 1) reveals that the largest oil blob always grew when the oil saturation increased and shrank when the oil saturation decreased. Similarly, the largest water blob always grew when the water saturation increased and shrank when the water saturation decreased.

Table 9—Summary of connectivity values for the largest blob.

	Berea, oil, %	Berea, water, %	PE, oil, %	PE, water, %
S_{or}			36.2	99.88
S_{wr}	98.9	5.04	99.93	4.15
S_{or}	1.76	97.9	46.1	99.76
gel	11.8	95.0	4.23	99.985
S_{wr} after gel	96.1	25.7	45.5	99.78
S_{or} after gel	77.6	80.5	32.3	99.98

Implications for the Mechanism of Disproportionate Permeability Reduction

A key finding from our XMT studies was that oil injection reduced the pore volume that was occupied by gel. This reduction created pathways for oil flow, thus restoring an important level of permeability to oil. How did this reduction in gel volume occur? At least two mechanisms are under active consideration. In one mechanism, oil ripped pathways through the gel.[1,2,9] In the second mechanism,[10,11] gel dehydrated (i.e., lost water and became more concentrated through compression.)

Our recent analysis supports the dehydration mechanism over the ripping mechanism. In particular, the apparent reduction in gel saturation during oil injection was insensitive to pore size in Berea (Fig. 11c) and was greatest in small pores in porous polyethylene (Fig. 12d). If ripping was the dominant mechanism, losses in gel volume should have been greatest in the largest pores. To explain, if gel failure (i.e., ripping) occurred at a gel-rock interface or within the gel, a force balance suggests that the pressure gradient for gel failure should be inversely proportional to the pore radius.[12,13] Thus, for a given applied pressure gradient, gel failure should occur dominantly in larger pores. Since this did not occur, our results argue against the ripping mechanism.

In contrast, the observed XMT results could be consistent with the dehydration mechanism. With a fixed pressure gradient applied through the porous medium, gel in all pores could be "squeezed" or dehydrated to the same extent, regardless of pore size. More work is needed to investigate this possibility.

Remaining Issues
A number of issues and questions were raised during this work. Among them are the following.

First, why were S_{wr} values not greater (i.e., near 100%) in Berea's small pores? Since S_{or} values were ~80% in strongly oil-wet porous polyethylene before gel, S_{wr} values in strongly water-wet Berea were expected to be at least as great. The pore and throat sizes in polyethylene were no smaller than those in Berea.

Second, why was oil mobilized during gelant injection even though the pressure gradients were less than those before gel placement?

Third, why did oil injection reduce gel volume by 55% in Berea and 16% in polyethylene even though the pressure gradients were less than those before gel placement?

Fourth, why was reduction of gel volume (during oil injection) insensitive to pore size in Berea?

Fifth, why was the residual oil phase in Berea after gel so highly connected? What pores participated in the largest residual oil blob? How did the blob throat, blob body, and blob aspect ratios compare with the participating pore throat, body, and aspect ratios?

Additional work is needed to answer these questions. Of course, our ultimate goal in these studies is to identify ways to maximize disproportionate permeability reduction in a predictable and controllable manner.

Conclusions
In previous work, we used X-ray computed microtomography to determine why gels reduce permeability to water more than that to oil in strongly water-wet Berea sandstone and strongly oil-wet porous polyethylene cores. At a recent Gordon Conference, attendees questioned a few of our findings. Therefore, to double check our results, our X-ray images were re-analyzed using a different method for segmenting the fluids (i.e., differentiating between water and oil). The following conclusions were reached.

Comparison of the first and second analyses:

1. The second analysis revealed larger pores in polyethylene (because a larger population was sampled). This finding validated one of our critics, who pointed out that Berea and polyethylene should have different pore size distributions.
2. The second analysis showed lower S_{wr} and S_{or} in Berea, which was more consistent with floods in larger cores.
3. The second analysis showed many more pores at high and low saturations in Berea than the first analysis.
4. In the transition from S_{wr} to S_{or}, many Berea pores gained oil in the first analysis but not in the second.
5. Both analyses confirmed that S_{wr} averaged about 60% in the smallest detected Berea pores and that a wide range of saturations could be found for any pore size. This average

saturation surprised a second critic of our work and also seemed unexpected in view of the next conclusion. No satisfactory explanation is apparent yet.

6. The average S_{or} was 80% in the smallest detected polyethylene pores (which were the same size as the smallest detected pores in Berea). The behavior in polyethylene followed conventional expectations for a strongly oil-wet porous medium.
7. Other qualitative trends were the same for both analyses.

Important findings from the combined analysis:

1. During the transition from S_{wr} to S_{or} in Berea before gel placement, pores in all detected size ranges experienced significant gains in water saturation. Pore size did not significantly influence the extent of the transition.
2. In contrast, in polyethylene before gel placement, oil was largely immobile in smaller pores.
3. Injection of our 20-cp gelant mobilized oil in both porous media even though the pressure gradients during gelant placement were less than those during previous oil or water floods.
4. Immediately after gel placement, an extremely high resistance (F_{rrw}>10,000) to water flow occurs (in either Berea or polyethylene), presumably because impermeable gel occupies nearly all of the aqueous pore space.
5. During oil flow after gel placement in Berea, much of the gel was destroyed or experienced a reduction in volume, thus leading to a relatively high permeability to oil (F_{rro}=15). A 55% reduction (on average) in gel volume occurred in pores of all detected size ranges. Gel volume was most likely to be reduced in pores that experienced the greatest saturation changes during floods before gel placement. After gel placement, 86.1% of the pores had higher S_{wr} values than before gel. Presumably, gel accounted for this increase. The gel that remained was widely distributed.
6. At S_{or} after gel placement in Berea, 93.3% of the pores had higher oil saturations than at S_{or} before gel placement. The overall S_{or} in Berea jumped from 18.4% before gel placement to 51% after. The greater level of trapped oil greatly restricted water flow (F_{rrw}=1,220). A wide range of saturation changes occurred for all pore sizes, and the average saturation change was insensitive to pore size.
7. In polyethylene, reduction in gel volume occurred mainly in small pores. Overall, oil injection apparently reduced gel volume by only 16.3%. However, in pores smaller than 10^{-4} mm^3, gel volume was reduced by 63.5%. A reduction of only 10.2% occurred in pores that were larger than 10^{-3} mm^3.
8. The above observations suggest that gel destruction or reduction in gel volume was probably caused by a dehydration mechanism rather than a gel-ripping mechanism.
9. In contrast to Berea, the overall S_{or} was significantly lower after gel placement than before gel placement (0.3% versus 17.0%). Thus, oil trapping could not explain the large disproportionate permeability reduction seen in porous polyethylene (F_{rrw}/F_{rro}=2,130/24=89).

Conclusions from a study of phase connectivity:

1. Before gel placement, at least 97.9% of the injected phase (oil or water) was contained within a single blob.
2. Before gel placement, the residual phase was widely distributed. In Berea, the largest oil blob accounted for 1.76% of the total residual oil phase. In polyethylene, the largest water blob accounted for 4.15% of the total residual water phase.

3. The analysis suggests that before gel placement, most residual non-wetting blobs were probably “singlets”—i.e., isolated within individual pores.
4. We suspect that most of the residual wetting phase was contained within a single blob. However, we could not prove this because our resolution was not sufficient to detect thin film connections smaller than 4.1 μm.
5. Changes in blob connectivity qualitatively followed the trends expected from the saturation changes. The largest oil blob always grew when the oil saturation increased and shrank when the oil saturation decreased. Similarly, the largest water blob always grew when the water saturation increased and shrank when the water saturation decreased.
6. In Berea at S_{or} after gel placement, 77.6% of the residual oil was contained within the largest blob. This blob was 122 times larger than the largest oil blob at S_{or} before gel placement (i.e., 77.6/1.76x51.0/18.4).

3. DISPROPORTIONATE PERMEABILITY REDUCTION IN FUSED SILICA

The ability of polymers and gels to reduce permeability to water more than that to hydrocarbon has tremendous potential for water shutoff applications. However, a critical issue with these materials is performance variability. Before disproportionate permeability reduction can be successfully exploited in widespread field applications, its behavior must be predictable and controllable.

Two main approaches have been taken toward creating disproportionate permeability reduction. One approach uses pore-filling gels, while the other uses polymers that adsorb onto pore walls. Pore-filling gels can show fairly reproducible permeability reductions (especially to water). However, a perceived disadvantage for the pore-filling gels is that they provide large permeability reductions (e.g., 30 to 300) to oil. These high values are unacceptable for unfractured (radial flow) production wells because oil productivity will be impaired too much. For radial-flow applications, the permeability reduction to oil should not exceed two. Adsorption-based polymers are more likely to provide low oil residual resistance factors. Unfortunately, the reproducibility of the behavior for these polymers is notoriously poor. The performance of the AquaCon™ polymer (a BJ product) illustrates this point.[1] During replicate experiments, solutions with 0.18% polymer in Berea sandstone exhibited oil residual resistance factors ranging from 2.6 to 46, while water residual resistance factors varied from 1.7 to 317. The three most obvious potential causes of this variability were differences in (1) the polymer, (2) the core material, and (3) the experimental technique. After extensive considerations described in Ref. 1, we suspect that the performance variations were caused by subtle mineralogical or other differences from one Berea core to the next—even though the cores were all taken from the same block of rock and had nearly the same permeability and porosity values. This possibility is disturbing because mineralogical variations within porous rock are unavoidable. If adsorption levels and consequent permeability reductions vary significantly, it may be impossible to predict or control disproportionate permeability reduction for adsorption-based polymers in field applications.

We are in the early stages of investigating this possibility. Our first experiments used a synthetic silica porous media from HP Technical Ceramics (Sheffield, UK). The pore structure of this material is comparable to that of Berea sandstone (see Figs. 25-28), but it contains no clays or carbonate minerals. Our hope was that this material would have a uniform morphology and distribution of adsorption sites and therefore provide reproducible disproportionate permeability reduction for adsorption-based polymers. The permeability and porosity of the silica porous media were about 3 darcys and 38%, respectively. When flooded with brine (0.95 cp) and oil (15% 1-bromohexadecane in hexadecane, 3.6 cp) at room temperature, the endpoint S_{wr}, S_{or}, k_{rw}, and k_{ro} values were reproducibly 25%, 17%, 0.82, and 0.61, respectively.

The objective of our first experiments was to establish baseline behavior in the silica porous media for a pore-filling gel [Cr(III)-acetate-HPAM] and an adsorption-based polymer (AquaCon). Four experiments were performed using four separate cores (3.75-cm diameter and 14-cm long). In two cores, 8-8.5 pore volumes of Cr(III)-acetate-HPAM gelant [0.5% Alcoflood 935 HPAM, 0.0417% Cr(III) acetate] were injected at a flux of ~75 ft/d. The 40-cp gelant exhibited resistance factors of 91 and 96 in the two cores. In the other two cores, 9 pore volumes of 0.18% AquaCon were injected at 35.6 ft/d. This 2.5-cp polymer solution showed resistance factors between 2.4 and 2.6 in both cores. After gel or polymer placement, oil was injected first in Cores 389 and 390, while

water was injected first in Cores 388 and 391. Table 10 lists oil (F_{rro}) and water (F_{rrw}) residual resistance factors obtained after gel or polymer placement.

Table 10—Residual resistance factors in silica cores.

	Cr(III)-acetate-HPAM gel		AquaCon polymer	
	Core 388	Core 389	Core 390	Core 391
F_{rrw}	217,000			1.2
F_{rro}	200	288	1.2	1.2
F_{rrw}	333,000	373,000	3.1	2.6
F_{rro}		131	1.2	

For the cores with Cr(III)-acetate-HPAM, the oil residual resistance factors ranged from 131 to 288. The behavior of the F_{rro} values was consistent with earlier findings.[14] In particular, the highest F_{rro} values were observed when oil was injected first after gel placement (e.g., the 1st F_{rro} =288 for Core 389), and F_{rro} values decreased through multiple cycles of oil and water injection (e.g., the 2nd F_{rro} =131 for Core 389). In Ref. 14, this behavior was interpreted to mean that gel experienced additional damage as it was subjected to cycles of oil and water flow.

Water residual resistance factors ranged from 217,000 to 373,000, so the final permeability to brine ranged from 5.2 to 9.4 μd. High residual resistance factors were expected when water was injected first after gel placement (Core 388). For this case, injected water must flow through the gel itself, which has a very low permeability. However, when oil was injected, previous work[2] revealed that pathways were created through the gel, and much of the gel was destroyed or dehydrated. When water injection followed oil flow, the remaining gel trapped substantial residual oil saturation, thus causing F_{rrw} values that were significantly higher than the F_{rro} values.[2] However, because oil flow damaged the gel, we expected F_{rrw} values measured after oil flow should be significantly lower than F_{rrw} values during first brine flow after gel placement. Since the results were not consistent with our expectations, we need to re-think why the final F_{rrw} values were so high.

The F_{rro} values were at least 1,000 times less than the F_{rrw} values. This behavior can be very useful when treating excess water production from fractured wells.[14-16]

For the two cores treated with AquaCon (Cores 390 and 391 in Table 10), the F_{rro} values were consistently 1.2. The F_{rrw} values were also very low, ranging from 1.2 to 3.1. These values suggest that very little polymer adsorption occurred. We are considering whether to make another silica porous media with a small, controlled amount of adsorbing material (e.g., clay) to increase the level of polymer adsorption.

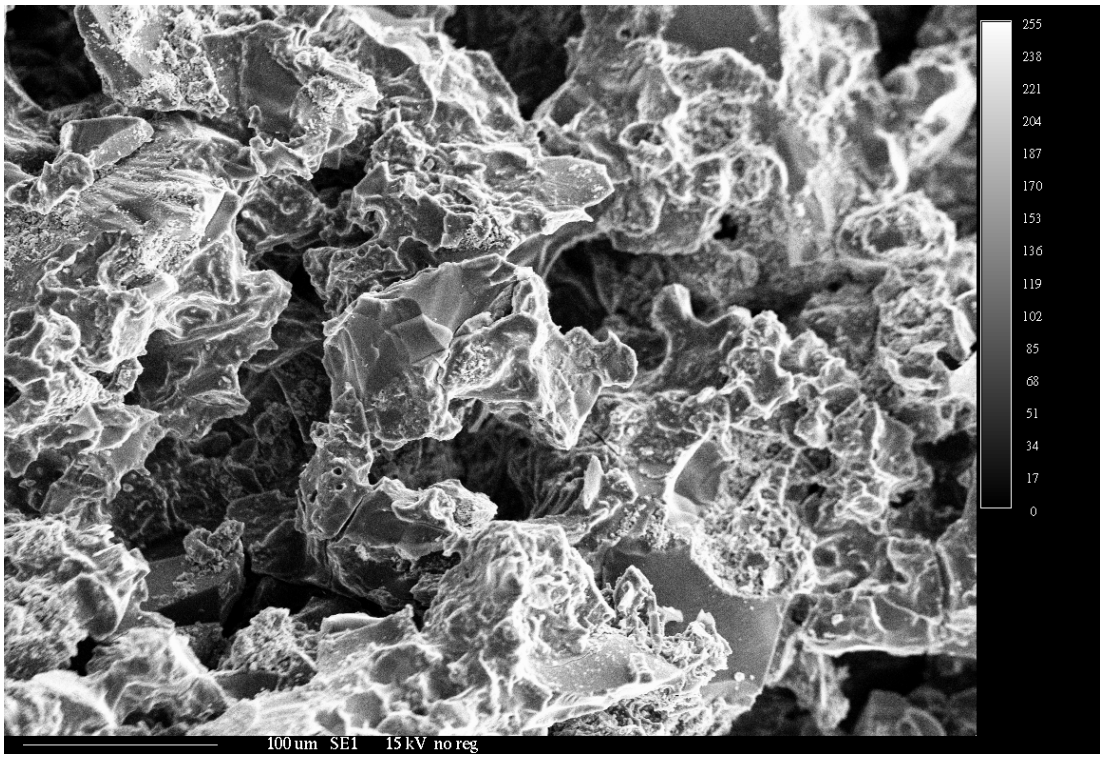

Fig. 25—Scanning electron micrograph (SEM) of silica porous media. 500 μm x 367 μm.

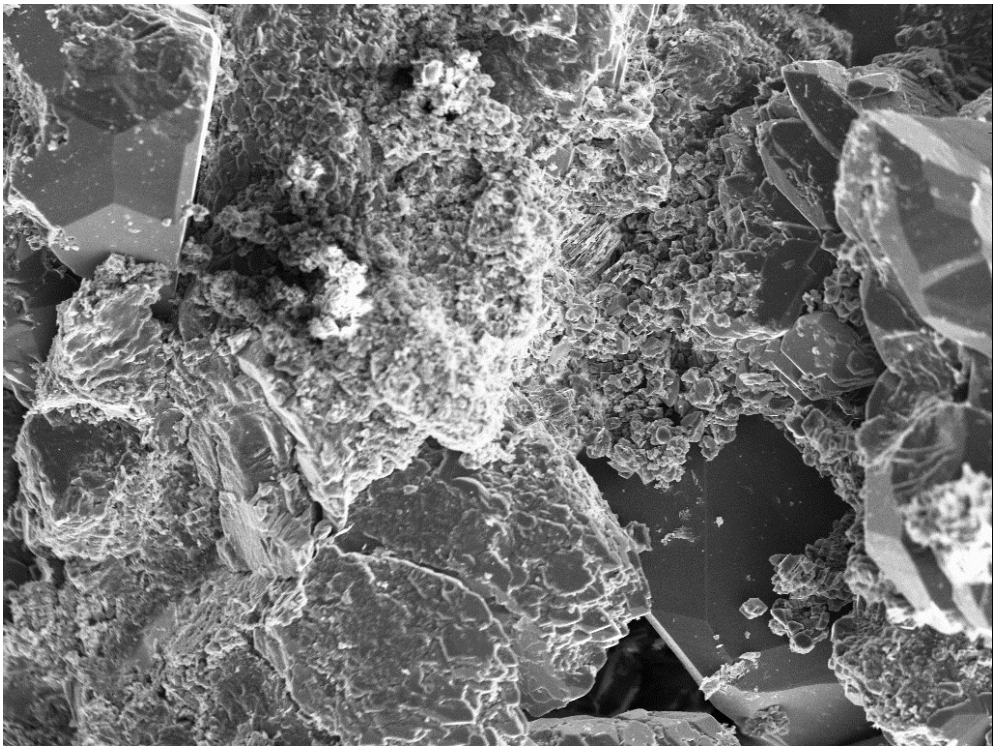
Fig. 26—SEM of Berea. 500 μm x 367 μm.

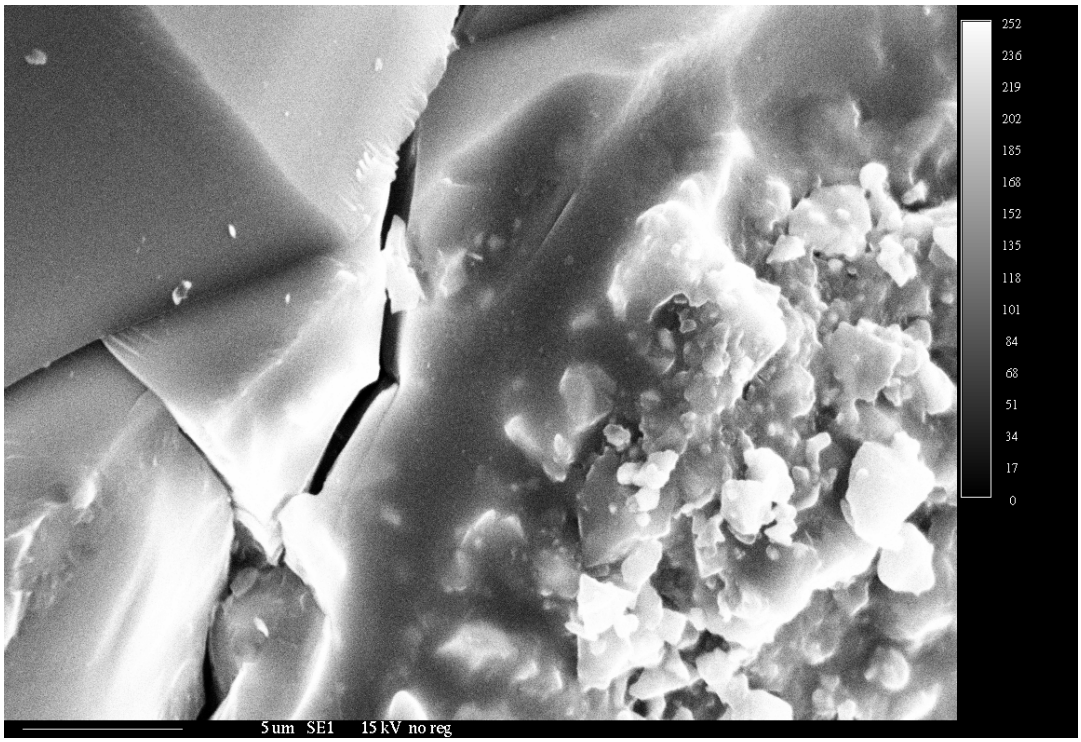

Fig. 27—SEM of silica porous media. 30 μm x 22 μm.

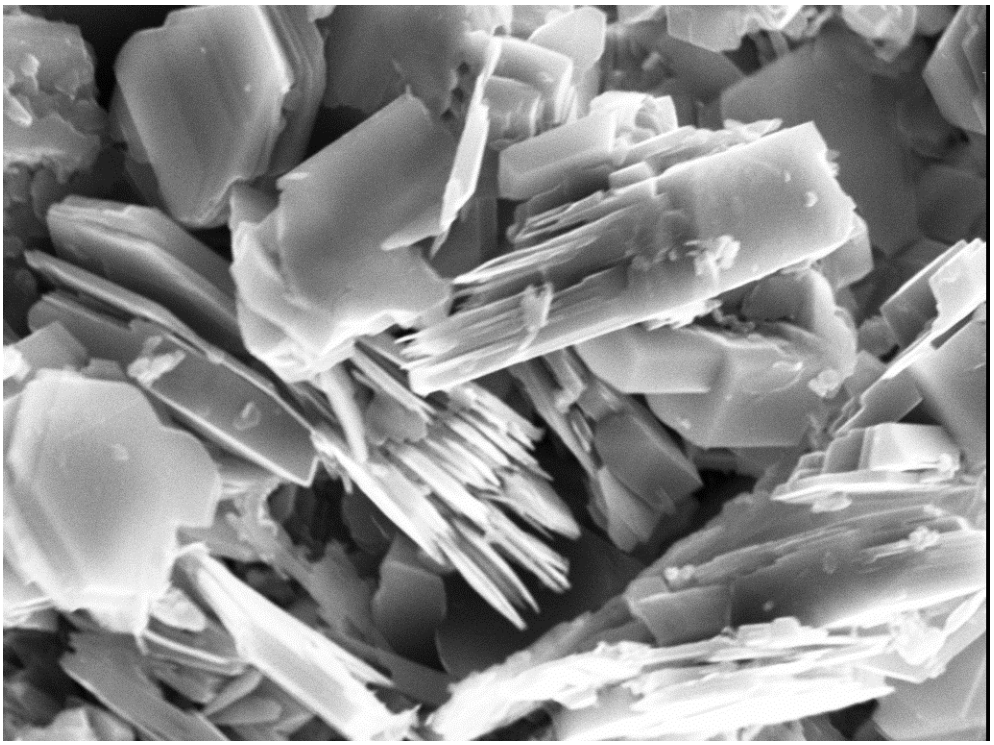
Fig. 28—SEM of Berea. 30 μm x 22 μm.

4. GEL TREATMENT IN AN ARBUCKLE PRODUCTION WELL

For many years, polymer and gel treatments have dramatically reduced the producing water/oil ratio, decreased water production, and increased oil production in naturally fractured production wells in the Arbuckle formation of western Kansas.[17] In most cases, the effects of these treatments were temporary (typically around one year). The main response occurred immediately after the gel treatment, followed by an exponential decay to pre-treatment production levels. In spite of the success of these treatments, much is unknown about them, including why they work, what is the best blocking agent to use (e.g., polymer versus gel), how much blocking agent should be injected, what is the optimum placement method, and what is the exact nature of the water channels.

Linear versus Radial Flow?

Gel-Tec and Vess Oil Company were kind enough to provide detailed information about a gel treatment in the Jennie Johansen #8 production well in the Arbuckle formation. The treatment was applied December 19-21, 2002. The well was completed at depths between 3367 and 3374 ft in the Arbuckle dolomite, which had an estimated permeability of 5 md. Immediately, before the gel treatment, the well produced 720 BWPD and 8 BOPD with a fluid level 1530 ft from the surface. Assuming fluid density of 1 g/cm^3, the flowing down hole pressure was 797 psi [i.e., (3370-1530)x62.4/144]. The static bottom hole pressure was 928 psi (measured with a downhole gauge), so the pressure drop from the formation to the wellbore was 131 psi.

To confirm that flow into the wellbore was not radial flow through matrix, we applied the Darcy equation for radial flow.

$$q/\Delta p = kh/[141.2\ \mu\ \ln(r_e/r_w)] \quad (1)$$

Assuming that μ was 0.67 cp and $\ln(r_e/r_w)$=6, the right side of Eq. 1 yields a value of 0.0617 BPD/psi [i.e., 5x(3374-3367)/(141.2x0.67x6)]. In contrast, the actual fluid productivity ($q/\Delta p$) was 5.56 BPD/psi (i.e., 728/131). Since 0.0617 BPD/psi was much less (90 times less) than 5.56 BPD/psi, most flow did not come to the well via matrix radial flow.

Estimated Fracture Width

If we assume that production was dominated by a single two-wing fracture, the fracture conductivity can be estimated from Eq. 2, while the effective average fracture width can be estimated using Eq. 3.

$$k_f w_f = (q/\Delta p)\ \mu\ (L_f/h_f)/2 \quad (2)$$

$$w_f = 0.0479\ (k_f w_f)^{1/3} \quad (3)$$

where $k_f w_f$ is in darcy-cm and w_f is in cm. Substituting values into Eq. 2 leads to Eq. 4.

$$k_f w_f = [5.56\text{x}350\text{x}454\text{x}14.7\text{x}0.67/(3600\text{x}24\text{x}2)]\ \text{x}\ (L_f/h_f) = 50.4\ \text{x}\ (L_f/h_f)\ \text{darcy-cm} \quad (4)$$

The ratio of fracture length to fracture height was not known. However, this ratio was probably between one and ten. If L_f/h_f=1, k_fw_f = 50.4 darcy-cm and w_f = 0.18 cm. If L_f/h_f=10, k_fw_f = 504 darcy-cm and w_f = 0.38 cm. Therefore, a rough estimate indicates that the **effective fracture width was between 0.2 and 0.4 cm**. Thus, the feature had a large flow capacity.

In a natural fracture system, multiple fractures are present, so one might question our assumption of a single two-wing fracture. However, two factors mitigate this concern. First, unless the fracture intensity is very high, the probability is low that more than one fracture will intersect the wellbore. Second, because fracture conductivity varies with the third power of fracture width (see Eq. 3), the widest fracture will probably dominate the flow system.

Estimated Tube Diameter

Alternative to a fracture, the conductive feature might be a vug, vug system, or solution channel. If the feature is treated as a single tube that was 100 ft long, standard calculations[18] reveal that the effective tube diameter was 0.66 cm. The feature could also be two 0.55-cm diameter tubes, four 0.46-cm diameter tubes, ten 0.37-cm diameter tubes, or one-hundred 0.21-cm diameter tubes (all with a length of 100 ft).

Gel Placement

The gelant used was MARCIT^{SM}, which contained Alcoflood 935^{TM} HPAM crosslinked with Cr(III) acetate. The polymer solutions were prepared in fresh water with less than 0.2% total dissolved solids (i.e., salinity). Table 11 shows the volumes, polymer concentrations, and injectivities for the stages of gelant injection. During gelant injection, pressures were measured both at the wellhead and downhole. The pressure difference between the surface and downhole was about 1,400 psi, regardless of gel composition or rate. Virtually all of this pressure difference was due to the gravity head. The pressure drop due to flow down the wellbore was quite small. In contrast, the pressure drop from the wellbore into the reservoir was much larger (typically 800 to 900 psi). The estimated wellbore volume was 15 bbl, and a typical transit time between the surface and the formation was about 15 minutes. The gelation time was several hours, so the formulation was in gelant form going down the wellbore. However, beyond the wellbore, a significant fraction of the formulation was older than the gelation time and was therefore crosslinked during much of the placement process.

Table 11—Gelant injection data.

Polymer concentration in gelant, %	Volume injected, bbl	Injection rate, BPD	Injection time, hours	Final injectivity, BPD/psi
0.0	5	1,440	0.08	23.8
0.4	1,057	1,800	14	1.92
0.55	1,440	1,488	23.5	1.75
0.7	482	1,073	10	1.27

Gelant Viscosities. Fig. 29 shows the viscosities of HPAM solutions relative to that of water for the three HPAM solutions of interest (i.e., containing 0.4%, 0.55%, and 0.7% HPAM in a 0.15% NaCl brine). These viscosities were measured at 19.3°C; however, the viscosity relative to water

was not sensitive to temperature. (The viscosity measurements were made by Ying "Annie" Wang.) The reservoir temperature was 40°C, while the minimum downhole temperature during gelant injection was 14°C.

For injection into a two-wing fracture, the shear rate at the fracture wall can be estimated using Eq. 5 (from Ref. 18).

$$dv/dx = 3\,q / (h_f w_f^2) \quad \text{.....(5)}$$

For the range of injection rates (1,073 to 1,800 BPD), probable fracture widths (0.18 to 0.4 cm), and probable fracture heights (roughly 100 ft), the shear rates in the fracture typically ranged from 10 to 100 s^{-1}. For example, Eq. 6 estimates 65 s^{-1} for a typical shear rate.

$$dv/dx = 3x(1BPMx350lb/bblx454cm^3/lbx1min/60sec)/[100ftx12x2.54cm/ftx(0.2cm)^2] = 65\ s^{-1} \quad \text{....(6)}$$

For shear rates from 10 to 100 s^{-1}, the relative viscosity ranged from 50 to 25 for 0.4% HPAM, from 95 to 44 for 0.55% HPAM, and from 180 to 65 for 0.7% HPAM.

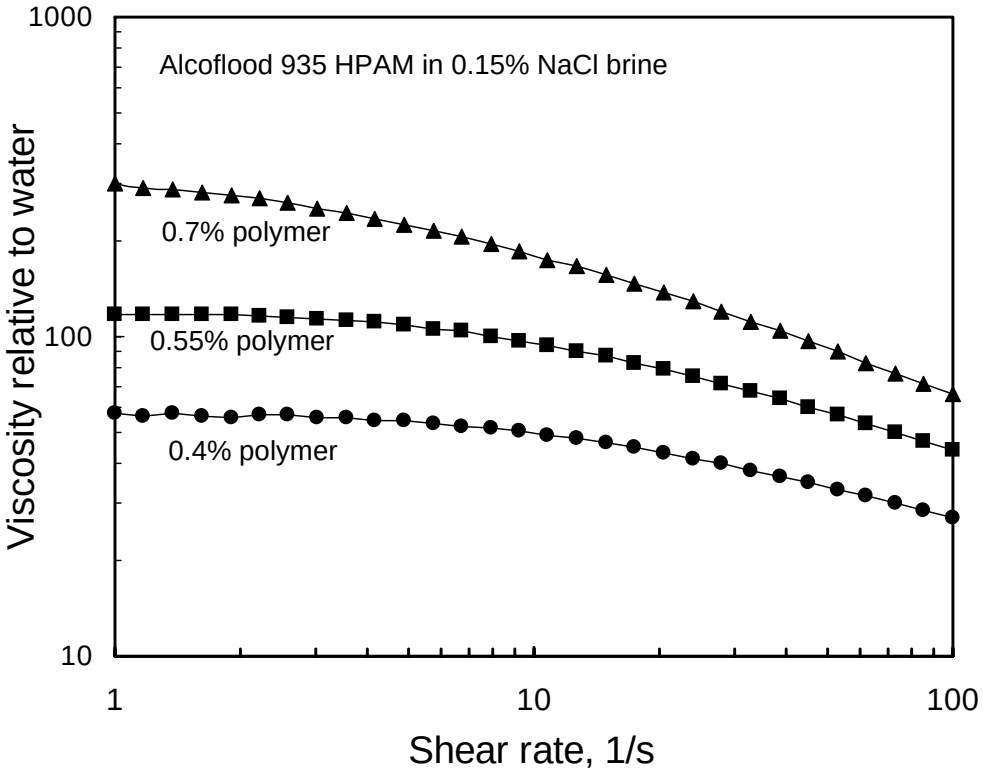

Fig. 29—Viscosity versus shear rate for polymer solutions.

Effective Viscosity in the Fracture. During gelant injection, if all resistance to flow could be attributed to gelant flowing or extruding down the fracture, then the gelant injectivity data from Table 11 could be used with Eq. 2 to estimate the *in situ* viscosities in the fracture. The estimates are listed in Table 12 and are substantially greater than viscosities measured in the laboratory

(Fig. 29). If the formulation is in the gelant state, this result indicates that we should not assume that all resistance to flow can be attributed to gelant flowing down the fracture. On the other hand, if the formulation is in the gelled state (i.e., mostly crosslinked), then Table 12 indicates the effective viscosities of formed gels as they extruded down the fracture. This possibility seems credible since the formulation ages were significantly greater than the gelation time for most of the placement process.

Table 12—Estimated *in situ* viscosities in the fracture.

Polymer concentration in gelant, %	Estimated *in situ* viscosities, cp
0.4	420
0.55	460
0.7	634

Assuming Most Resistance Occurs during Gelant Leakoff. An alternative approach assumes that flow down the fracture shows negligible resistance compared to that for flow through the porous rock. In this approach, the pressure all along the fracture is assumed to be that at the wellbore, and all pressure losses occur from the fracture face to some distance into the porous rock. If this is valid, Eq. 7 (from Ref. 16) estimates the area associated with the fracture during gelant injection.

$$A_f = \{V_{gelant}\, q\, \mu_{gelant} / [\Delta p\, k_m\, \phi\, (1\text{-}S_{or})]\}^{0.5} \quad \text{.....(7)}$$

And the distance of gelant leakoff from the fracture face is estimated by Eq. 8.

$$L_p = V_{gelant} / [A_f\, \phi\, (1\text{-}S_{or})] \quad \text{.....(8)}$$

Here, the $\phi\,(1\text{-}S_{or})$ term also includes any retardation or acceleration from chemical retention or inaccessible pore volume effects. We assume that $\phi\,(1\text{-}S_{or})$=0.1 and k_m=5 md.

For 0.4% HPAM gelant (1057 bbl over 14 hours), μ_{gelant}=35 cp @45 s^{-1} (from Fig. 29):

A_f = {(1057x350x454)x[1.92x350x454x14.7/(3600x24)]x35/[0.005x0.1]}$^{0.5}$ = 26600 ft^2.
L_p = 1057x350/62.4/[26600x.1] = 2.2 ft.

For 0.55% HPAM gelant (2497 bbl total, final 1440 bbl over 23.5 hours), μ_{gelant}=60 cp @45 s^{-1}:

A_f = {(2497x350x454)x[1.75x350x454x14.7/(3600x24)]x60/[0.005x0.1]}$^{0.5}$ = 51100 ft^2.
L_p = 2497x350/62.4/[51100x.1] = 2.7 ft.

For 0.7% HPAM gelant (2979 bbl total, final 482 bbl over 10 hours), μ_{gelant}=100 cp @45 s^{-1}:

A_f = {(2979x350x454)x[1.27x350x454x14.7/(3600x24)]x100/[0.005x0.1]}$^{0.5}$ = 61400 ft^2.
L_p = 2979x350/62.4/[61400x.1] = 2.7 ft.

Note that the estimated distances for gelant leakoff were fairly constant, between 2.2 and 2.7 ft. The implication from these results is that additional gelant injection is not increasing the distance of gelant leakoff but instead is increasing the fracture area contacted by gelant (with basically a fixed distance of gelant leakoff). This finding seems reasonable. However, two considerations indicate that the above estimates of fracture area are too low and the distances of gelant penetration are too high. First, Alcoflood 935 has a molecular weight of about 5 million Daltons and is not expected to penetrate very readily into 5-md dolomite—even in the uncrosslinked state. Second, the gelation times for the injected formulations were less than 5 hours, so once a virgin area of fracture surface was contacted by gelant, gelant leakoff should not occur after 5 hours. An alternative estimate of the distance of gelant penetration can be made using Eq. 9.

$$L_p = \{t\,\Delta p\,k_m/[\mu_{gelant}\,\phi\,(1\text{-}S_{or})]\}^{0.5} \quad (9)$$

Given a 800-psi pressure drop, the maximum distances of gelant penetration into 5-md dolomite after 5 hours would be 1.7, 1.3, and 1.0 ft for gelant viscosities of 35, 60, and 100 cp, respectively. Acceptance of these values leads to fracture areas of 34,400, 106,000 and 166,000 ft^2, respectively (from Eq. 7). High molecular weight polymers show a greater resistance to flow in low-permeability rock than is expected from viscosity data. Consequently, the distance of gelant penetration could be significantly less than 1 ft, and the open fracture area could be significantly larger than the values calculated above. Perhaps, the most important indication from these calculations is that the fracture area being contacted by gelant/gel increases significantly with increased gelant volume.

Productivity Changes from the Gel Treatment

After the gel treatment was completed, production rates and fluid levels were measured on several dates indicated in the first column of Table 13. The fluid levels were converted to downhole pressure drops (i.e., between the wellbore and the formation) and listed in the fourth column of Table 13. Given the rates and downhole pressure drops, oil and water productivity values were calculated (fifth and sixth columns), along with the productivity values relative to those before the gel treatment (last two columns).

Table 13—Productivity values before and after gel placement.

Date	BOPD/ BWPD	Fluid level, ft	Δp, psi	$q/\Delta p$, BOPD/psi	$q/\Delta p$, BWPD/psi	J_{oil}/J_{oil0}	J_{water}/J_{w0}
Before gel	8/720	1,530	131	0.061	5.496	1.0	1.0
After gel: 1/7/2003	130/130	1,500	118	1.102	1.102	18.0	0.20
2/8/2003	48/216	1,800	248	0.194	0.871	3.2	0.16
3/7/2003	29/237	1,680	196	0.148	1.210	2.4	0.22
4/3/2003	22/206	1,680	196	0.112	1.052	1.8	0.19
5/13/2003	15/217	1,590	157	0.096	1.383	1.6	0.25
6/23/2003	16/329	1,860	274	0.058	1.201	1.0	0.22

The Gel Treatment *Increased* Oil Productivity! The major surprise from Table 13 was that the gel treatment actually increased oil productivity. Shortly after the gel treatment, the oil productivity was about 18 times greater than that before the treatment. Usually, we expect that the gel will cause some reduction in both oil and water productivity, but we hope that the reduction in oil productivity will be minimized. (Commonly, the oil production rate can be increased by a gel treatment even though the oil productivity decreases. This occurs because lower fluid levels in the well allow for greater pressure drawdowns between the formation and the well.) An increase in oil productivity suggests that the gel treatment somehow selectively stimulated the well. From Table 13, the largest oil productivity occurred immediately after the gel treatment (January 7). Over the next month, the oil productivity fell from 18 times the pre-treatment productivity to 3.2 times the pre-treatment value. Over the next four months, oil productivity decreased further, ultimately approaching the pre-treatment value.

Possible Mechanisms for Oil Stimulation. We envision two possible mechanisms for oil stimulation. First, the fracture system may be forced open during injection of the viscous gelant, followed by a prolonged closing of the fracture system during the six months after the treatment. During gelant injection, the downhole pressures were roughly 1,000 psi greater than during production. These higher pressures may have significantly extended and/or increased the effective area associated with the fracture system. Upon return to production and significantly lower pressures, the fracture system closed.

If the above mechanism is valid, an obvious method to prolong oil productivity would be to keep the fracture system open after the stimulation. In particular, a proppant could be injected with the gelant to accomplish this goal. Hopefully, this approach will be applied to an Arbuckle production well in the near future.

A second possible mechanism involves mitigation of a water block in the matrix next to the fractures. This mechanism speculates that before the gel treatment, water imbibed into the oil-bearing rock, thus increasing water saturation and decreasing oil relative permeability near the fractures. In order for oil to be produced, it must flow through the region of high water saturation. When the gel treatment is applied, water flow through the fracture system is reduced substantially, thus allowing oil in the matrix to displace the water block and increase oil productivity.

Incidentally, the fact that oil productivity was stimulated increases the likelihood that fractures caused the excess water production (before the treatment). If a vug system was responsible, oil productivity should not have been stimulated.

Potential Flaws with Proposed Mechanisms. Concerning the first mechanism above, the apparent slow closing of the fracture system (over six months) seems surprising. Normally, the fracture system is expected to close almost immediately after the pressure reduction. At present, we can’t explain why the closing should take so long or whether the presence of the gel influences the closing rate. The second mechanism above also seems inadequate. After the gel treatment, the water production rates and productivity values do not change enough to explain why six months should be required to re-establish the water block in the oil-bearing rock.

If the first mechanism above (the fracture-opening mechanism) was correct, why did this process not stimulate water productivity as well as oil productivity? Note in Table 13 that water productivity after the treatment was fairly constant at about 20% of the pre-treatment value. Several possible explanations come to mind. First, after gel placement, the oil might re-establish flow paths to the wellbore much more easily than did water. Our previous work supports this possibility if gelant leaked off some distance into the porous rock and then reduced permeability to water much more than that to oil.[14-16] This possibility could also occur if gelant or gel experienced gravity segregation during placement, thereby plugging the lower part of the fracture system (i.e., the aquifer) more than the upper part of the fracture system (i.e., the oil zones).

A second possible reason why oil productivity was stimulated while water productivity was not is that the distance to the oil sources (i.e., the oil-bearing rock) may be less than the distance to the water sources. For a given fracture width and applied pressure difference, the pressure gradient from the oil source to the well may be significantly greater than that from the water source to the well. Consequently, oil may force a viable pathway through the gel in a fracture more readily than water.

A third possibility is that gel in fractures reduced permeability to water more than that to oil. However, this effect requires that an oil or water pathway must first be established through the gel. For work to date, the pressure gradient to establish the first pathway through the gel was about the same for water as for oil.[13]

A fourth possibility is that the fracture system happened to open/extend more into oil zones than into water zones. However, this possibility seems unlikely.

***In Situ* Residual Resistance Factors**. Because the gel treatment actually stimulated oil production, it is not possible to obtain reliable *in situ* residual resistance factors from the field data. With our available methods,[15,16] these calculations indicated oil residual resistance factors that were less than one or even negative. For water residual resistance factors, a value of about 66 is estimated using these methods and the data from Table 13. However, this number should not be considered reliable for two reasons. First, if fracture extension was important, it probably occurred in the water zones as well as in the oil zones. Thus, the final water productivities reflect the composite effect from opening the fracture system (which would increase water productivity) and from gel damaging the water pathways (which would decrease water productivity). Second, the Cr(III)-acetate-HPAM gel should provide much higher water residual resistance factors (i.e., greater than 1,000).

Conclusions

We analyzed results from a Cr(III)-acetate-HPAM gel treatment that was applied by Gel-Tec and Vess Oil Company in the Jennie Johansen #8 production well in the Arbuckle formation. The availability of accurate pressure data before, during, and after the treatment was critical for the analysis. Productivity values before the treatment were 90 times greater than those expected from the Darcy equation for radial flow—indicating the presence of a very conductive feature, such as a fracture. The productivity data was used to estimate an effective average fracture width between 0.2 and 0.4 cm. Based on injectivity data during gelant injection, the fracture area that

was contacted by gelant or gel increased significantly with increased volume of gelant injection. This fracture area was probably greater than 166,000 ft^2 by the end of the 3,000-bbl treatment. Some doubt exists whether any significant gelant leakoff occurred into the 5-md dolomite matrix. If it did occur, the distance of gelant leakoff from the fracture faces was fairly constant with additional injection. The gelant leakoff distance was less than 2 ft and may have been significantly less than 1 ft. After the gel treatment, water productivity was fairly constant at about 20% of the pre-treatment value. However, oil productivity was stimulated by a factor of 18 immediately after the treatment. During the six months after the treatment, oil productivity gradually decreased to approach the pre-treatment value. Two mechanisms were considered to explain why the gel treatment increased oil productivity. Consistent with the observations during gelant injection, one mechanism suggested that the fracture area open to oil flow was increased substantially by the gel treatment, followed by a gradual closing of the fractures during subsequent production. If this mechanism is correct, the longevity of these gel treatments may be increased by including a proppant during gelant placement.

5. DISPROPORTIONATE PERMEABILITY REDUCTION IN FRACTURES

Gels in Fractures

Previous Work. In our first annual report[1], results from two sets of experiments suggested that gels might exhibit disproportionate permeability reduction in fractures. One set of experiments was performed in 0.02-in. (0.5-mm) wide fractures, while the second set was performed in 0.04-in. (1-mm) wide fractures. Both sets of experiments involved our standard 1-day-old Cr(III)-acetate-HPAM gel (0.5% Alcoflood 935 HPAM crosslinked with 0.0417% Cr(III) acetate, 41°C) placed at 2,000 cm^3/hr in 4-ft long, 1.5-in. high, fractured Berea sandstone cores. Within each set, two separate experiments were conducted (using two separate fractured cores)—one where brine (1% NaCl, 0.1% $CaCl_2$) was injected after gel placement and a second where Soltrol 130 oil (1.05 cp at 41°C) was injected. In each experiment, injection rates from 100 to 16,000 cm^3/hr were investigated.

For both fracture widths, the final fracture conductivity during oil flow was higher than that for brine. The average pressure gradients during oil injection at low rates were 10 to 20 times less than those during water injection (Fig. 30). At high rates, the differences between water and oil pressure gradients were less pronounced—especially in the 0.02-in. wide fractures. These results suggested that disproportionate permeability reduction in fractures was most evident at low flow rates. Prior to this study, the presence of a porous medium was thought necessary to observe disproportionate permeability reduction.[2]

Sequential Oil and Water Banks after Placement of Formed Gels. Several additional experiments were performed to explore this behavior in fractures. Two sets of experiments used sequential injection of oil and water banks after gel placement. In both sets, our standard 1-day-old Cr(III)-acetate-HPAM gel was placed at 2,000 cm^3/hr (8,260 ft/d) in 4-ft long, 1.5-in. high, fractured Berea sandstone cores. In both cases, the fracture width was 0.02 in. (0.5 mm), and 2 liters (80 fracture volumes) of Soltrol 130 oil were injected after a 1-day shut-in. Oil was injected at 2,000 cm^3/hr (8,260 ft/d) for the first set of experiments (Fig. 31) and 200 cm^3/hr (826 ft/d) for the second set (Fig. 32).

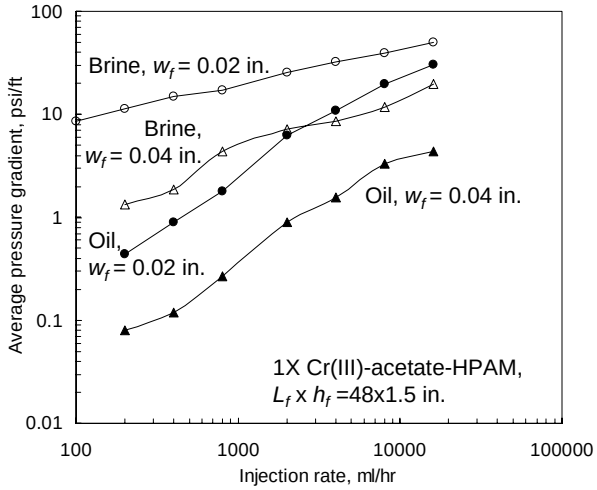

Fig. 30—Gel washout using oil versus brine at various rates.

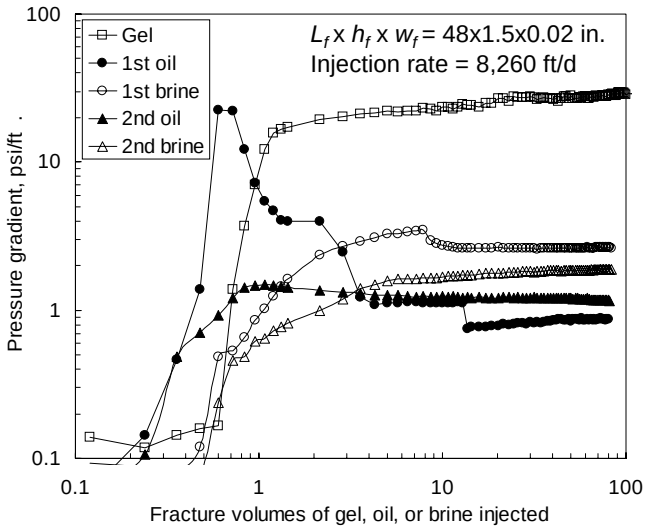

Fig. 31—Gel washout during oil/brine/oil/brine sequence at 8,260 ft/d.

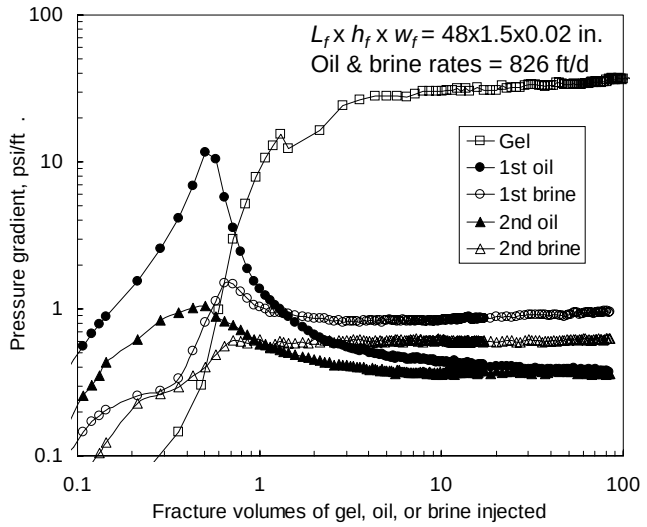

Fig. 32—Gel washout during oil/brine/oil/brine sequence at 826 ft/d.

For the first set of experiments (at 8,260 ft/d), the solid circles in Fig. 31 show that the pressure gradients during the first oil injection peaked at 22.6 psi/ft—roughly similar to the 28.8 psi/ft associated with gel placement (open squares in Fig. 31). As with brine injection, the pressure gradient for gel washout was about the same as that for gel placement. After the peak, pressure gradients dropped and approached 0.87 psi/ft after 80 fracture volumes of oil.

Next, sequential banks of brine, oil, and brine (80 fracture volumes each) were injected at 2,000 cm^3/hr (8,260 ft/d). For these three banks, a prominent peak, like that associated with the first oil bank, was not observed. After 80 fracture volumes, the final pressure gradients were 0.87 psi/ft for the first oil bank, 2.6 psi/ft for the first brine bank, 1.2 for the second oil bank, and 1.9 psi/ft for the second brine bank. Since the oil viscosity was 1.05 cp, brine viscosity was 0.67 cp, and

depending on which pair of oil and water pressure gradients were chosen, the ratio of water permeability reduction to oil permeability reduction ranged from 2.5 to 4.7 [i.e., (1.9x1.05)/(1.2x0.67)=2.5 to (2.6x1.05)/(0.87x0.67)=4.7]. Thus, the gel showed a moderate disproportionate permeability reduction. However, one could argue that this effect was of minor importance, considering that the pressure gradient for the first gel failure (i.e., in the wormholes) was the same for oil and brine flow.

For the second set of experiments (at 826 ft/d), the solid circles in Fig. 32 show that the pressure gradients during the first oil injection peaked at 11.6 psi/ft—significantly lower than the corresponding value from the high-rate experiment (Fig. 31) and less than half the value associated with gel placement at 826 ft/d (open squares in Fig. 32). Nevertheless, a significant pressure peak was observed during the first oil injection. After the peak, pressure gradients dropped and approached 0.37 psi/ft after 80 fracture volumes of oil.

Next, sequential banks of brine, oil, and brine (80 fracture volumes each) were injected at 200 cm^3/hr (826 ft/d). For these three banks after 80 fracture volumes, the final pressure gradients were 0.95 psi/ft for the first brine bank, 0.37 for the second oil bank, and 0.62 psi/ft for the second brine bank. Depending on which pair of oil and water pressure gradients were chosen, the ratio of water permeability reduction to oil permeability reduction ranged from 2.6 to 4.0 [i.e., (0.62x1.05)/(0.37x0.67)=2.6 to (0.95x1.05)/(0.37x0.67)=4.0]. This range of disproportionate permeability reduction was similar to that observed for the first experiment (Fig. 31). Thus, contrary to the discussion associated with Fig. 30, a rate dependence for the disproportionate permeability reduction was not evident.

Failure of Gels Placed as Gelants in Fractures

In the above work, we studied failure or washout of gels in fractures after they were extruded into place as formed gels. We wondered how the pressure gradients for gel failure would compare when the gels were placed as gelants rather than as formed gels. Several sets of experiments were performed where short fractured cores were saturated with either a 1X or 2X Cr(III)-acetate-HPAM gelant (where the 1X gelant contained 0.5% Alcoflood 935 HPAM and 0.0417% Cr(III)-acetate, while the 2X gelant contained twice the polymer and crosslinker concentrations). Two sets of experiments (one with 1X gel and the other with 2X gel) were performed using fused silica as the core material, while the core material was polyethylene for two other sets. Within each of the polyethylene and silica sets, four cores were used with fracture widths of 0.2, 0.5, 1, and 2 mm. All cores were 0.65 cm in diameter, and all experiments were performed at room temperature. The polyethylene cores were 3.5 cm in length, while the silica cores were 5.4 cm in length. All cores were saturated with either 1X or 2X gelant and shut in for several days. In about half of the experiments, hexadecane (3.3 cp) was injected into each core for two hours using a fixed rate of 1 cm^3/hr while pressure gradients were monitored continuously. Next, brine (1% NaCl, 0.1% $CaCl_2$) was injected at the same rate for two hours. In the other half of the experiments, brine was injected first after gel placement, while oil was injected second.

For the experiments with 1X gel, Fig. 33 plots the peak pressure gradient observed during the first fluid injection after gelation. These peaks indicate the point of gel failure. The solid symbols show results when oil was injected first after gel placement, while the open symbols show results when water was injected first. As expected, the peak pressure gradients generally decreased with

increased fracture width, however, a wide degree of data scatter was evident. A regression analysis indicated that the failure pressure gradient was inversely proportional to fracture width, but the correlation coefficient (r^2) was only 0.48. A correlation was not evident between failure pressure gradient and whether oil or water was injected first after gelation. Also, a correlation was not evident between failure pressure gradient and type of core material (silica or polyethylene).

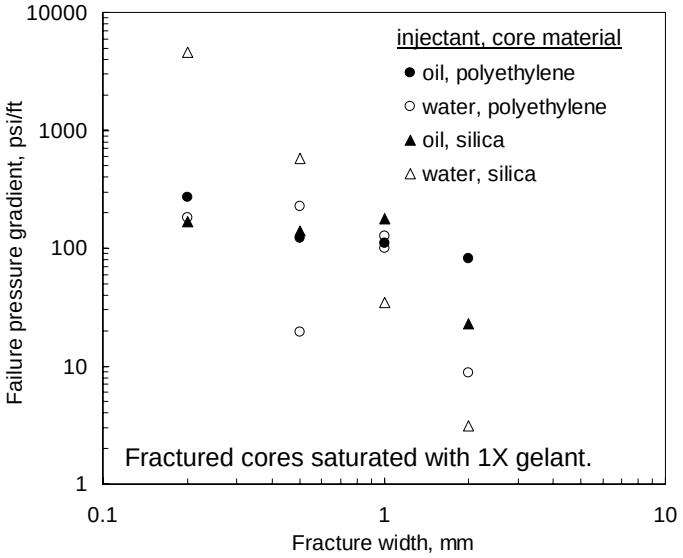

Fig. 33—Failure pressure gradients for 1X gel in short fractures.

Consistent with the regression analysis, a force balance predicts that the failure pressure gradient should be inversely proportional to fracture width. Data from Ganguly *et al.*[11] matched this prediction very well for a Cr(III)-acetate-HPAM gel [0.75% Alcoflood 935 HPAM, 0.0417% Cr(III) acetate] in plastic tubes with diameters from 2.4 to 7.6 mm.

For the experiments with the 2X gel, Fig. 34 plots the peak pressure gradient observed during the first fluid injection after gelation. In general, the failure pressure gradients were greater than those observed for the 1X gel (compare with Fig. 33), and the failure pressure gradients decreased with increased fracture width. Again, significant data scatter was evident, and there was no obvious correlation between the failure pressure gradient and whether oil or water was injected first after gelation. The pressure gradients for the narrow fractures in the silica cores were lower than those in the polyethylene cores, but this observation does not appear definitive in view of the results in Fig. 33.

In these experiments in short fractured cores, the pressure gradients were allowed to stabilize during two hours of fluid injection at 1 cm^3/hr. Subsequently, the complementary phase (water if oil was injected first; oil if water was injected first) was injected for two hours. Pressure gradients at the end of these oil and water flow periods were used to estimate the degree of disproportionate permeability reduction exhibited by the gels. In particular, a measure of the disproportionate permeability reduction is the ratio of oil/water viscosity (i.e., 3.3 cp ÷ 0.95 cp)

times the ratio of the ending water/oil pressure gradients. These disproportionate permeability reduction values are plotted in Fig. 35 for the 1X gel and in Fig. 36 for the 2X gel. These figures suggest that the gel generally provided a significant disproportionate permeability reduction. The average F_{rrw}/F_{rro} was 10 for the 1X gel and 40 for the 2X gel. However, a large variability was noted. The magnitude of the effect did not show a definitive correlation with fracture width, gel concentration, or core material. The variability of the disproportionate permeability reduction values reflects the variability of the oil and water pressure gradients.

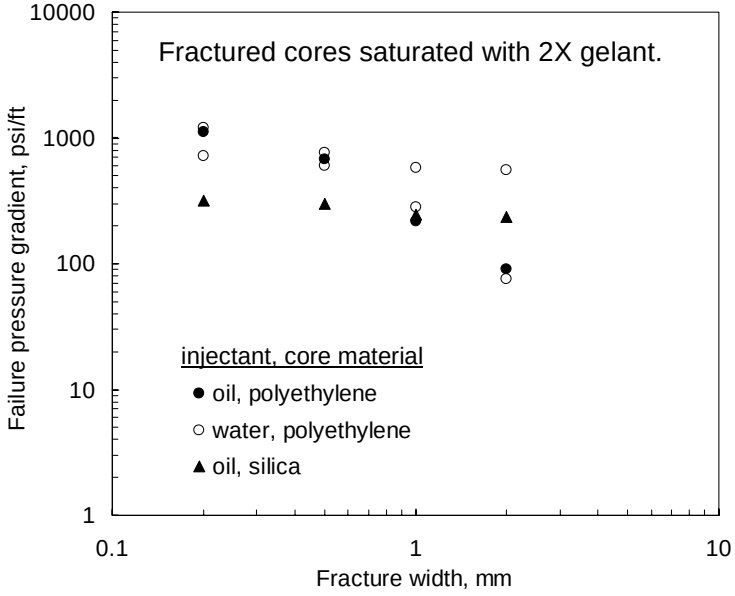

Fig. 34—Failure pressure gradients for 2X gel in short fractures.

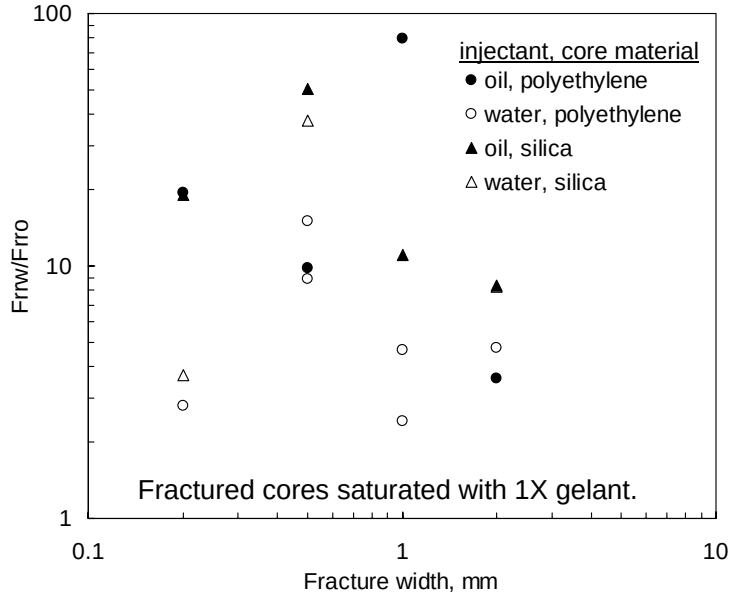

Fig. 35—Disproportionate permeability reduction for 1X gel in short fractures.

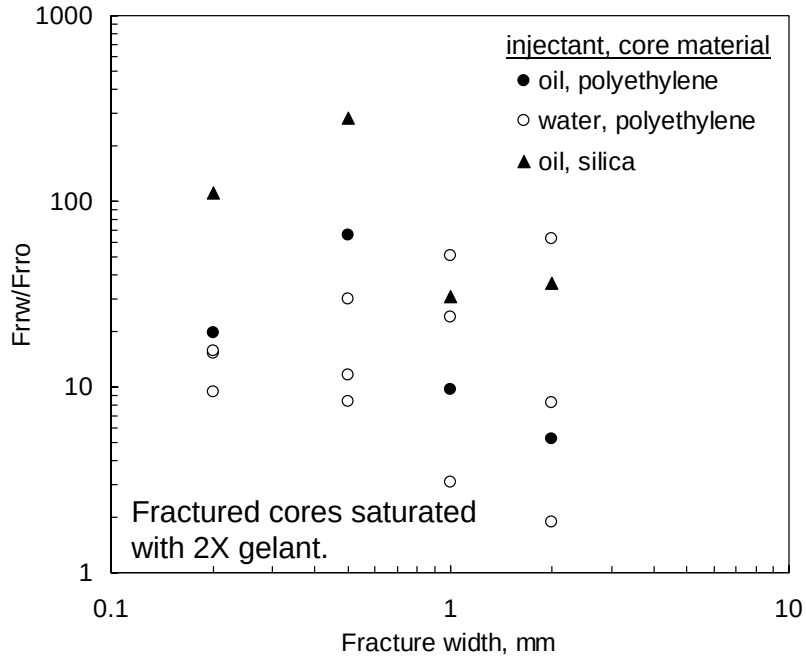

Fig. 36—Disproportionate permeability reduction for 2X gel in short fractures.

Gel Failure in Tubes

Why did gel failure and disproportionate permeability reduction show such large variability (e.g., Figs. 33-36)? Was it caused by variations in the gel, the fracture, our experimental technique, or a combination of factors? We knew the fractures were not identical in the above experiments. To remove this factor as a variable, we switched to uniform-diameter tubes in place of fractures.

Replicate Experiments. Several replicate experiments were performed in 1-ft-long, 1-mm-inside-diameter stainless steel tubes. Our standard 1X Cr(III)-acetate-HPAM gelant was placed and gelled in all tubes. For five experiments, oil (hexadecane) was injected to find the failure pressure, while brine was injected in six other experiments (all performed in separate tubes). To minimize variations in experimental technique and gel composition, all tubes were filled with the same gelant at the same time. After gelation, either brine or oil was injected at a fixed rate of 1 cm^3/hr (0.0343 cm/s or 97 ft/d) to determine the failure pressure gradient. Table 14 lists the results for each experiment, including the maximum pressure gradient and the final stabilized pressure gradient. For oil injection, the maximum pressure gradient averaged 219 psi/ft, with a standard deviation of 32 psi/ft. The maximum pressure gradient during water injection averaged 308 psi/ft (± 67 psi/ft)—40% greater than during oil injection. Given standard deviations ranging from 15% to 22% of the average values, the results suggest that gel failure can be reasonably reproducible.

The final stabilized pressure gradient averaged 15 psi/ft during oil injection and 31 psi/ft during water injection. In both cases, the standard deviation was large relative to the average. For all cases during oil injection, the final pressure gradients indicated that some gel remained in the tubes. In contrast, for four cases during water injection (i.e., those with peak pressure gradients above 300 psi/ft), the low final pressure gradients suggested that all gel may have blown out

from the tubes. For the two water-injection cases where the peaks were less than 300 psi/ft, the final stabilized pressure gradients were significant—suggesting that some gel remained.

Table 14—Failure pressure gradients during replicate experiments (1-mm ID tubes).

	Oil injection		Water injection	
Experiment	Peak, psi/ft	Final, psi/ft	Peak, psi/ft	Final, psi/ft
1	164	0.5	315	0
2	231	14	315	0
3	218	17	269	116
4	242	31	367	0
5	240	14	200	72
6			382	0
Average	219	15	308	31
Std. deviation	32	11	67	50

Effect of Tube Length. Another set of experiments tested the effect of tube length on gel failure. These stainless steel tubes had an inside diameter of 2.16 mm, and the tube lengths ranged from 1 to 5 ft. Again, our standard 1X Cr(III)-acetate-HPAM gel was placed as gelant in the tubes. For each tube length, water was injected after gelation for one set of tubes, while oil was injected for a second set. Oil and brine injection rates were 1 cm^3/hr (0.0076 cm/s or 21.5 ft/d). The results are summarized in Table 15. For oil or water injection after gel placement, the maximum pressure gradient averaged about 140 psi/ft, with the standard deviation about one-third of the average value. Final stabilized pressure gradients were generally low for both oil and water injection. Disproportionate permeability reduction was not evident.

Table 15—Failure pressure gradients versus tube length (2.16-mm ID tubes).

	Oil injection		Water injection	
Tube length, ft	Peak, psi/ft	Final, psi/ft	Peak, psi/ft	Final, psi/ft
1	106	3	111	0
2	173	0.8	94	17
3	156	0.5	127	1
4	143	0.2	199	2
5	81	5	188	0
Average	132	2	144	4
Std. deviation	38	2	47	7

Effect of Tube Diameter and Tube Material. Other experiments were performed to examine the effect of tube diameter and tube material on gel failure. These tubes were 1-ft long, with two identical tubes per set. Five sets of tubes were stainless steel, with diameters of 0.25, 1.02, 1.27, 1.75, and 2.16 mm. Two sets of tubes were teflon, with diameters of 0.8 and 2.49 mm. One set was glass, with a diameter of 2.21 mm. The final set of tubes was PEEK (polyetheretherketone), with a diameter of 2.36 mm.

All tubes were filled with the same batch of 1X Cr(III)-acetate-HPAM gelant at the same time. After gelation, brine was injected at a fixed rate of 1 cm^3/hr to determine the failure pressure gradient for one tube in a given set, while oil was injected at 1 cm^3/hr into the second tube of the set. Fig. 37 plots the results from these experiments, along with those from Tables 14 and 15. A power regression analysis of the data confirmed that the failure pressure gradient was inversely proportional to tube diameter; however, a fair amount of data scatter was evident. The correlation coefficient for a regression on all data was only 0.6. The correlation coefficient was improved to 0.8 when only water data in stainless steel tubes were included in the regression. The correlation between failure pressure gradient and the tube material was weak.

The dashed line in Fig. 37 plots the failure pressure gradient, assuming that this value can be estimated from a force balance and that the elastic modulus, *G'*, is 10 Pa (the value measured in a mechanical spectrometer).[12] Fig. 37 shows that these predictions are dramatically lower than the measured failure pressure gradients in the tubes. In order for the force balance equation to match the tube data (solid line in Fig. 37), the elastic modulus must be about 5,000 Pa—500 times the value measured in a mechanical spectrometer. Perhaps, there was a problem with our rheological measurements (e.g., wall slip?). This possibility will be checked in our future research.

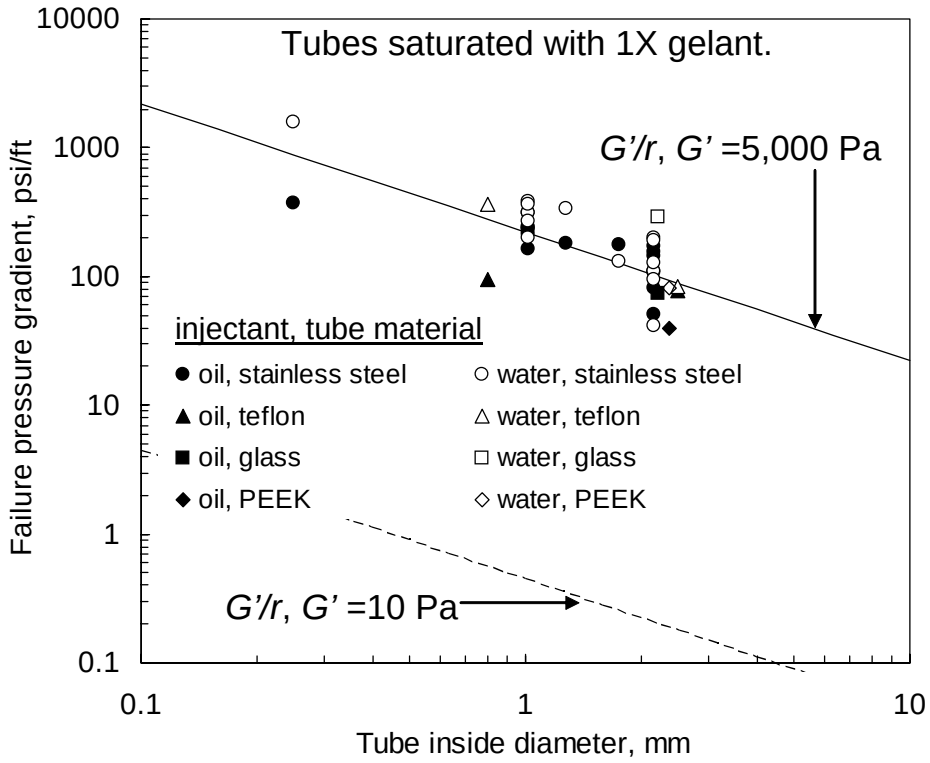

Fig. 37—Failure pressure gradient for 1X gel in tubes.

Oscillatory Behavior. Many of the experiments exhibited an interesting oscillatory behavior during oil injection. The thick curve in Fig. 38 shows an example of this behavior for the 2.49-

mm ID teflon tube. After experiencing the first (and largest) pressure peak of 78 psi/ft, subsequent peaks occurred on average every 10 minutes (±3.5 minutes). One can envision elastic gel globs that act as check valves to allow oil blobs of a certain size to pass when the pressure rises to a certain level. Following this idea and considering the injection rate and tube volume, this 10-minute period translates to oil blobs that were 3.5 cm in length (±1.2 cm), assuming that the oil blobs had the same diameter as the tube. During these oscillations, the minimum pressure gradient averaged 5.7 psi/ft (±0.7 psi/ft). The maximum values during the oscillations generally decreased with time—perhaps indicating erosion of the gel that caused this "check-valve" effect. After oil flow, water was injected (thin line in Fig. 38). The pressure gradients during water injection were sometimes higher and sometimes lower than those during oil injection—perhaps indicating rearrangement of residual gel within the tube.

Figs. 39-41 show that the oscillatory behavior was also observed during oil flow in PEEK, glass, and stainless steel tubes that were about 2 mm in diameter. The behavior was not observed during subsequent water flow, although other variations were seen. As noted for Fig. 38, during water flow (after oil flow), pressure gradients were sometimes higher and sometimes lower than those during oil flow. Thus, disproportionate permeability reduction was not clearly evident.

For Figs. 39-41, oil was injected first, followed by water. Fig. 42 shows a case where water was injected first, followed by oil. The oscillatory behavior associated with oil flow was noted.

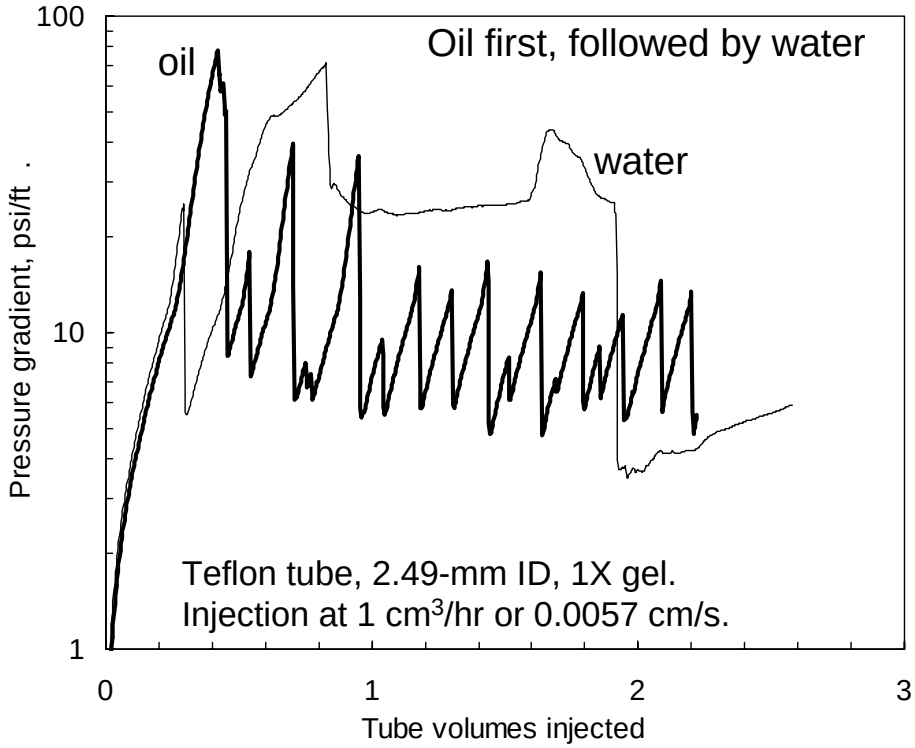

Fig. 38—Oil flow followed by water flow in the 2.49-mm ID teflon tube.

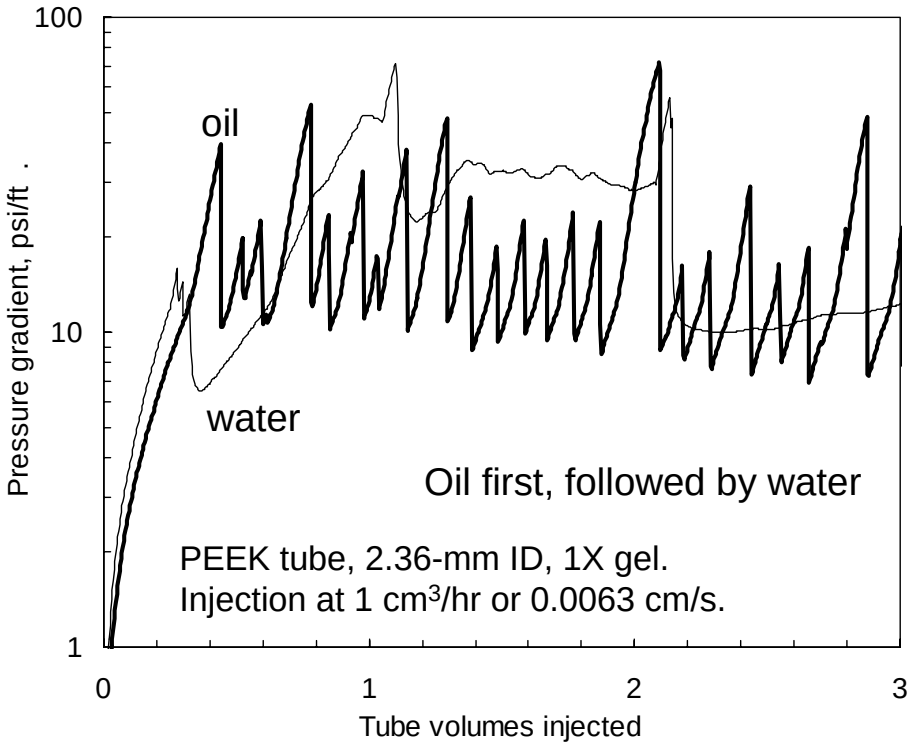

Fig. 39—Oil flow followed by water flow in the 2.36-mm ID PEEK tube.

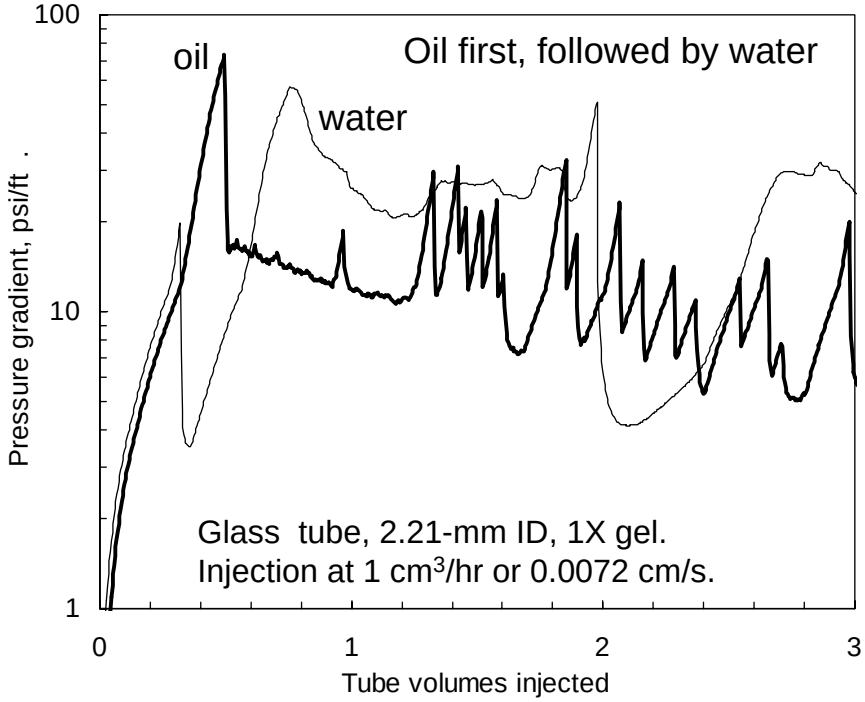

Fig. 40—Oil flow followed by water flow in the 2.21-mm ID glass tube.

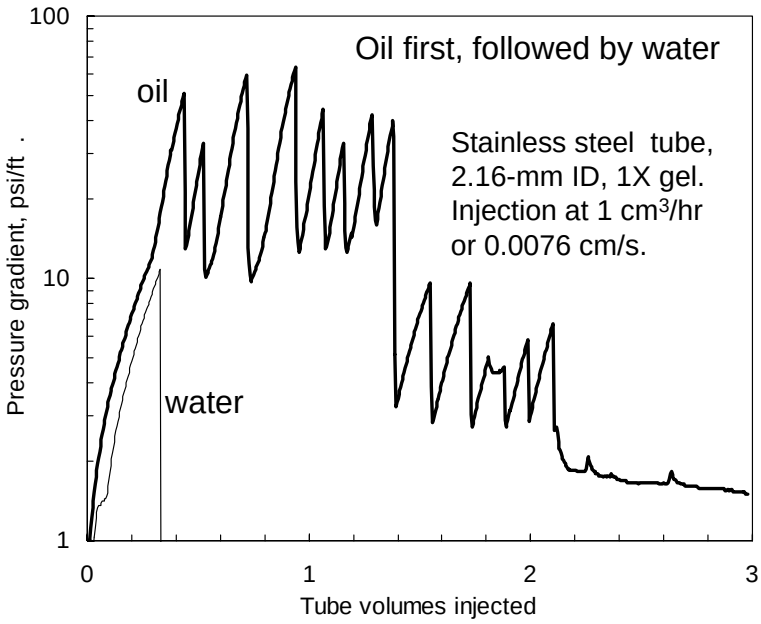

Fig. 41—Oil flow followed by water flow in the 2.16-mm ID stainless steel tube.

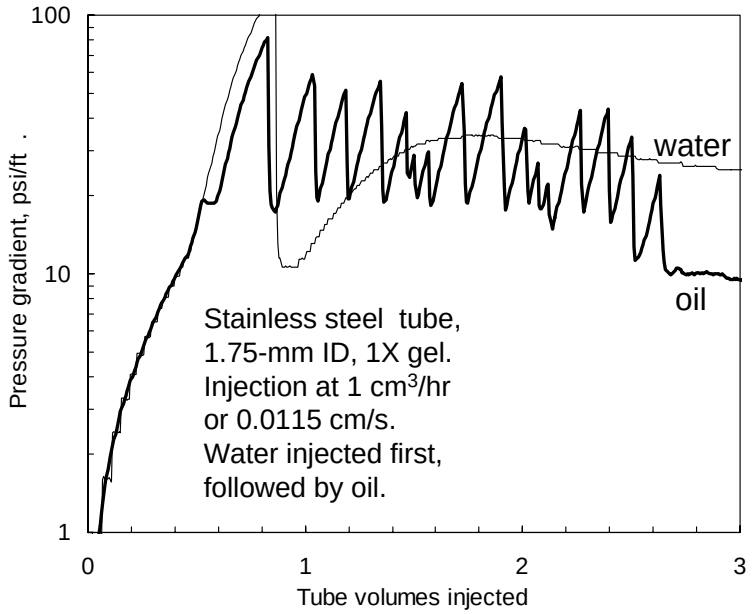

Fig. 42—Water flow followed by oil flow in the 1.75-mm ID stainless steel tube.

For many other cases, a single pronounced peak was seen. Often, the pressure gradients fell permanently to low values after the first peak—suggesting total washout of the gel. Fig. 43 shows this behavior for several tubes when water was injected first after gel placement. When oil followed water for these cases, the pressure gradients remained very low.

We suspect that the oscillatory behavior for oil flow shown in Figs. 38-42 is related to a balance between viscous, capillary, and elastic forces associated with the gel and oil flow. We plan additional experiments and analysis of this behavior in our future work.

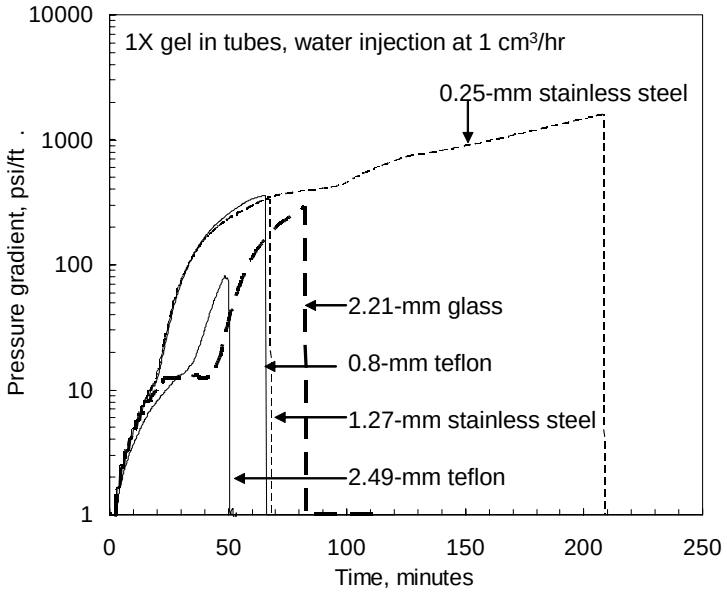

Fig. 43—Single peaks during water injection after placement of 1X gel in tubes.

Addition studies of disproportionate permeability reduction by partially formed gels in fractures will be presented at the end of Chapter 8.

Conclusions

We investigated whether Cr(III)-acetate-HPAM gels show disproportionate permeability reduction in open fractures. After extrusion of formed gels into fractures, the pressure gradients for first gel failure were similar for either brine or oil flow, which in turn, were similar to the pressure gradient observed during gel placement. In contrast, during steady state flow after first breaching the gel, the permeability to water (within the fracture) was reduced moderately more than that to oil. For these measurements, disproportionate permeability reduction was most evident at low flow rates. However, additional experiments that employed sequential injection of oil and water banks into the same fractured core did not show a rate dependence for the effect. Experiments where gels were placed as gelants (rather than extruded into place as formed gels) in short fractures exhibited reductions in water permeability that were significantly greater than those to oil. However, these results showed substantial variability that did not definitively correlate with fracture width, gel concentration, or core material.

Gel failure in tubes was also studied (using gel placed as gelant). Consistent with predictions from a force balance, the failure pressure gradient was inversely proportional to tube diameter; however, significant data scatter was noted. Within this scatter, it was not evident that the pressure gradient for gel failure depended on the tube material. Disproportionate permeability reduction was not clearly demonstrated.

6. EFFECT OF INJECTION DELAY ON GEL PROPERTIES IN FRACTURES

In most of our previous studies of gel extrusion through fractures, a Cr(III)-acetate-HPAM gel was aged for one day (or five times the gelation time) before injection into a fractured core.[13,19-24] Our base-case 1X gel contained 0.5% Ciba Alcoflood 935™ HPAM (molecular weight ≈$5x10^6$ daltons; degree of hydrolysis 5% to 10%), 0.0417% Cr(III) acetate, 1% NaCl, and 0.1% $CaCl_2$. The gelation time for this formulation was about 5 hours at 41°C. This chapter examines the effect of gel age (before injection) on (1) pressure gradient during extrusion, (2) gel dehydration/water leakoff behavior, (3) effectiveness in sealing a fracture, and (4) resistance to washout.

In the present study, we again focused on our standard 1X Cr(III)-acetate-HPAM gel. However, before injection into fractured cores, the aging time was varied during 12 separate experiments. The aging times included 12 minutes, 2 hours, 4 hours, 5 hours, 8 hours, 12 hours, 16 hours, 24 hours, 48 hours, 72 hours, 120 hours, and 240 hours. All experiments were performed at 41°C using 0.04-in.-wide (1-mm wide) fractures in 48x1.5x1.5-in. Berea sandstone cores. At the end of each 4-ft long fracture, a special outlet fitting segregated the effluent from the fracture and that from the porous rock. These fractured cores were initially saturated with brine only.

Pressure Gradients during Gelant/Gel Placement

In each of the twelve experiments, after gel aging, 3,700 cm^3 (80 fracture volumes) of the formulation were injected at a fixed rate of 2,000 cm^3/hr or 4,130 ft/d effective average velocity in the fracture. Fig. 44 shows pressure gradients (in the middle 60% of the fractured core) during gel placement. Table 16 lists the final pressure gradient after 80 fracture volumes. Generally, pressure gradients increased sharply as the gelant/gel displaced water from the fracture, followed by relatively stable pressure gradients for the remainder of gelant/gel injection. However, the 5-hour to 24-hour experiments showed a steady increase in pressure gradient—i.e., by 1 to 2.5 psi/ft over the final 70 fracture volumes. Fig. 44 and Table 16 demonstrate that before the gelation time (i.e., before 5 hours), pressure gradients were low—i.e., less than 0.5 psi/ft. Between 5 and 16 hours, the final pressure gradient increased to about 10 psi/ft. Presumably, the gel strength continuously increased up to 16 hours. For longer delay times, increases in pressure gradient were less pronounced. The 16-hour and 24-hour curves were very similar, and the 2-day, 3-day, and 5-day curves were similar. The highest pressure gradients occurred after 10 days.

Leakoff Rates

During gelant/gel injection, we measured the rate of fluid leakoff from the fracture faces (Fig. 45). Experimentally, this was accomplished by monitoring the rate of fluid production from the matrix. Dividing these values by the total fracture area (i.e., 1 ft^2 or 929 cm^2) gives the rate of fluid leakoff (e.g., in units of ft^3 of fluid per ft^2 of fracture area per day or ft/d). For injection delay times of 5 hours or less, the experiments exhibited leakoff rates that were similar and low (typically less than 0.03 ft/d). Presumably for these experiments, the leakoff fluid consisted of gelant (uncrosslinked polymer solution and Cr(III) acetate).

For injection delays of 16 hours or longer, leakoff rates were similar and high (typically greater than 0.3 ft/d). Based on previous work during extrusion of formed gels,[19] the leakoff fluid was brine (with no crosslinked polymer). Intermediate leakoff rates were noted for the 8-hour and 12-

hour experiments. Figs. 44 and 45 suggest that the leakoff and extrusion properties of these gels experienced their greatest changes between 5 and 16 hours after gelant preparation.

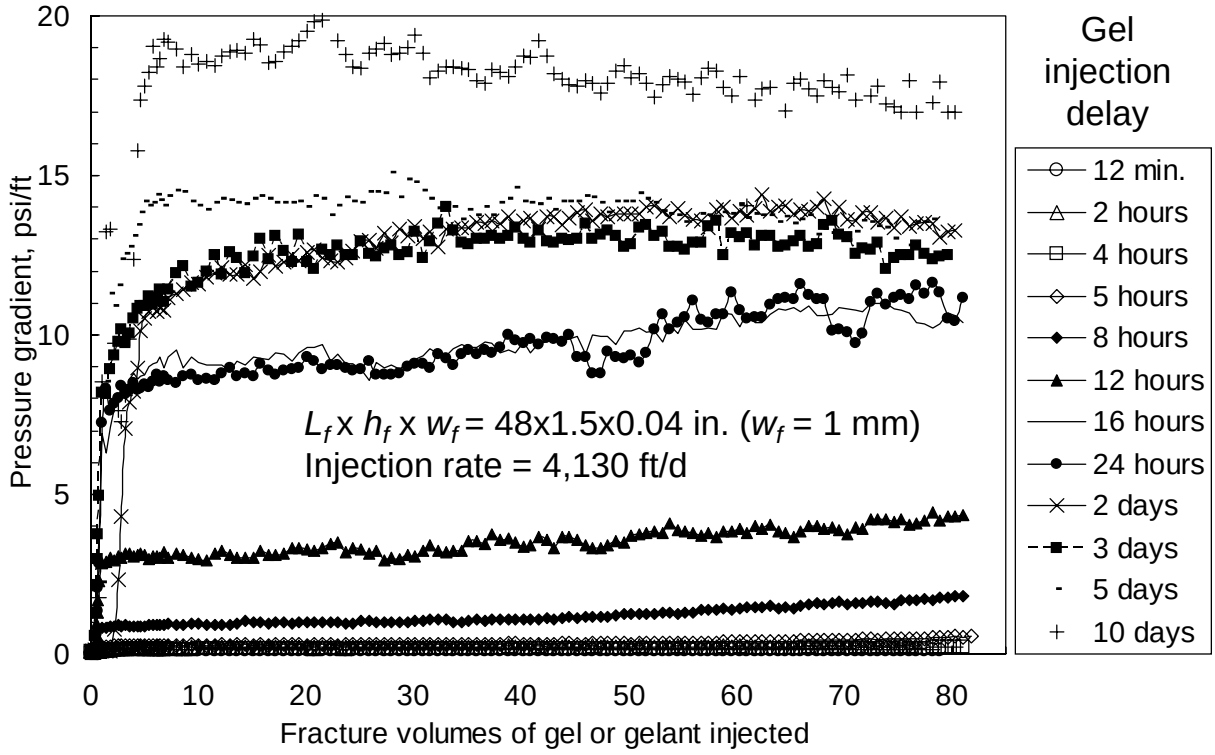

Fig. 44—Pressure gradients during gel placement.

Table 16—Final pressure gradients at the end of gel/gelant placement.

Delay time before injection	Final pressure gradient, psi/ft
12 minutes	0.13
2 hours	0.23
4 hours	0.20
5 hours	0.55
8 hours	1.82
12 hours	4.4
16 hours	10.4
24 hours	11.2
2 days	13.3
3 days	12.5
5 days	13.5
10 days	17.0

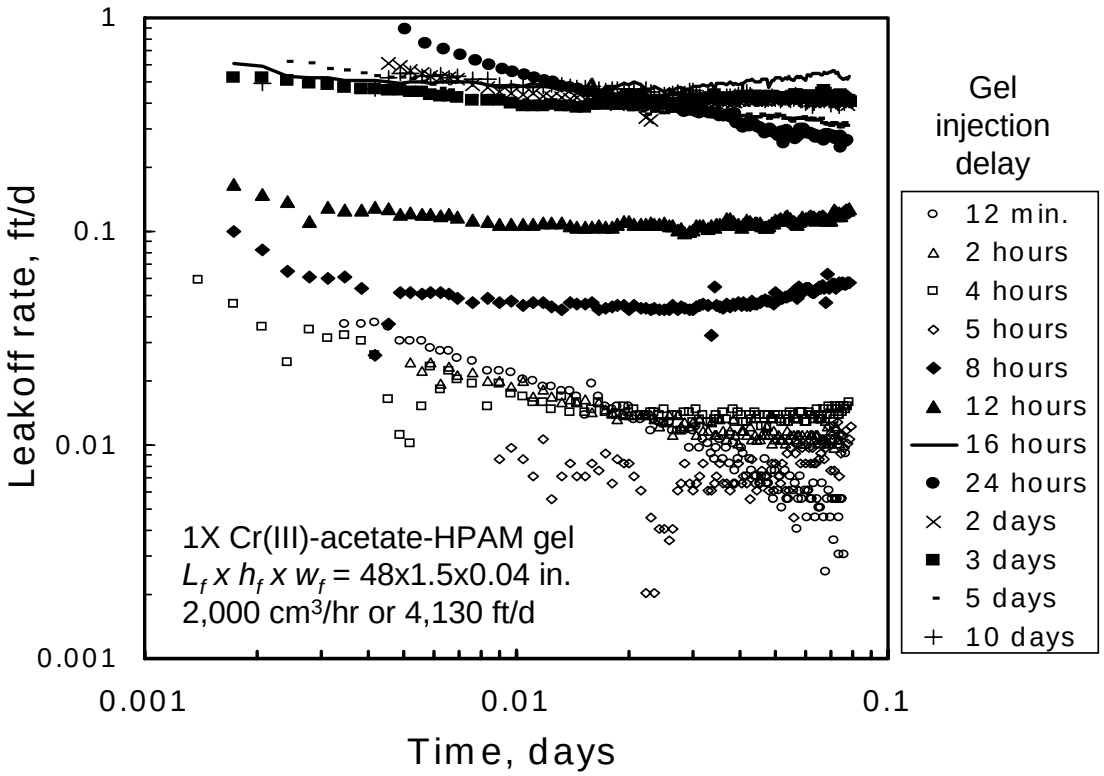

Fig. 45—Leakoff rates (in $ft^3/ft^2/d$ or ft/d) during gelant/gel injection.

First Brine Injection after Gel Placement

After placement, the cores were shut in for one day. Next, brine was injected at a low rate of 100 cm^3/hr (206 ft/d effective average velocity in the fracture). Fig. 46 plots pressure gradients (in the middle 60% of the fractured core) during this first brine injection after gel placement. Commonly, the pressure gradient rose to a maximum, followed by a rapid decline to approach a stabilized value. Table 17 lists peak (or maximum) values from the experiments along with the pressure gradient at the end of brine injection at 206 ft/d (100 cm^3/d). Presumably, the peak pressure gradients indicate the first breach of the gel in the fracture. These peaks typically occurred within the first 0.5 fracture volumes of gel injection.

For injection delay times from 12 minutes to 8 hours, only small peaks were noted. The peak values were only about 1.4 psi/ft for the 12-minute and 2-hour experiments and about 3.5 psi/ft for the 4-, 5-, and 8-hour experiments. The highest peaks occurred for the 12-, 16-, and 24-hour delays, with maximum pressure gradients ranging from 5.2 to 8.2 psi/ft. Incidentally, for our previous experiments using 24-hour delays, the peak pressure gradient during brine injection was typically about the same as the pressure gradient observed when gel was extruded into place.[13] Interestingly, for the longest delays (2 days and greater), the peak pressure gradients were noticeably lower—2 to 3.6 psi/ft.

After the peak, pressure gradients experienced some fluctuations (Fig. 46), but ended at values between 0.2 and 2.8 psi/ft. No obvious correlation was evident between the peak and final pressure gradients.

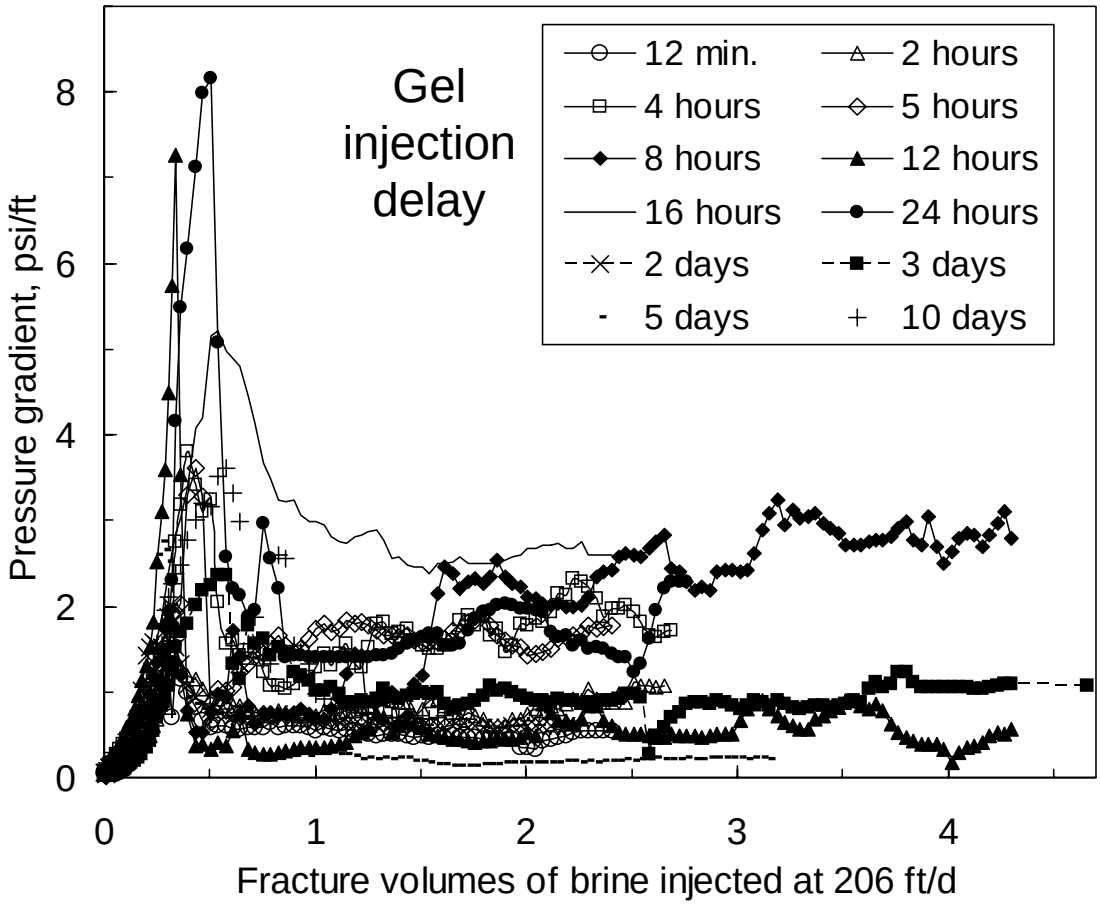

Fig. 46—Pressure gradients during first brine injection after gel placement.

Table 17—Pressure gradients during first brine flow after gel/gelant placement.

Delay time before injection	Peak pressure gradient, psi/ft	Final pressure gradient, psi/ft	Total brine injected, fracture volumes
12 minutes	1.3	0.5	2.4
2 hours	1.4	1.1	2.7
4 hours	3.8	1.7	2.7
5 hours	3.6	1.8	2.4
8 hours	3.2	2.8	4.3
12 hours	7.3	0.6	4.3
16 hours	5.2	2.6	2.6
24 hours	8.2	2.3	2.8
2 days	2.0	0.6	2.2
3 days	2.4	1.1	4.7
5 days	2.8	0.2	3.2
10 days	3.6	0.7	1.7

In interpreting the above results, we presume that the fracture was basically filled with the 1X gel for the experiments that used injection delays of 4 hours or less. For gels with longer delays, the gels were expected to experience some degree of dehydration (concentration) as they extruded through the fracture.[19] During the dehydration process, gel of the original (injected) composition formed wormhole pathways through immobile concentrated gel. During brine flow after gel placement, these wormholes provided the point of failure where the brine first breached the gel.[13] Gel in the wormholes was the first material to be displaced, while the concentrated immobile gel was more resistant to washout. These concepts were used earlier to explain the behavior for the 24-hour experiment.[13] The peak brine pressure gradient (8.2 psi/ft from Table 17) was similar to the pressure gradient observed when the gel was extruded into place (8 to 11 psi/ft from Fig. 44). The pressure gradient near the end of brine injection (2.3 psi/ft from Table 17) was substantially greater than the value expected for brine flow through an open 1-mm-wide fracture. Standard calculations for laminar flow of brine in tubes or slits[18] (coupled with the brine pressure gradients and flow rates) suggested that less than 1% of the gel washed out during brine injection. In contrast, if the entire gel mass had washed out, the brine pressure gradients should have been lower by a factor of 4,000. Thus, these observations were consistent with a small fraction of gel being displaced from wormholes, while the concentrated immobile gel remained in place to reduce fracture conductivity.

The above arguments can explain why the peak pressure gradients in Fig. 46 (i.e., the pressure gradient for first breach of gel in the fracture) generally increased with increased injection delay up to 24 hours. Presumably, more concentrated immobile gel formed with increased injection delay—leading to less wormhole area and greater resistance to first gel breach. However, this logic does not explain why the peak pressure gradient decreased for delay times greater than 24 hours. Also, it does not explain why all the final pressure gradients were fairly similar (in the range from 0.2 to 2.8 psi/ft, with no obvious correlation to injection delay). Concerning the decrease in peak pressure gradients after 24 hours, it seems possible that mechanical degradation may be more important during extrusion for the longer delay times. Presumably during gel extrusion, bonds are being broken. This breakage is balanced to some extent by reformation of bonds by reaction of polymer with free Cr(III). In the early stages (perhaps before 24 hours) enough free chromium may be present to ultimately form a strong gel structure. However, for longer injection delays (i.e., after 24 hours) insufficient free chromium may be present to repair degradation caused during extrustion.

Pressure Gradients for Other Brine Rates

After brine injection at 100 cm^3/hr (206 ft/d), the injection rate was doubled, and the measurements were repeated. This process was repeated in stages up to a final brine flow rate of 16,000 cm^3/hr (33,000 ft/d). The final stabilized pressure gradients at other brine rates are shown in Figs. 47 and 48. In Fig. 47, the heavy solid line indicates the behavior expected if the core contained no fracture, while the dashed line shows the behavior if the fracture was open and unaffected by the gel. In all experiments, the pressure gradients were substantially larger (by factors ranging from 65 to 8,600) than the values expected for an open fracture. Consequently, all gels caused significant conductivity reductions in the fracture. In particular, residual resistance factors ranged from 2,000 to 8,600 at 100 cm^3/hr and from 65 to 337 at 16,000 cm^3/hr.

Fig. 48 shows the same information with a greatly reduced range plotted on the *y*-axis. For most of the data curves, the pressure gradient varied with rate raised to the 0.3 power. This variation indicates that some incremental erosion of the gel occurred with each increase in brine injection rate. If no gel erosion occurred, the slopes of the curves should have been unity.

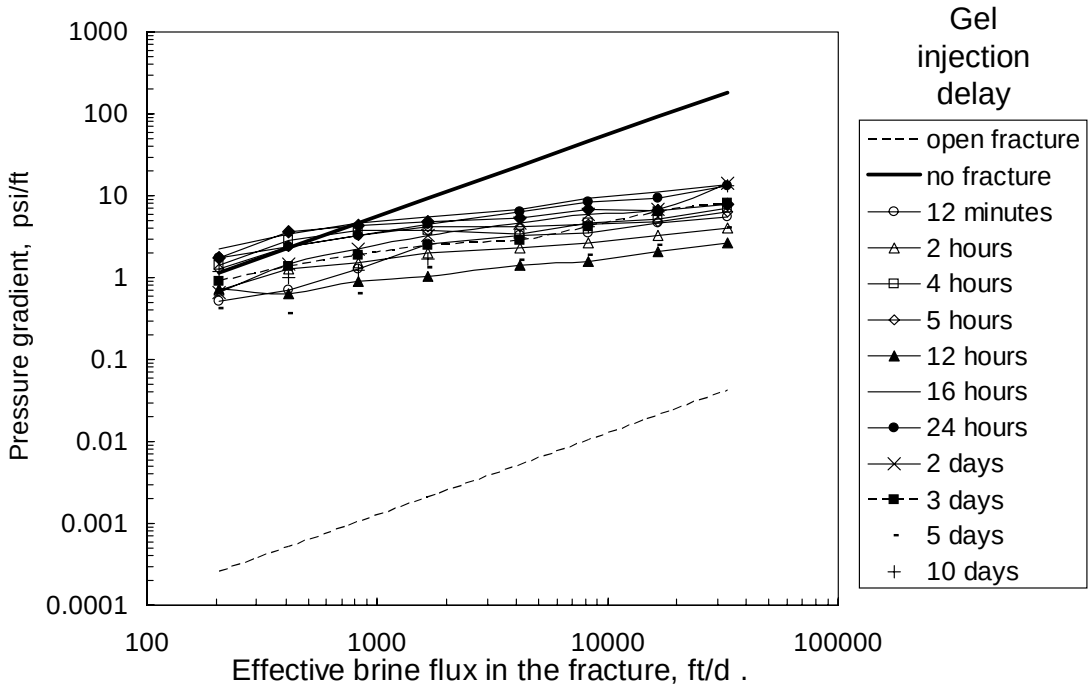

Fig. 47—Final stabilized pressure gradients at various brine rates.

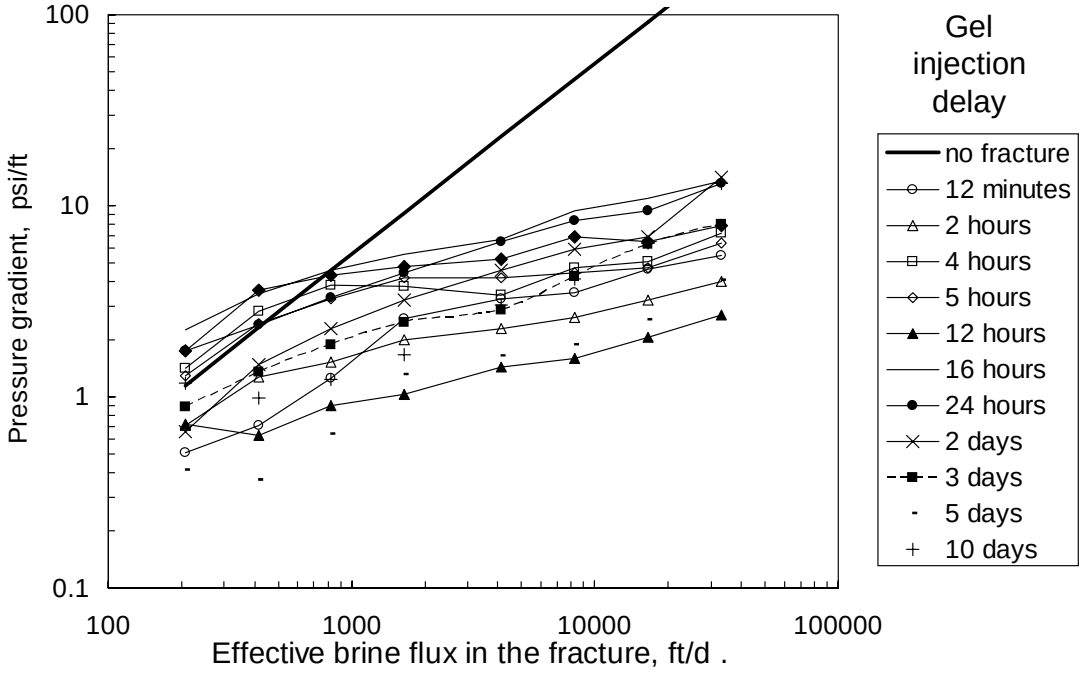

Fig. 48—Final stabilized pressure gradients at various brine rates: reduced range.

For a given brine injection rate, the pressure gradients generally increased with increased injection delay up to 24 hours. For injection delays beyond 24 hours, the pressure gradients were lower. The 12-hour experiment provided a notable exception (solid triangles in Fig. 48). In this case, perhaps the large pressure peak during first brine injection (Fig. 46) displaced more gel than normal from the fracture.

For a given brine injection rate, the largest pressure gradient (typically associated with the 16-hour delay) was 5 to 6 times greater than the lowest pressure gradient (typically associated with the 12-hour delay). Presumably, brine forced at least one pathway through the gel for each experiment shown in Fig. 48. Although the exact shapes of these pathways are not known, we note that flow capacity varies with the third power of width for slit openings and with the fourth power of diameter for circular openings. Consequently, the width of the brine pathway (through the gel) for the 12-hour experiment should be no more than twice that for the 16-hour experiment. Thus, the data curves in Fig. 48 represent a relatively narrow range of brine pathways sizes. For example, assuming tube-shaped brine pathways, the diameters ranged from 0.07 to 0.11 cm for the experiments at 16,000 cm^3/hr (33,000 ft/d) in Fig. 48.

The maximum pressure gradient observed at any given brine injection rate is plotted in Fig. 49 for each of the experiments. At the lowest rate (206 ft/d or 100 cm^3/hr), the maximum pressure gradients were often much larger (by factors up to 11) than the corresponding final stabilized pressure gradients from Fig. 48. This occurred because the gel was first breached during brine injection at this rate. At higher rates, the maximum pressure gradients paralleled and were moderately higher (typically by factors from 1.3 to 2) than the corresponding stabilized values from Fig. 48.

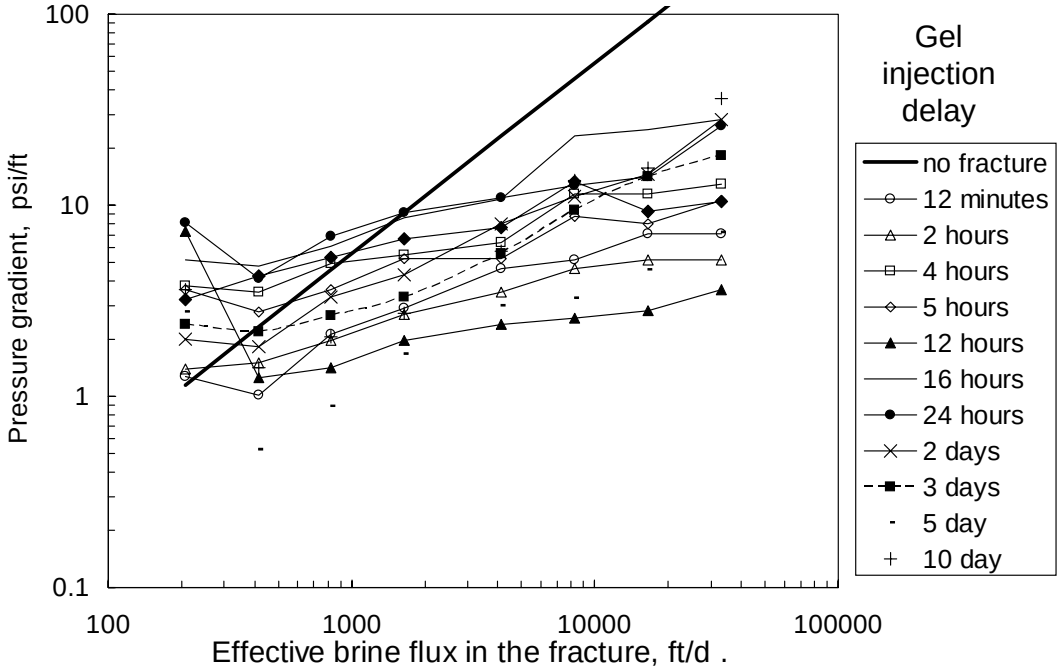

Fig. 49—Maximum pressure gradients at various brine rates.

Flow Diversion

How effectively did the gel divert brine flow into the matrix instead of the fracture? Fig. 50 plots the percent of the brine that was produced from the matrix during the various experiments.

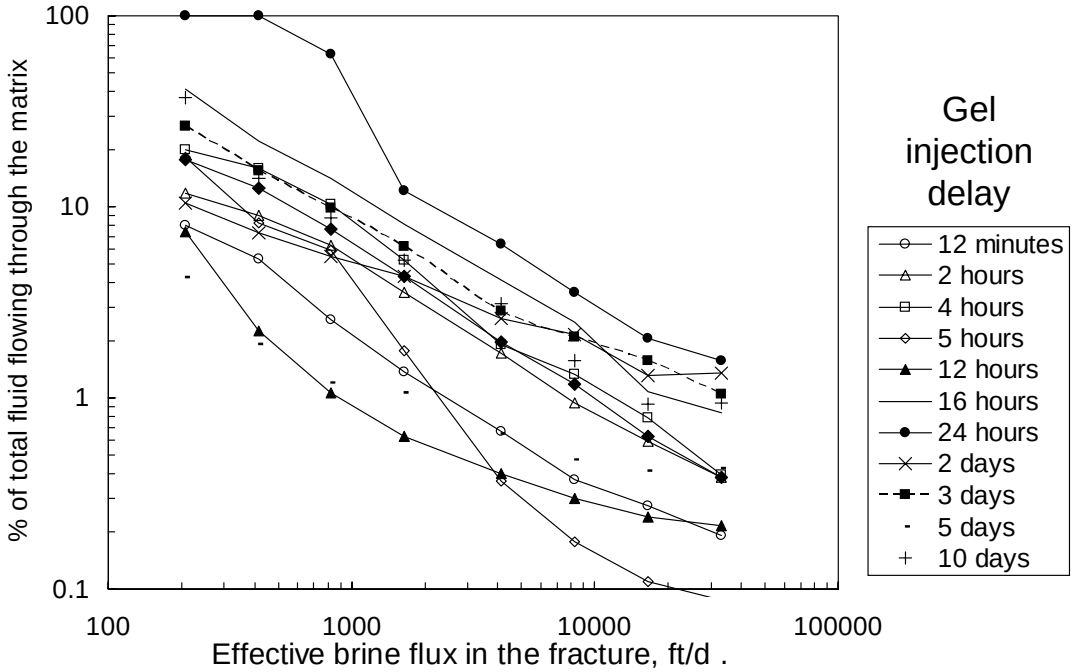

Fig. 50—Percent of brine flowing through the matrix.

The 24-hour experiment showed the best behavior, with 100% of the brine being forced to flow through the matrix (i.e., no flow occurred in the fracture) at rates of 413 ft/d and lower. In general, longer gel injection delays (up to 24 hours) lead to better fluid diversion. (The 12-hour experiment was a notable exception.) For all injection delays, the favorable diversion properties deteriorated substantially upon exposure to successively greater brine injection rates.

Conclusions

For our 1X Cr(III)-acetate-HPAM gel (with 0.5% Alcoflood 935, 0.0417% Cr(III) acetate at 41°C), the following conclusions were reached during a study of the effects of gelant/gel aging (i.e., delay between gelant preparation and subsequent injection into a fractured core) on the extrusion, leakoff, and washout properties in 1-mm-wide fractures:

1. Leakoff rates and pressure gradients during gel extrusion increased most significantly between 5 hours (i.e., the gelation time) and 16 hours after gelant preparation.
2. For gelant injection delays less than 5 hours and for gel injection delays greater than 16 hours, leakoff rates and pressure gradients were relatively insensitive to the aging time.
3. During first brine injection after gel placement, the pressure gradient where brine first breached the gel was greatest (~8 psi/ft) for the gel that was aged from 12 to 24 hours before injection. Significantly lower breaching pressure gradients were seen at either longer or shorter injection delays.

4. After breaching the gel during brine injection at 206 ft/d, the pressure gradient declined to a final stabilized value around 2.5 psi/ft for gels aged from 16 to 24 hours.
5. As brine injection rate increased to 33,000 ft/d, the stabilized pressure gradient increased in proportion to rate raised to the 0.3 power. This behavior was not sensitive to injection delay.
6. For a given brine injection rate, the stabilized pressure gradient was generally greatest for gels aged from 16 to 24 hours before injection. However, when comparing behavior for gel aging times between 12 minutes and 10 days at a given rate, the largest stabilized pressure gradient was no more than 6 times greater than the smallest pressure gradient.
7. Gels aged from 16 to 24 hours showed the maximum diversion of brine into the matrix (i.e., minimized brine flow through the fracture). Regardless of injection delay, the diversion provided by the gels deteriorated substantially as the brine rate increased to 33,000 ft/d.

7. USE OF SWELLING POLYMERS TO PLUG FRACTURES

Addition of Partially Dissolved Alcoflood 935 HPAM

We explored the use of swelling polymers to plug fractures. In particular, suspensions of powder-form polymers (Alcoflood 935 HPAM) were quickly prepared and injected before they had a chance to dissolve fully. Hopefully, the partially dissolved polymer "fisheyes" would lodge and swell to plug the fracture. Several experiments were performed to investigate this idea. All experiments used 1-mm-wide (0.04-in.) fractures in 4-ft-long Berea sandstone cores. All mixtures had total polymer concentration of 0.5% and contained 1% NaCl and 0.1% $CaCl_2$. The polymer or gel placement rate was 2,000 cm^3/hr or 4,130 ft/d, and the temperature was 41°C.

In the first experiment (referred to as "fisheye polymer without Cr"), powder-form polymer was rapidly added to a swirling vortex of brine, placed in our ISCO pumps, and injected into a fractured core. Only 15 minutes elapsed between the first addition of polymer to the brine and the start of injection. In Figs. 51 and 53-56, open circles show data points for this case.

In the second experiment (referred to as "$CrCl_3$ added to fisheye polymer"), the procedure was identical to that for the first experiment, except that sufficient $CrCl_3$ was added immediately after polymer addition to make the $CrCl_3$ concentration 0.0513%. In Figs. 51 and 53-56, open triangles show data points associated with this case.

In the third experiment (referred to as "fisheye polymer & $CrCl_3$ mixed on the fly"), the procedure was identical to that for the second experiment, except that the polymer and $CrCl_3$ mixtures/solutions were pumped separately and plumbed to mix just before entering the fractured core. Again, the final $CrCl_3$ concentration was 0.0513%. Data points for this case are represented by open squares in Figs. 51 and 53-56.

These three cases were compared with results obtained previously using a pre-formed 1-day-old Cr(III)-acetate-HPAM gel [0.5% HPAM, 0.0417% Cr(III) acetate] that was extruded into place (solid circles in Figs. 51 and 54-56).

Pressure Gradients during Gel Injection. Fig. 51 plots the pressure gradients (averaged over the middle 60% of the 4-ft-long fracture) for each of the cases during the course of injecting 80 fracture volumes (3,700 cm^3) of gel or polymer formulation at 2,000 cm^3/hr (4,130 ft/d). For the formed gel (solid circles), the pressure gradient rapidly stabilized at 13 psi/ft. In contrast, for the three "fisheye polymer" cases, pressure gradients were very low for the first 75 fracture volumes of injection and rose only near the end of the injection process. These "fisheye" formulations experienced severe gravity segregation so that the polymer globs quickly settled to the bottom of the pump cylinder—and therefore were the last part of the fluid injected. The highest final pressure gradient (76 psi/ft) occurred for the second fisheye experiment, where $CrCl_3$ was mixed with the polymer before injection. (This formulation showed pressure fluctuations beginning at 40 fracture volumes—presumably indicating entry of the first polymer globs into the fracture.) The lowest final pressure gradient (1.8 psi/ft) was noted at the end of injection of the first fisheye experiment, where no chromium was added.

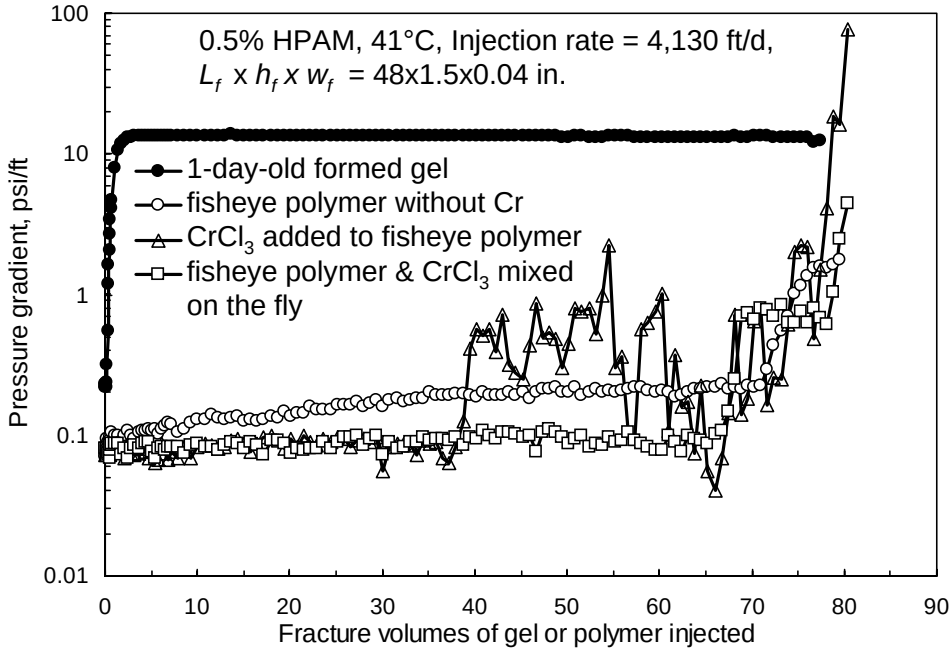

Fig. 51—Pressure gradients during gel or polymer placement.

Fig. 52 plots the pressure gradients (near the end of the injection process) in each of the five sections of the fracture for the second fisheye experiment, where $CrCl_3$ was mixed with the polymer before injection. Confirming an observation from Fig. 51, the highest pressure gradients occurred at the end of the injection process. Interestingly, at any given time, the pressure gradients were generally fairly uniform in the five fracture sections. One might have expected higher pressures gradients in the first sections of the fracture.

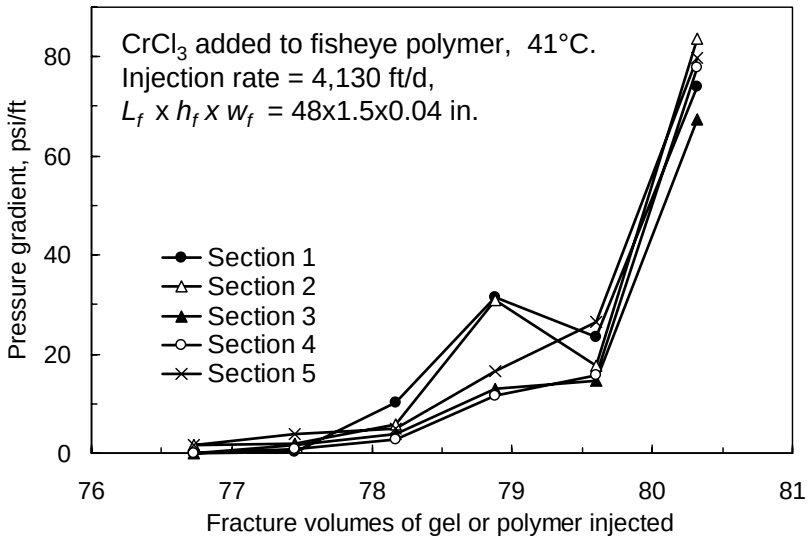

Fig. 52—Pressure gradients near the end of the second fisheye experiment.

Leakoff Rates. Leakoff rates during the course of the four experiments are plotted in Fig. 53. The solid curve shows leakoff rates versus time for extrusion of a formed gel.[19] The open symbols show leakoff results from the fisheye experiments. Except at the end of the second fisheye experiment (open triangles), the leakoff rates during placement of the fisheye polymer mixtures were dramatically lower than those during extrusion of the formed gel. Leakoff rates for the fisheye polymer without chromium (i.e., the first fisheye experiment) were less than 0.01 ft/d throughout the injection process. The low pressure gradients during most of the fisheye experiments (i.e., less than 1 psi/ft from Fig. 51) provided virtually no pressure difference between the fracture and the porous rock, and consequently, little potential for fluid leak off and gel dehydration. In contrast, the pressure gradient during extrusion of the formed gel (13 psi/ft) resulted in significant leakoff and gel dehydration.

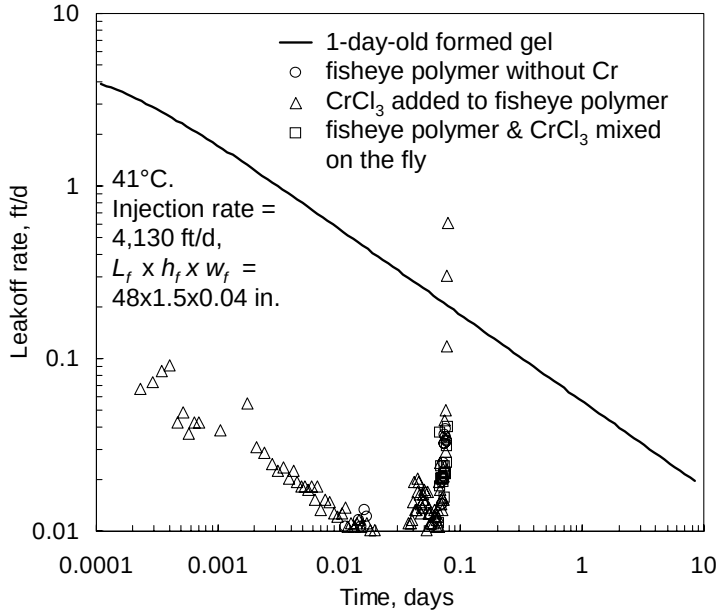

Fig. 53—Leakoff rates during placement of the fisheye formulations.

First Brine Injection. After placement of the gel or fisheye polymer, the fractured cores were shut in for one day at 41°C. Then, brine was injected at 100 cm^3/hr (206 ft/d effective average velocity in the fracture). Fig. 54 plots pressure gradients during the course of this first brine injection. The solid circles show the results for brine injection after placement of the formed gel. In this case, the pressure gradient rose to a sharp peak of 8.2 psi/ft at 0.5 fracture volumes. This peak pressure gradient (associated with first failure or mobilization of the gel) was a bit lower than the 13 psi/ft observed during extrusion of the gel into the fracture (Fig. 51). After the peak value, the pressure gradient dropped rapidly to about 2 psi/ft. In contrast, for the first fisheye experiment where no chromium was used (open circles), the pressure gradients remained near 0.03 psi/ft during the entire course of brine injection.

The most favorable result was noted for the second fisheye experiment, where $CrCl_3$ was added to the polymer (open triangles). Here the peak pressure gradient was 9.7 psi/ft (at 0.7 fracture volumes of brine). Rather than dropping sharply after the peak, the pressure gradients decreased

gradually to 8 psi/ft after 2.7 fracture volumes. Interestingly, the peak pressure gradient for this case was substantially lower than the final pressure gradient observed during polymer placement (76 psi/ft from Fig. 51).

Results from the third fisheye experiment (polymer and $CrCl_3$ mixed on the fly) were intermediate in behavior (open squares in Fig. 54). The pressure gradient peaked at 5.0 psi/ft (comparable to 4.4 psi/ft at the end of polymer placement shown in Fig. 51) and then declined to 2.3 psi/ft.

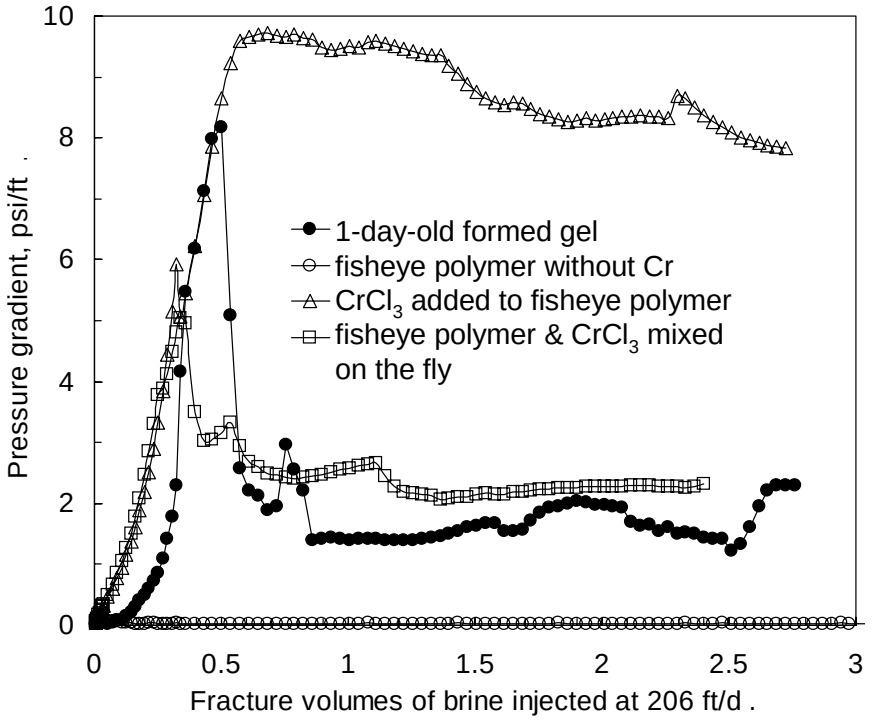

Fig. 54—Pressure gradients during first brine injection after polymer or gel placement.

Other Rates. For each experiment, after obtaining the results shown in Fig. 54, the brine injection rate was doubled and pressure gradients were monitored until they stabilized. Then, the rate was doubled again. This process was repeated in steps to a maximum brine injection rate of 16,000 cm^3/hr (33,100 ft/d). For each step, the final stabilized pressure gradient was converted to a composite permeability for the gel-treated fractured core. In turn, this value was divided by the permeability of the matrix rock (~700 md) to provide a measure of the degree of gel failure. This permeability ratio is plotted on the *y*-axis of Fig. 55. If the gel healed the fracture without damaging the porous rock, this permeability ratio would have a value of unity. If the permeability ratio is greater than one, the fracture must be open to some extent. As the permeability ratio increases, a greater degree of polymer or gel failure is indicated. Thus, resistance to failure increases as the curves progress to the right side of Fig. 55. The first fisheye polymer treatment (without chromium) showed the least resistance to failure, while the second fisheye treatment (open triangles) showed the greatest resistance.

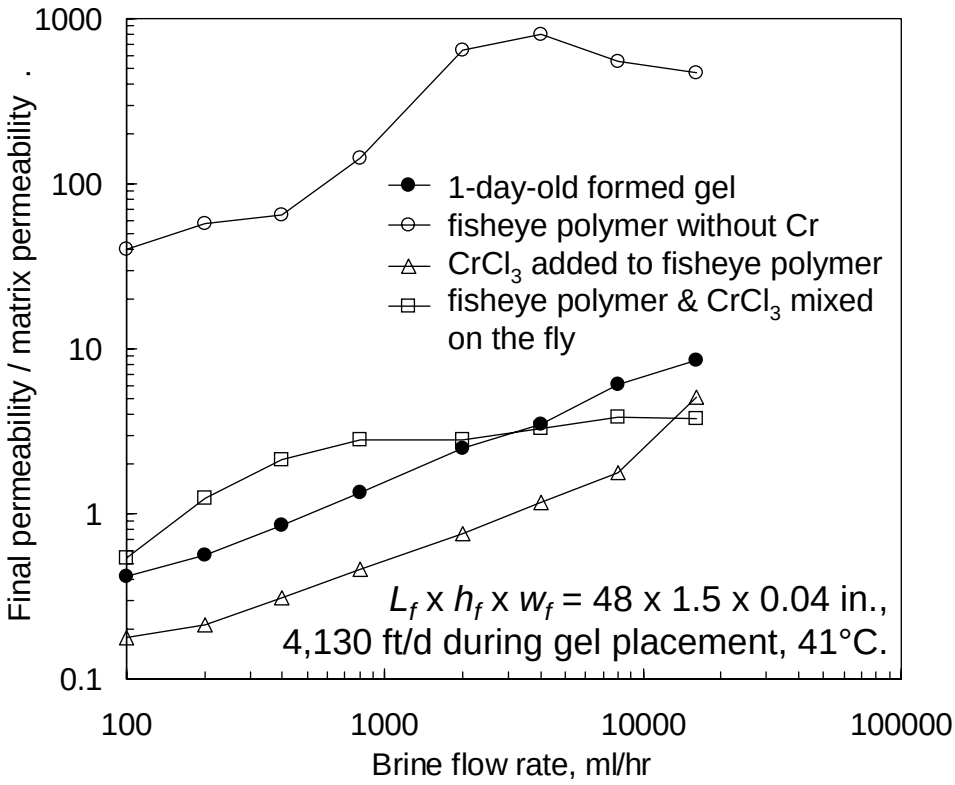

Fig. 55—Effect of brine rate on final permeabilities for fisheye polymers and gels.

Diversion. Another measure of gel failure is the fraction of the fluid produced from the fracture versus from the matrix during brine injection at various rates. These results are plotted in Fig. 56 for the four experiments. A high fractional flow through the matrix is desirable, since that indicates effective plugging of the fracture and brine diversion into the matrix. For brine rates up to 400 ft/d, Fig. 56 suggests that the third fisheye experiment (polymer and $CrCl_3$ mixed on the fly) exhibited the most complete plugging of the fracture. However, for higher rates, the second fisheye experiment (polymer and $CrCl_3$ mixed as a batch before injection) showed the best results.

At the end of the experiments, the fractures were opened to view the polymer/gel lodged within. Contrary to previous experiments involving extrusion of formed gels,[13] we did not see signs of brine wormholes through concentrated gel. Instead, polymer globs were distributed fairly uniformly throughout the fracture.

In summary, injection of fisheye (i.e., swelling or incompletely dissolved) polymer has potential for plugging fractures and deserves further investigation. However, results to date indicate that this method is ineffective unless a crosslinker (e.g., $CrCl_3$) is included. These formulations experienced severe gravity segregation, so that the polymer concentrated in the bottom 10% of the pump volume and was the last material injected into the fracture.

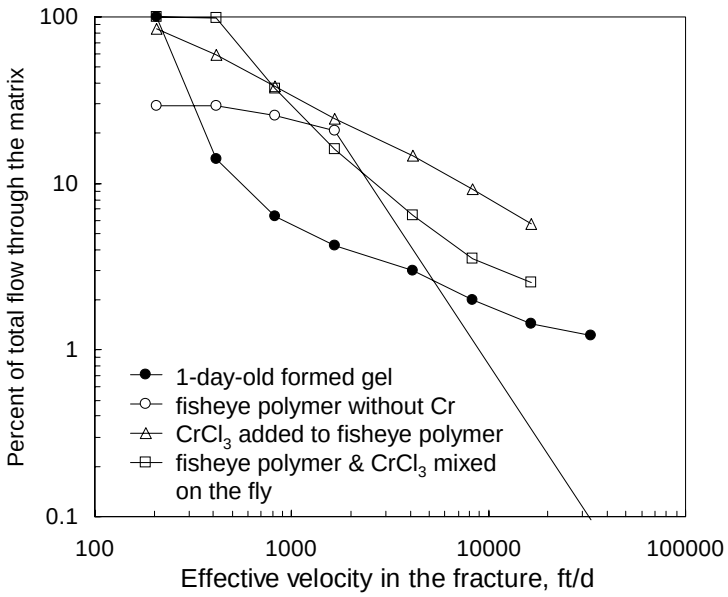

Fig. 56—Percent of brine flow through matrix after polymer or gel placement.

Alcosorb Polymers

Our initial polymer choice (Alcoflood 935) may not have been optimum for this application. Therefore, we wished to study polymers that were designed more specifically to swell after contacting water. With this in mind, we asked Ciba (Jim Sutphen) to recommend and provide polymers that might work in our intended application. In response, Ciba kindly provided two polymers, Alcosorb 400™ and AlcosorbAB3C™. For each polymer, we prepared formulations that contained 0.5% polymer, 0.0513% $CrCl_3$, 1% NaCl, and 0.1% $CaCl_2$. These formulations were injected immediately after preparation. (The typical delay time between chromium addition and injection into the fracture was 10 to 15 minutes.) All experiments were performed at 41°C.

Pressure Gradients during Gel Injection. We performed a series of tests that were analogous to those for the fisheye polymers described above. In all cases, the fractures were 4-ft long and 1.5-in. high. Also, 3,700 cm^3 of the polymer formulation were injected at a rate of 2,000 cm^3/hr. Fig. 57 plots pressure gradients during injection of the polymer formulations. The open circles and triangles show results when injecting the Alcosorb 400 and Alcosorb AB3C into 1-mm-wide fractures. In both cases, pressure gradients were relatively low until the last portions of the formulation were injected. Then, the pressure gradients rose abruptly, resulting in rupture of the core. Even though the polymer formulations were well mixed, gravity segregation rapidly occurred after they were placed in the pumps. Consequently, mostly water was injected during the first part of the experiment, resulting in low pressure gradients for the first part of Fig. 57. When the concentrated polymer finally entered the fracture, pressure gradients quickly rose to high values, breaking the core.

These experiments were repeated in 4-mm-wide fractures (open squares and diamonds in Fig. 57). Similar behavior was observed, although the entire 3,700 cm^3 was placed (for both Alcosorb 400 and Alcosorb AB3C) without breaking the cores. A comparison of Figs. 51 and 57 reveals qualitatively similar behavior for the Alcosorb polymers and the fisheye gels. In contrast, the

solid symbols in Fig. 57 show the pressure gradients during placement of our standard 1-day-old 1X Alcoflood 935 gel in 1-mm- and 4-mm-wide fractures. Note that the Alcoflood 935 gel showed stable pressure gradients once brine was displaced from the fracture (i.e., no sharp increase in pressure gradient occurred near the end of gel injection).

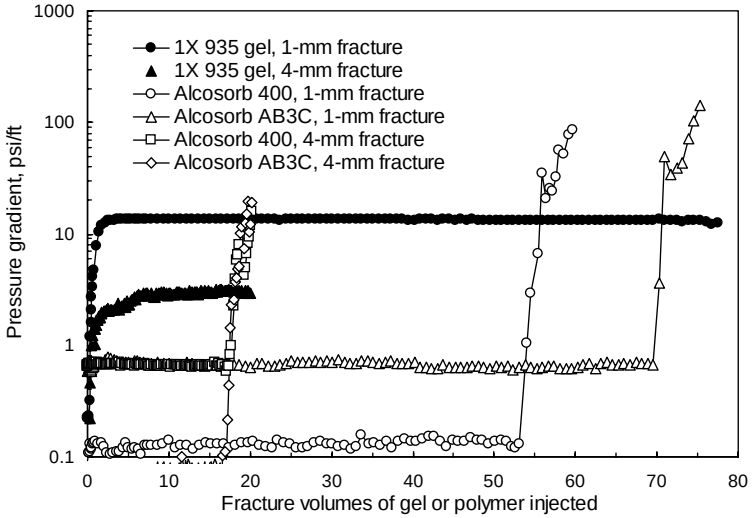

Fig. 57—Pressure gradients during Alcosorb placement.

Leakoff Rates. Leakoff rates during injection of the Alcosorb polymers are shown in Fig. 58. In both 1-mm- and 4-mm-wide fractures, the leakoff rates were quite low during the entire injection process. Recall from Fig. 53 that the leakoff rates during injection of the fisheye polymers were also generally low. In contrast, during extrusion of the formed 1X Alcoflood 935 gel, leakoff rates were much higher in both 1-mm- and 4-mm-wide fractures (Fig. 58).

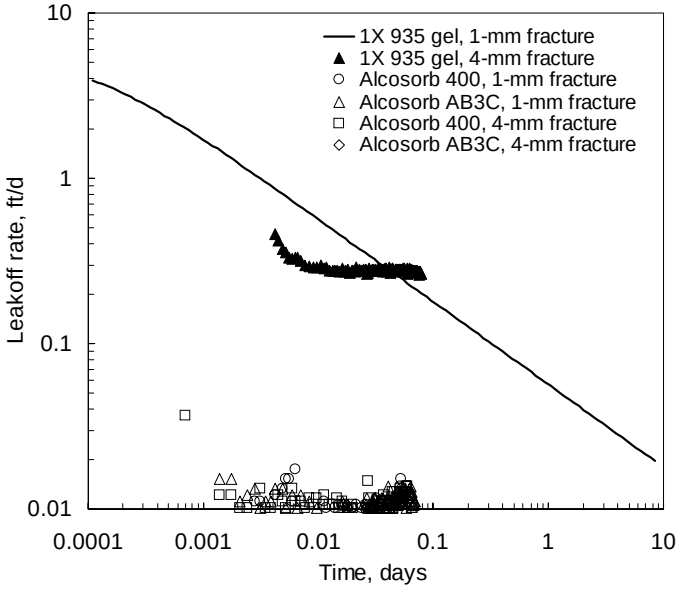

Fig. 58—Leakoff rates during placement of Alcosorb formulations.

First Brine Injection. After polymer placement and a 1-day shut-in, brine (1% NaCl, 0.1% $CaCl_2$) was injected at 100 cm^3/hr. For both Alcosorb polymers (Fig. 59), the peak pressure gradients during first brine injection (6 to 12 psi/ft) were significantly greater than those for the 1X Alcoflood 935 gel (2.8 psi/ft maximum) in 4-mm-wide fractures. (Recall that the cores with 1-mm fractures broke when injecting Alcosorb polymers, so no brine results were available.)

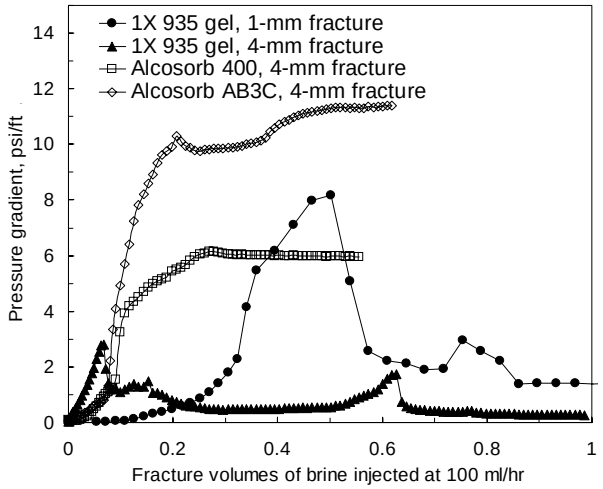

Fig. 59—Pressure gradients during first brine injection after Alcosorb placement.

Other Rates. Subsequently, the brine injection rates were increased in stages to a maximum of 16,000 cm^3/hr. Fig. 60 plots the final permeability of the polymer/gel-treated fractured cores relative to the permeability of the Berea sandstone rock (700 md). As mentioned earlier for this type of plot (Fig. 55), we desire polymers and gels that provide low permeability ratios at all rates. In 4-mm-wide fractures, Fig. 60 indicates that both Alcosorb polymers provided lower permeability ratios than the 1X Alcoflood 935 gel up to ~2,000 cm^3/hr. Interestingly, at higher rates, the 1X Alcoflood 935 gel provided better performance.

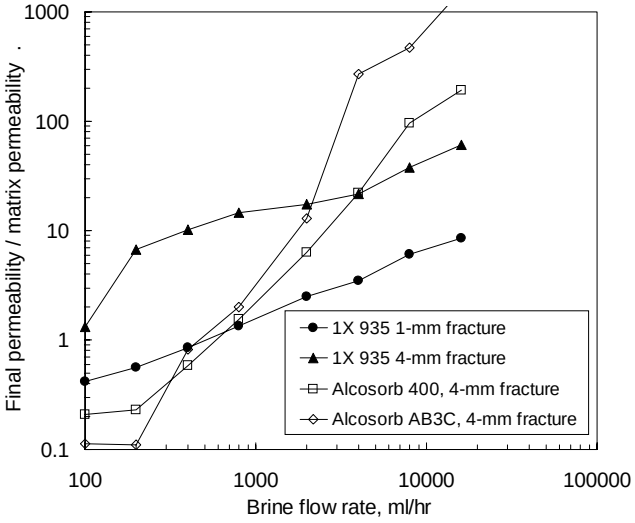

Fig. 60—Effect of brine rate on final permeabilities for Alcosorb.

Diversion. Ideally, a gel treatment will stop flow through the fracture and divert brine so that it must flow through the rock matrix. Fig. 61 shows the fraction of brine that was produced from the matrix for each injection rate. For the Alcosorb polymers, some odd variations occurred, in that the fraction of brine flowing through the matrix did not always decrease with increased injection rate. Perhaps, this result was caused by fortuitous mobilization and re-entrainment of gel. Nevertheless, in 4-mm-wide fractures, the diversion performance of the Alcosorb polymers was not generally significantly better than that for the 1X Alcoflood 935 gel. Again, ideally, we desire 100% of the brine to be forced through the matrix (so that the fracture is effectively "healed").

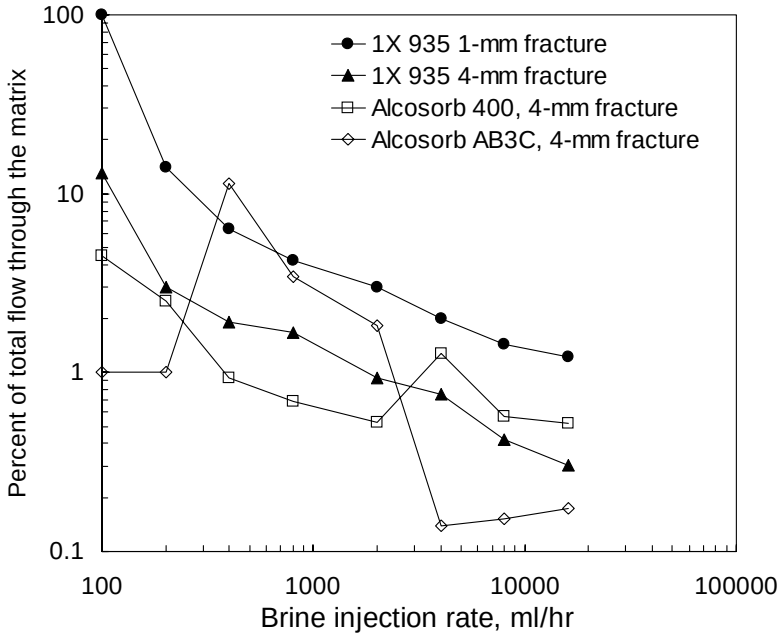

Fig. 61—Percent of brine flow through matrix after Alcosorb placement.

PolyCrystal or Diamond Seal

Halliburton indicated that they also had a swelling polymer, called PolyCrystal or Diamond Seal™. This material is a dehydrated crystal of a copolymer. (The exact composition was not specified.) A field application of this material is discussed in Ref. 25. Prentice Creel of Halliburton was kind enough to provide us with a sample of this material. We tested this material using the same procedures described above, except that the formulations contained 2.5% Diamond Seal, 1% NaCl, and 0.1% $CaCl_2$ in water. This concentration of Diamond Seal was selected because we observed the material to swell by a factor of 40 when placed in our brine. Thus, 2.5% Diamond Seal left little free water standing with the gel, and gravity segregation was not a problem.

The dry Diamond Seal granules were typically 2 mm to 4 mm in diameter. Thus, we chose to inject the Diamond Seal formulations into 2-mm- and 4-mm-wide fractures (both 4-ft long and 1.5-in. high). We felt that 1-mm-wide fractures were too narrow for the material to propagate effectively, although this limitation probably could have been circumvented by simply grinding the dry granules to a smaller size.

Pressure Gradients during Gel Injection. During injection at 2,000 cm^3/hr into a 2-mm-wide fracture, the Diamond Seal exhibited a fairly stable pressure gradient of about 12 psi/ft for the first 3,000 cm^3 (~30 fracture volumes) of injection (open squares in Fig. 62). For comparison, the 1X Alcoflood 935 gel showed a pressure gradient of 4 psi/ft in a 2-mm-wide fracture at the same rate (solid squares in Fig. 62). Interestingly, for the final volume of Diamond seal injected into the 2-mm-wide fracture, the pressure gradient shot up to 111 psi/ft. This behavior was noted in all five sections of the 4-ft-long fracture, so it did not appear to be a screen-out at one particular point. (Note the analogous behavior in Fig. 52.)

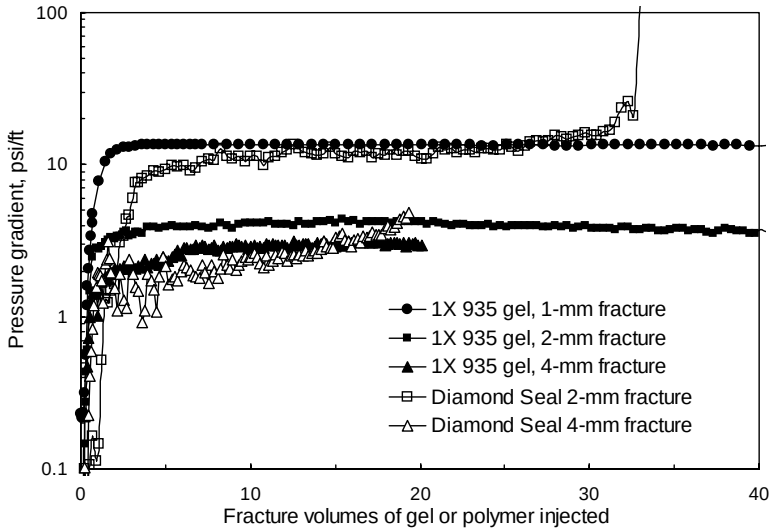

Fig. 62—Pressure gradients during Diamond Seal placement.

During Diamond Seal injection into a 4-mm-wide fracture (open triangles in Fig. 62), the pressure gradients were comparable to those for the 1X Alcoflood 935 gel (solid triangles)—roughly 3 psi/ft. However, over the course of 20 fracture volumes, the Diamond Seal showed a moderate increasing trend, while the Alcoflood 935 behavior was more stable.

Leakoff Rates. Fig. 63 compares leakoff rates during Diamond Seal injection into 2-mm- and 4-mm-wide fractures with those of the 1X Alcoflood 935 gel. Leakoff rates associated with the Diamond Seal were generally lower than those for the Alcoflood 935 gel. However, comparison of Figs. 53, 58, and 63 reveals that the leakoff rates for placement of the fisheye and Alcosorb polymers and gels were generally lower than those for the Diamond Seal formulations.

First Brine Injection. For first brine injection after gel placement, Fig. 64 compares pressure gradients for the Diamond Seal and the 1X Alcoflood 935 gels. In the 4-mm-wide fractures, the performance of the Diamond Seal was modestly better than that for the Alcoflood 935 gel. However, in the 2-mm-wide fractures, the pressure gradients associated with Diamond Seal were substantially better. At 100 cm^3/hr, the pressure gradient peaked at 18.2 psi/ft for the Diamond Seal, compared to 1.2 psi/ft for the Alcoflood 935 gel.

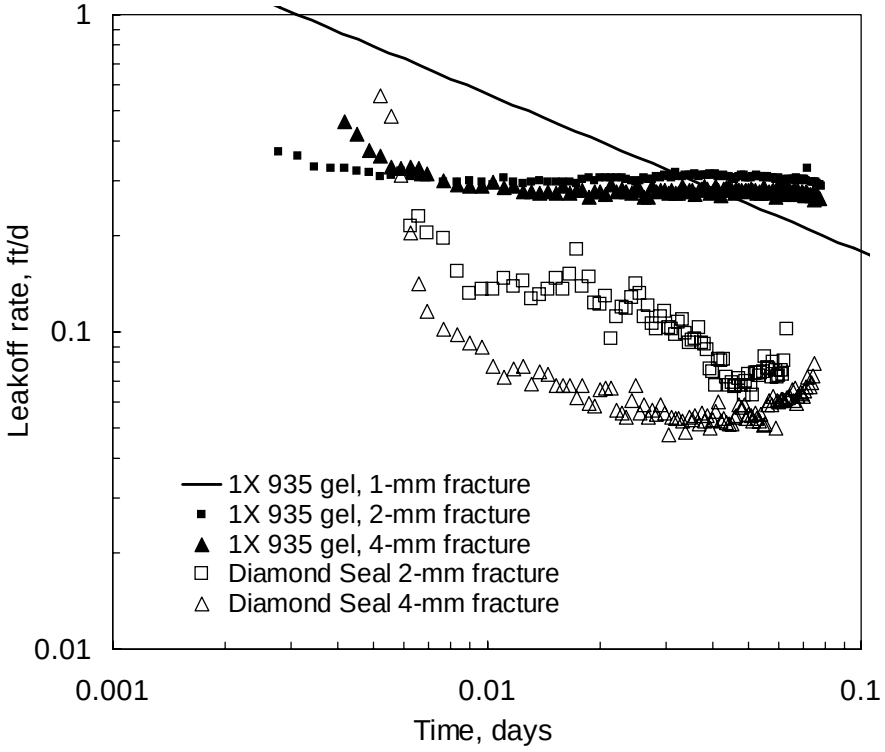

Fig. 63—Leakoff rates during placement of the Diamond Seal.

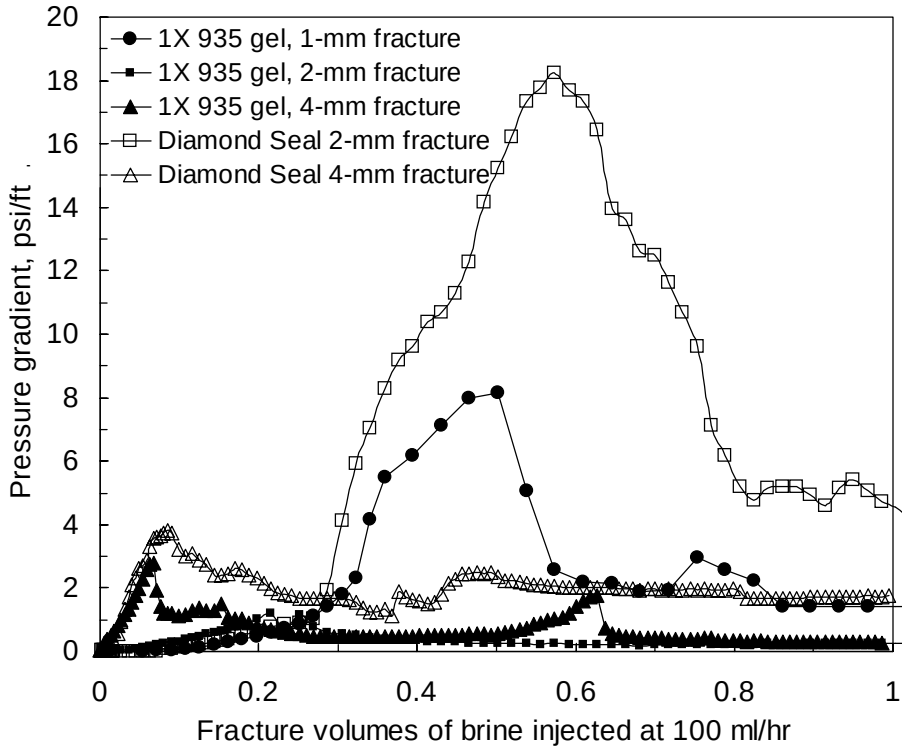

Fig. 64—Pressure gradients during first brine injection after Diamond Seal placement.

Other Rates. The final permeabilities (for the composite gel-treated fractured cores) are compared as a function of rate in Fig. 65. This figure suggests that the Diamond Seal resisted washout better than the 1X Alcoflood 935 gel for brine rates below 1,000—2,000 cm^3/hr. Above 2,000 cm^3/hr, the performance advantage shifted to the Alcoflood 935 gel. Qualitatively, a similar trend was also noted in Fig. 60.

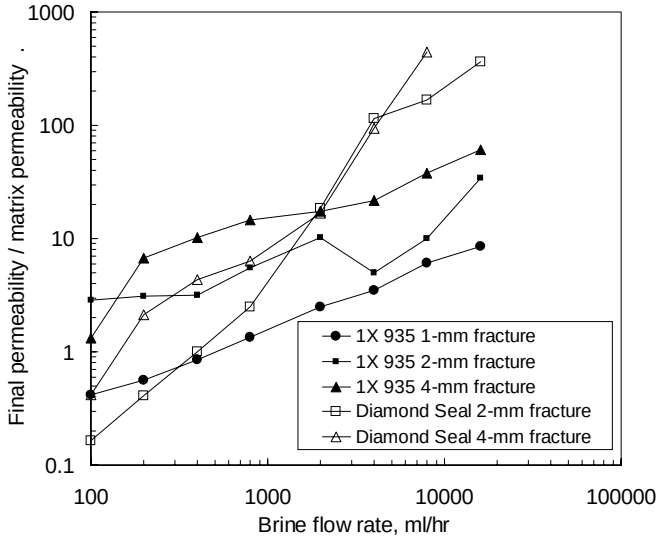

Fig. 65—Effect of brine rate on final permeabilities for Diamond Seal.

Diversion. Fig. 66 shows the fraction of brine produced from the matrix for each injection rate. In spite of the positive indications shown in Figs. 64 and 65, Fig. 66 does not suggest that the diversion behavior for Diamond Seal was superior to that for the 1X Alcoflood 935 gel.

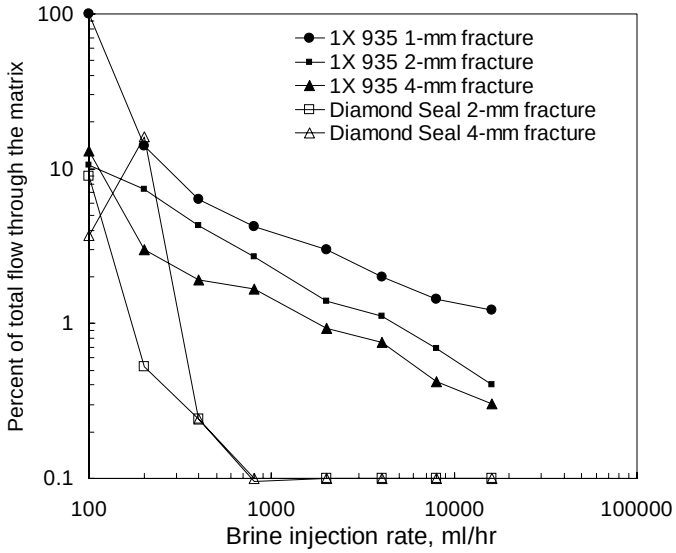

Fig. 66—Percent of brine flow through matrix after Diamond Seal placement.

Summary of Swelling Polymer Results

We compared the behavior of three types of swelling polymers with that of our standard 1-day-old 1X Cr(III)-acetate-HPAM gel (that was prepared using Alcoflood 935). The three swelling polymers included (1) undissolved Alcoflood 935 [with or without Cr(III) crosslinker], (2) Alcosorb polymers with $CrCl_3$, and (3) Diamond Seal. The undissolved Alcoflood 935 and the Alcosorb polymers showed significant problems with gravity segregation. Although the Diamond Seal used five times the concentration of the Alcoflood 935 and Alcosorb polymers, it did not exhibit a problem with gravity segregation. During first brine injection after polymer or gel placement, all three types of swelling polymers showed promise in requiring significant pressure gradients for the brine to first breach the polymer or gel. In 1-mm-wide fractures, the breaching pressure gradients were 8.2 psi/ft for the 1X Alcoflood 935 gel and 9.7 psi/ft for an undissolved Alcoflood 935 polymer that was mixed with $CrCl_3$. In 2-mm-wide fractures, the breaching pressure gradients were 1.2 psi/ft for the 1X Alcoflood 935 gel and 18.2 psi/ft for the Diamond Seal. In 4-mm-wide fractures, the breaching pressure gradients were 2.8 psi/ft for the 1X Alcoflood 935 gel, 3.7 psi/ft for the Diamond Seal, and 11.4 psi/ft for Alcosorb AB3C with $CrCl_3$. After breaching the gel, the Alcosorb and Diamond Seal formulations tended to be more effective than the 1X Alcoflood 935 gel in reducing fracture conductivity at low brine injection rates, but less effective at high rates.

Gravity Segregation for Gelants with Particulates

In several field applications, the addition of particulates to injected gelants reportedly increased the gel's resistance to failure. Thus, we are interested in identifying the optimum material to use for this purpose. In previous work,[1] we noted that suspensions of mica, nut plug, diatomaceous earth, and cellophane flakes experienced severe gravity segregation when mixed with gelants. In contrast, suspensions of fiberglass and shredded polypropylene were less prone to this problem. In continuing our search for effective particulates that will not experience severe gravity segregation, we investigated four new materials (obtained from Fiberglass Supply of Bingen, Washington): (1) strand fibers, (2) milled glass fibers (bag form), (3) milled glass fibers (canister form), and (4) acrylic deck dust. With each material, we prepared 2%, 5%, and 10% suspensions of the material using two different gelants—0.5% Alcoflood 935, 0.0417% Cr(III) acetate (Marathon's MARCIT—CT^{SM}, our standard 1X gel) and 5% Alcoflood 254S, 0.417% Cr(III) acetate (Marathon's MARASEAL^{SM}). After mixing and allowing the suspensions to gel, we noted that the particulates had settled to the bottom. The formulations visibly had a particulate-laden fraction underlying particulate-free gel. In Table 18, we record the fraction of the total formulation that was particulate-laden gel. This table suggests that the milled glass fibers (supplied in bag form) had the best suspension qualities. However, gravity segregation was significant with all of the materials.

Table 18—Fraction of gel volume laden with particulates.

Fiber type	Concentration, %	0.5% Alcoflood 935, 0.0417% Cr(III) acetate	5% Alcoflood 254S, 0.417% Cr(III) acetate
Strand	2	5%	3%
	5	15%	10%
	10	30%	20%
Milled glass (bag)	2	15%	15%
	5	33%	40%
	10	55%	80%
Milled glass (canister)	2	5%	7%
	5	10%	15%
	10	18%	18%
Acrylic deck dust	2	3%	5%
	5	10%	10%
	10	25%	20%

8. PARTIALLY FORMED GELS IN FRACTURED PRODUCTION WELLS

Introduction

During this study, we focused on water-shutoff polymer gels injected in the *partially formed* state into fractures. Ultimately, we want to consider whether our findings are applicable to other high-permeability anomalies that are connected to petroleum production wells. Other than fractures, these high-permeability anomalies could include solution channels, interconnected vugs, karsted features, joints, faults, rubblized zones, and ultra-high matrix rock permeability. These features generally have permeabilities greater than two darcies.

For water-shutoff applications in fractured productions wells (i.e., in field applications), injected polymer gels are usually in the partially formed state during transit from the wellbore into the formation. For classical fracture-plugging gel treatments, the injected polymer-gel solution should develop enough gel structure (including microgel structure) to minimize detrimental gelant leakoff into the matrix reservoir rock that is adjacent to the fracture. On the other hand, the gel should not be fully formed during initial injection because excessive pressures may be encountered. Use of partially formed gels permit manageable injectivities during placement, may provide minimum damage to matrix rock, and yet ultimately yield strong gels with good resistance to washout. Gels must be in the partially formed state when injecting gels that will ultimately be strong or rigid.

The objective of this chapter is to characterize the performance of polymer gels that are injected into fractures in the partially formed state. The intent was to investigate near-wellbore gel properties for a small-volume gel treatment (treatment pumped in less than a day) in a fractured production well. Thus, during our experiments, a relatively large number (on the order of 40) of fracture volumes (FV) of gel were injected as rapidly as possible into the fracture (injected within about seven minutes). An explicit goal was to minimize time-dependent gel dehydration,[24] and in turn, minimize the associated gel wormhole formation. By injecting the partially formed gel rapidly, gel dehydration was minimized. As will be noted later in this chapter, the gels in the fractures at the end of our flooding experiments were 1.2 to 2.5 times more concentrated than the injected gels.

Experimental

All but one of the flooding experiments were conducted in 1.5-in. by 1.5-in. by 2.0-ft long rectangular, 700-md, 19% porosity, unfired Berea sandstone cores, where a 1-mm (0.04-in.) clean-sawed fracture ran down the middle of the length of the sandstone core. An earlier study[24] showed that it makes little difference for this type of experiment whether the fracture surface is “rough” (as occurs during core splitting) or the fracture surface is “smooth” (as occurs with a cleaned-sawed rock surface). The fractured core was flooded with the fracture in the vertical position.

The single exception to the core setup described above was one flood that was conducted in an identical manner except: 1) the core was only 1.0 ft long, 2) there were no internal pressure taps along the length of the fracture, and 3) there were no matrix-flow effluent ports present.

In all cases, gel (and other fluids), exiting from the downstream end of the fracture, flowed into a chamber in the core's acrylic end cap that was ~4-mm (~0.16-in.) deep and ~26x26-mm (~1.0x1.0-in.) square. The gel then flowed into a stainless steel effluent port fitting having an ID of 4.5 mm (0.18 in).

Two ports for the flow of fluids from the matrix rock were placed at the downstream end of the core material. The injected fluids, including gel fluids, were distributed over the majority of the injection face, which included both the fracture and the matrix sandstone rock. The matrix-rock effluent end of the core slab was sealed such that fluids could only flow out of the fracture at this point, and could not flow out of the matrix rock. All effluent fluid flow out of the matrix rock occurred by exiting the downstream matrix-rock effluent ports. The fractured Berea sandstone slab was cast in epoxy.

During each flooding experiment, the rates of fluid production from both the fracture and the matrix-rock effluent ports were recorded versus time. The one exception to this was the 1.0-ft-long core (as discussed above) where only the rate of fluid produced from the fracture was recorded as a function of time.

Fig. 67 shows a fractured core prior to casting it in sand-filled epoxy resin. Fig. 68 shows the core residing in PVC pipe after casting in epoxy resin. The core and the core-holder setup for flooding the fractured sandstone core are similar to that discussed in Ref. 22.

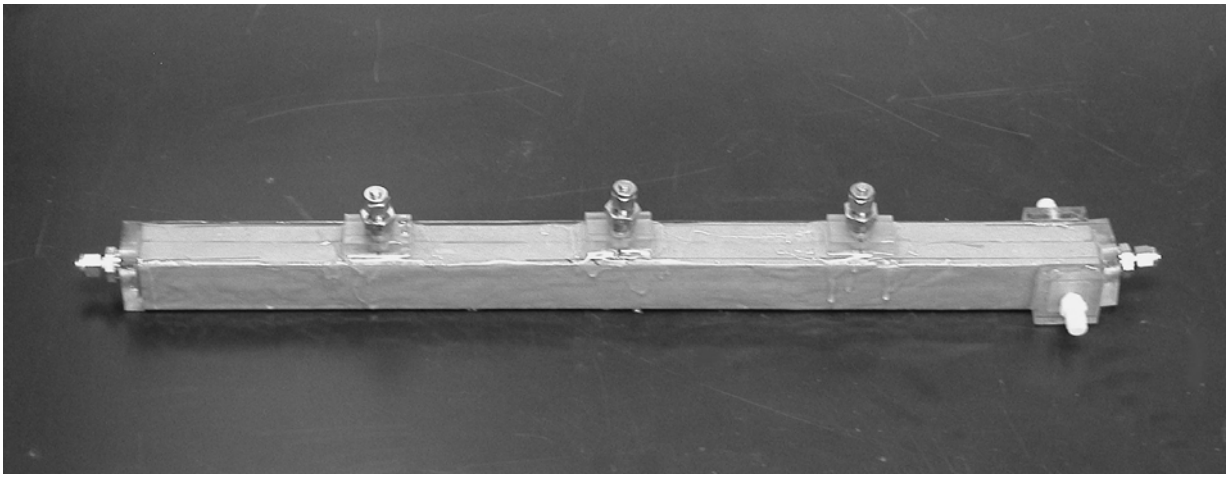

Fig. 67—Fractured core used during the gel/fracture floods.

Differential pressures along the fracture length were continuously monitored during all flooding experiments using Honeywell Series 100e quartz differential-pressure transducers. Pressure taps divided the core into four intervals of equal length. During the second half of this study, an extra pressure transducer was added to measure the differential pressure across the entire core and fracture length. Except for the first flooding experiments, all final measurements of differential pressure were corrected for transducer-reading baseline drift. These values were used when calculating the stabilized and/or final permeabilities and residual resistance factors.

All flooding experimental work was conducted at 105°F (41°C). The brine and gel formulations contained 1.0 wt% NaCl and 0.1 wt% $CaCl_2$. The oil used was Soltrol 130^{TM} (mixed C10-C13 isoparaffins).

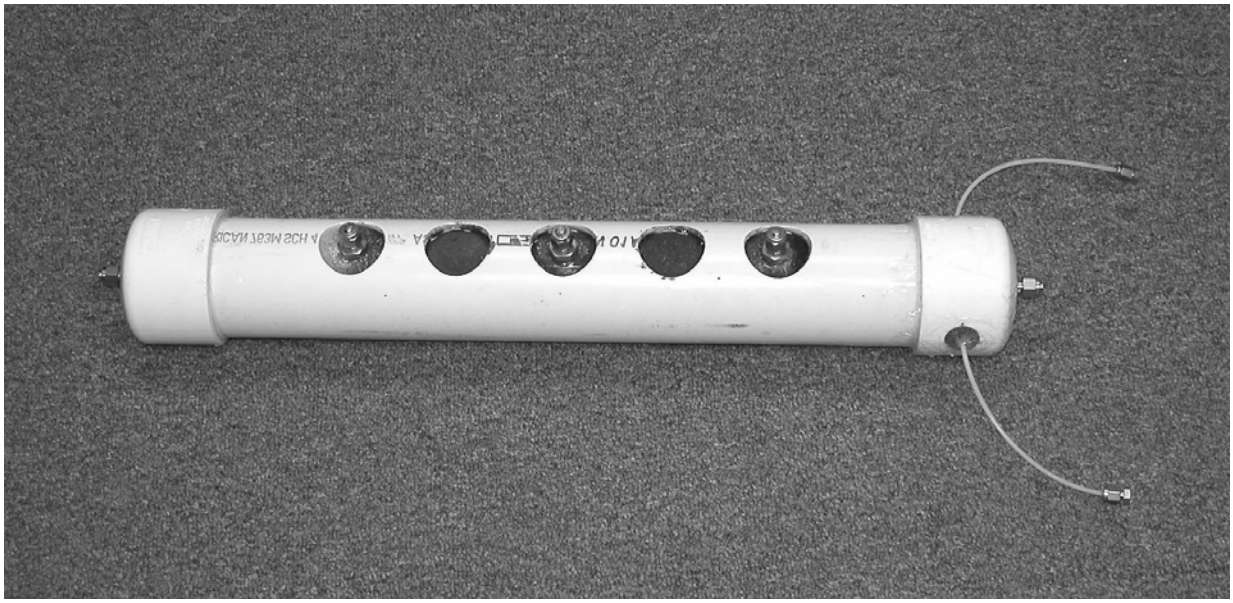

Fig. 68—Final form of the fractured core.

The CC/AP [or Cr(III)-acetate-HPAM] gels in this study used chromic triacetate as the chemical crosslinking agent. All gels were formulated in the brine that was described in the previous paragraph. No pH adjustment was made to any of the solutions. The crosslinking agent, chromic triacetate, was obtained from McGean as a 50 wt% active aqueous solution and was added to the polymer solutions in this form. The polymer was Ciba Alcoflood 935^{TM} commercial HPAM (hydrolyzed polyacrylamide). This acrylamide polymer has a nominal Mw of $5x10^6$ daltons and is 5-10 mole% hydrolyzed. The concentration of active polymer was 92%. Pertinent information regarding the three CC/AP gel formulations employed in this study is provided in Table 19.

Table 19—CC/AP gels used in this study.

Gel designation	1X	2X	3X
As-supplied concentration of "high" Mw HPAM, wt%	0.5	1.0	1.5
Concentration active Cr(III), ppm	95	150	200
Aging time prior to injection, hr	7.0	2.5	1.0
Viscosity of the polymer solution without crosslinker added (at 28 sec^{-1} shear rate and 41°C), cp	15	72	220

For those experiments involving partially formed gels, the gel aging time (i.e., from crosslinker addition to the polymer solution to initiating gel solution injection) was selected using the bottle-testing procedure that is described in Ref. 26. Utilizing the gel-strength-code assignment as a

function of gel aging time at 41°C (105°F), the aging time was determined when the first visually detectable gel formation occurred. At this aging time, we estimated very roughly that 10% of full gel maturation and gel strength was attained. At a minimum, substantial microgel formation occurred by this time.

For quality control, a sample of the gel to be injected was set in the air bath along side the core to verify that the newly prepared gel formulation matured (crosslinked) at the proper rate and that the final gel attained the expected ultimate strength.

In this chapter, superficial velocities for brine or oil flow through gel-treated fractures will be reported in units of ft/d. These superficial velocities were calculated assuming that the fluid flow occurred through the original fracture without any gel. As will become evident later in this chapter, the actual superficial velocity of brine or oil flow through the gel-treated fractures was probably more than ten times larger than stated in this chapter because the fluid flow actually occurred through relatively small channels in the gel.

Characterization of Partially Formed Gels

Flooding-experiments in this chapter addressed three facets:

1) Determination of the effective viscosity of partially formed gels in a fracture during gel injection,
2) Determination of the stabilized (equilibrium or "final") residual resistance factor (F_{rr}) for oil or water flow through a gel-filled fracture, and
3) Characterization of disproportionate permeability reduction (DPR) during oil and water flow through gel-filled fractures.

Effective Viscosity of Partially Formed Gels during Injection. During the gel/fracture flooding experiments of this study, 40 fracture volumes (FV) of gel solution were initially injected into the fracture/core assembly at 8,000 cm^3/hr (16,600 ft/d superficial velocity in the fracture). Using our experiments, the gel formulation was injected in less than 7 minutes.

During the injection of the *partially formed 1X* (0.5 wt% polymer) CC/AP gel, the effective viscosity of the gel in the fracture ranged from **30 to 34 cp**. These viscosity values are based on the average differential pressures between the two internal pressure taps in the fracture. This effective viscosity range for the partially formed CC/AP is relatively low for a gel. Formulations with such viscosities should be readily injectable into fractures that are commonly treated during water-shutoff applications. The injectivity index of the partially formed CC/AP gel during this experiment ranged from 27 to 34 (cm^3/min)/psi [0.25-0.31 BPD/psi].

During injection of the "fully formed" (1-day-old) 1X CC/AP gel, the effective viscosity of the gel within the fracture ranged from **280 to 320 cp**. *The effective viscosity of the "fully formed" gel was nearly an order of magnitude greater than the effective viscosity of the partially formed gel during injection.* Fig. 69 shows the apparent viscosities of the partially formed (7-hr-old) versus "fully formed" (1-day-old) gels as they propagated through the fractures.

As polymer concentration was increased (along with an appropriate increase in the crosslinking agent concentration), the strength of the final gel increased. Also, as the polymer concentration

was increased in an otherwise identical polymer-gel formulation, the effective viscosity of the gel formulation increased.

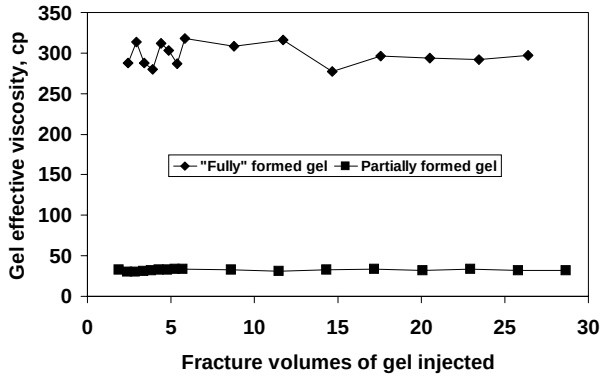

Fig. 69—Effective viscosity during injection of "fully" and partially formed 1X CC/AP gels.

Fig. 70 shows how the effective viscosity of partially formed gels in fractures increased with polymer concentration for three formulations. The effective viscosities increased from about 35 cp for the 1X gel (0.5% polymer) to about 110 cp for the 3X gel (1.5% polymer).

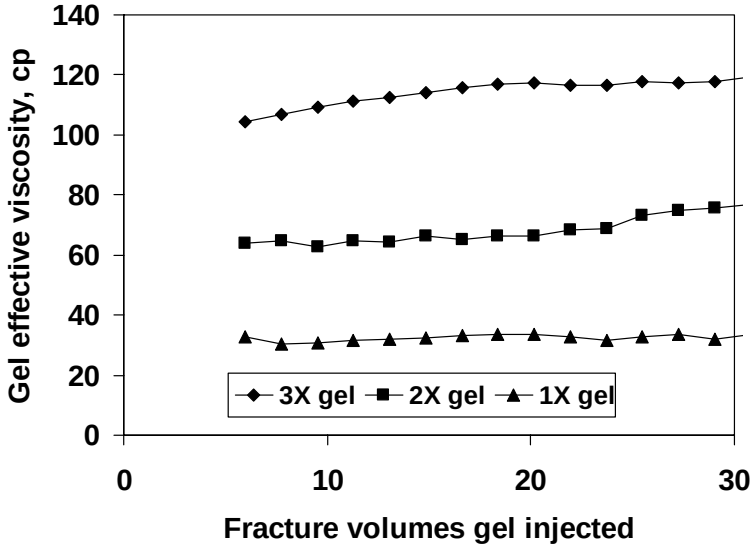

Fig. 70—Effective viscosity during injection of the three gel formulations.

Peak Pressure Gradient for First Gel Breaching. After gel placement and a one-day shut-in, brine was injected at a fixed rate of 100 cm^3/hr (206 ft/d superficial velocity in the fracture). In each experiment, the pressure gradient rose to a peak, followed by a pressure gradient decline to a more or less stabilized value. The peak pressure gradient indicates the point when brine first

breached the gel in the fracture. (As will be discussed shortly, breaching the gel does not constitute total washout. The flow capacity of the fracture remains dramatically less than before gel placement.) As shown in Table 20, the peak pressure gradients ranged from 5 psi/ft for the 1X gel to 99 psi/ft for the 3X gel.

Table 20—Peak pressure gradients for brine flow through a gel-filled fracture.

Gel state when injected	"Fully formed"	"Gelant"	Partially formed	Partially formed	Partially formed
Time gel aged prior to injection, hr	24	~0.25	7.0	2.5	1.0
Polymer concentration in gel, wt%	0.5	0.5	0.5	1.0	1.5
Peak or critical pressure gradient for initial brine flow, psi/ft	**9**	**3**	**5**	**32**	**99**

In the above table, each value represents the average pressure gradient measured for the four individual pressure taps along the length of the gel-filled fracture. Table 20 indicates that the peak pressure gradient increased substantially with polymer concentration and increased moderately with aging time (i.e., aging prior to injection into the fracture) for the 1X gel.

Stabilized Residual Resistance Factors. In this portion of the study, we determined the stabilized (equilibrium or "final') residual resistance factor (F_{rr} or permeability reduction factor) for brine flow through a gel-filled fracture. Using an equation from Ref. 27, the permeability of the original unobstructed 1-mm fracture was calculated to be 84,000 darcies. A fracture aperture of 1 mm is fairly typical of the average fracture aperture that is found in many naturally fractured oil reservoirs in the Big Horn Basin of Wyoming and the Permian Basin of Texas.

During the first 30 FV of brine injection at 100 cm^3/hr (following placement of the 3X CC/AP gel in a 1-mm-wide fracture), a "stabilized" permeability for brine flow through the gel-containing fracture was observed (Fig. 71). As shown in Table 21, the final stabilized F_{rr} values were substantial for the gels in these experiments. These F_{rr} values were determined using the final differential pressures after flooding with ~30 FV of brine (injected at a constant rate of 100 cm^3/hr). Differential pressures for the F_{rr} calculations of this table were not baseline corrected. As a result, the actual values for the F_{rr} that are shown in Table 21 may be somewhat larger than what is reported.

Table 21 suggests that the stabilized F_{rr} values for brine flow 1) were comparable for gel injected in the gelant, the partially formed, and the fully formed states and 2) increased with polymer concentration.

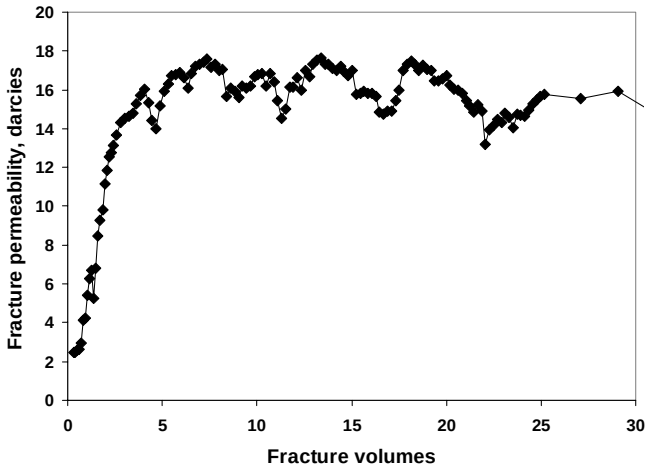

Fig. 71—Fracture permeability versus fracture volumes of brine injected for the 3X gel.

Table 21—Stabilized F_{rr} values for the first brine flood through gel-filled fractures.

Gel state when injected	"Fully formed"	"Gelant"	Partially formed	Partially formed	Partially formed
Time gel aged prior to injection, hr	24	~0.25	7.0	2.5	1.0
Polymer concentration in the gel, wt%	0.5	0.5	0.5	1.0	1.5
Final F_{rr} value	**7,000**	**6,500**	**6,400**	**9,300**	**12,000**

In wells with moderate or narrow fractures, the residual resistance factors in Table 21 should be sufficient to greatly reduce water production. However, for wide fractures, larger residual resistance factors may be needed to reduce the fracture flow capacity to an acceptable level.

The results in Tables 20 and 21 differ from results reported in Ref. 28, which reported that similar gels did not form in fractures when leakoff was not permitted. However, gel-mixing procedures and a number of experimental factors differed between the experimental studies of Ref. 28 and those of the present study.

As an aside, we briefly mention an experiment involving the placement of the 1X gel in a 1.0-ft-long fractured core where no effluent ports were present in the matrix sandstone. In all other respects, this flood was comparable to the experiment for the 1X "partially formed" gel flood that is cited in Tables 20 and 21. For the 1.0-ft-long core (with no effluent ports), both the peak (critical) pressure gradient and the stabilized F_{rr} for the post-gel brine were comparable to those values for the 1X partially formed gel experiment of Tables 20 and 21 where matrix effluent ports were present.

The relatively large stabilized F_{rr} values in Table 21 suggest that 1) only a small portion of the gel residing in the fracture was displaced (washed out) and 2) the brine formed a relatively small flow channel or "finger" through (or around) the gel in the fracture.

Several additional observations suggest that the brine flow channels through the gel are relatively small (likely <10% FV). First, no gel was visually observed in the produced brine, no blue color was visually noted in the produced brine [qualitatively indicating no dissolved chromium(III)], and there was no slippery feeling to the produced brine (a qualitative indication that little, or no, polymer or gel was present). During first brine flow after gel placement, four of five effluent brine samples contained less than 5% of the injected gel's chromium or polymer concentration (the exception contained 7% polymer concentration). In fact, the majority of effluent samples contained less than 1% of the chromium or polymer concentration in the injected gel. Thus, very little gel was produced from the fracture during the first post-gel-placement brine flood.

Second, brine breakthrough occurred substantially before one fracture volume was injected. During four experiments, brine breakthrough indicated that the brine flow channel was <<10% of the fracture volume. The brine breakthrough volume was determined from the volume of fluid that had been injected when the peak differential pressure for brine injection passed the furthest downstream of the four pressure taps.

Third, the large stabilized (final and equilibrium) residual resistance factors (Table 21) could only occur if the final flow channels were small. Assuming a single cylindrical brine pathway through the gel, standard calculations[18] indicated effective tube diameters between 0.06 and 0.07 mm. These values suggest that more than 99% of the gel remained in the fracture after brine injection.

Fourth, upon termination of the experiment, the fracture was opened and visually inspected. The fracture was filled with gel having the same consistency and strength as the mature gel that was originally placed in the fracture. Little of the gel was displaced from the fracture during brine flow. In fact, chromium analysis of gel samples taken from the fracture after termination of the experiments indicated that the gel was concentrated 1.2 to 2.5 times. Also, several small flow channels through the gel were noted.

Fifth, at the end of the experiments, several "wormhole" channels were observed through the gel. The flow channels within the gel were easy to observe because the last fluid injected was Soltrol 130 oil that was dyed red. The relatively small wormhole channels (<10% FV) appeared similar to the wormhole channels that were reported for "fully formed" gels in similar fractures.[13]

The photograph in Fig. 72 shows the wormhole channels after the fracture was split open. In this instance, the experiment involved the 2X CC/AP gel after four cycles of brine and oil flooding. During the final flood of the experiment, red-dyed oil was injected into the gel-filled fracture. Flow occurred from left to right in the photograph. In this photo, the core material resides in roughly the middle half of the photo, with the remaining outer material (top and bottom) being core-holder materials.

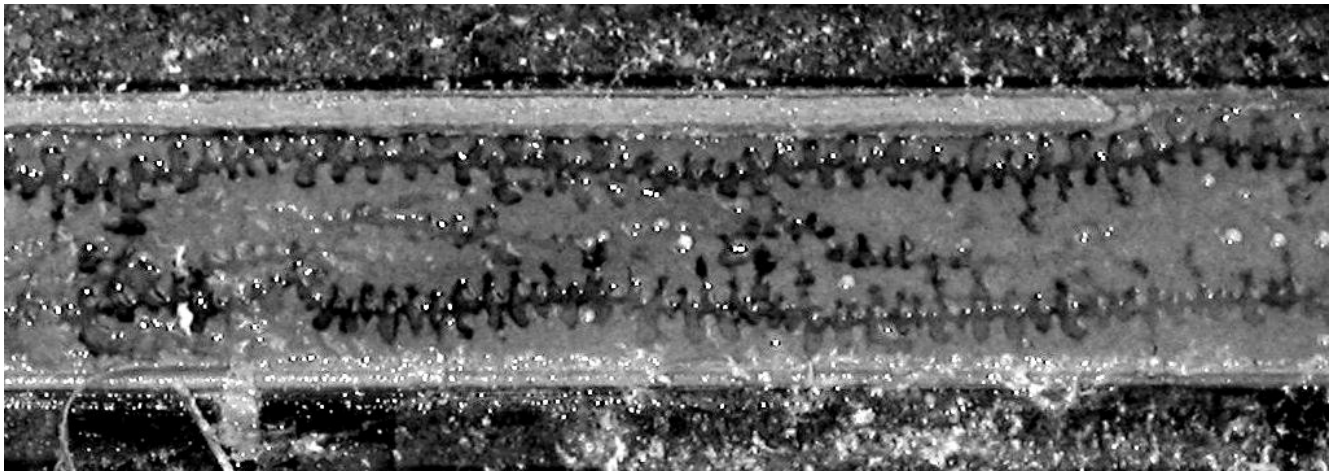

Fig. 72—Post-gel-treatment “wormhole” channels in the gel.

In Fig. 72, immediately adjacent to the oil-flow channels, a series of short dead-end flow channels appear to emanate perpendicular to the direction of the main oil-flow channels. These “railroad track” features may be an artifact. When a fracture and associate gel were split open, the resulting gel surface was not perfectly smooth. The freshly opened gel surface had alternating series of inward and outward protruding dimples. After splitting open the fracture, a portion of the oil may have accumulated in the inwardly protruding dimples (that were immediately adjacent to the wormhole channels)—thus forming the “railroad tracks”.

“Healing” a Fracture. An important point from the above discussion was that the gel caused substantial reductions in the fracture conductivities (i.e., residual resistance factors were between 6,400 and 12,000). These reductions occurred because very little gel washed out when brine was injected after gel placement. Ideally, a gel treatment should “heal” the fracture without damaging the porous rock. In that case, the final composite permeability of the core plus the fracture would revert to the permeability of the unfractured core. The last row of Table 22 lists composite permeabilities (after injecting 30 FV of brine) for the five cases considered. Interestingly, these overall permeabilities were insensitive to the gel state when injected (aged 0.25-24 hr) and polymer concentration in the gel formulation. In all cases, the overall fractured-core permeabilities were less than the 700-md permeability of the Berea sandstone. It is not surprising that the gel reduced the permeability of the matrix rock somewhat because most of inlet core face was exposed during gel injection. Thus, the core inlet face was damaged to some extent by the injected gel.

Reduction of the composite fracture-core permeability below 700 md does not insure that the fracture was “healed” (i.e., that the fracture conductivity was reduced to a negligible value). It is possible that the fracture may still be open to some extent and the rock matrix is damaged enough so that the composite permeability falls below 700 md. The extent to which brine is diverted away from the fracture and into the matrix can be assessed by examining the ratio of brine produced from the fracture versus from the matrix, as was described in Fig. 50. For the experiments of Table 22, the final rate of brine production from the matrix effluent ports ranged from 14% to 21% of the total flow rate. In contrast, at the time of the peak pressure, 21% to 92% of the total flow rate was produced from the matrix ports. Before gel placement, no fluid was

produced from the matrix ports. Thus, the gel diverted brine flow away from the fracture and into the matrix sandstone rock. Of course, in the ideal case, all flow would be produced from the matrix port after the gel treatment.

Table 22—Composite stabilized fracture-core permeability for the first brine flood.

Gel state when injected	"Fully formed"	"Gelant"	Partially formed	Partially formed	Partially formed
Aging time prior to injection, hr	24	~0.25	7.0	2.5	1.0
Polymer concentration in gel, wt%	0.5	0.5	0.5	1.0	1.5
Composite stabilized permeability, md	**330**	**380**	**380**	**300**	**440**

Gel-Treated Fractures Exhibit Disproportionate Permeability Reduction.
In previous literature, disproportionate permeability reduction (DPR) and its synonym, relative permeability modification (RPM), refer to polymers or gels that reduce the permeability to water more than that to oil or gas *in porous rock*. Recall in Chapter 5, we showed that disproportionate permeability reduction could also be observed in fractures. In one set of experiments with gels that were aged one day before placement (Fig. 30), permeability to brine was reduced 10-20 times more than that to oil at low rates, and the disproportionate permeability reduction was significantly moderated at high rates. In a second set of experiments (Figs. 31 and 32), the same "fully formed" gel provided only modest disproportionate permeability reduction (F_{rrw} / F_{rro} ranged from 2.5 to 4.7) that was not sensitive to rate. Disproportionate permeability reduction occurred to a much greater extent for gels placed as gelants, although the effect showed a wide variation (F_{rrw} / F_{rro} ranged from 2.4 to 80 for 1X gels and from 1.9 to 280 for 2X gels, from Figs. 35 and 36). Disproportionate permeability reduction was not evident in tubes (Figs. 37-42).

A series of experiments were conducted during this study to determine if partially formed CC/AP polymer gels promote disproportionate permeability reduction within a fracture. During six experiments involving three gel formulations, the CC/AP gels that were placed in a partially formed state exhibited varying degrees of disproportionate permeability reduction in fractures.

1X Gel Exhibits DPR. Here, we will only discuss results of one of the six experiments. After the first brine flood following gel placement in a 1-mm-wide fracture, we performed an oil flood at a rate of 500 cm^3/hr. Results of this experiment are summarized in Table 23. "Final permeability" in this table refers to the permeability after injection of 30 FV of brine or oil.

In Table 23, the ratio of oil permeability to water permeability (k_{of}/k_{wf}) was 166. Thus, *CC/AP gel placed in the partially formed state reduced the permeability to water in the fracture to a much greater extent than the permeability to oil*. The level of disproportionate permeability reduction was toward the high end of the values for gels placed as gelant, as described in Figs. 35 and 36.

Table 23—Disproportionate permeability reduction by a 1X gel.

Polymer concentration in gel, wt%	0.5
Final brine permeability, md	**12,000**
Final oil permeability, md	**2,000,000**
Ratio, k_{of}/k_{wf}	**166**
Brine F_{rr}	7,000
Oil F_{rr}	42

As a cautionary note, the above value (166) is one of the largest that we observed to date. Later in this chapter and in the next chapter, we will discuss examples and conditions where the disproportionate permeability reduction was substantially less. The value of 166 was determined during experiments that were conducted at relatively low flow rates and where the brine was flooded before oil. In the next chapter, the effect of flow rate on disproportionate permeability reduction will be discussed.

We repeated the water/oil flooding sequence three more times during this experiment sequence. Fig. 73 plots the brine and oil residual resistance factors (F_{rr}) for the four series of post-gel-placement brine and oil floods. During each cycle, 30 FV of brine and oil were injected into the gel-filled fracture. All these floods were conducted at an injection rate of 500 cm^3/hr.

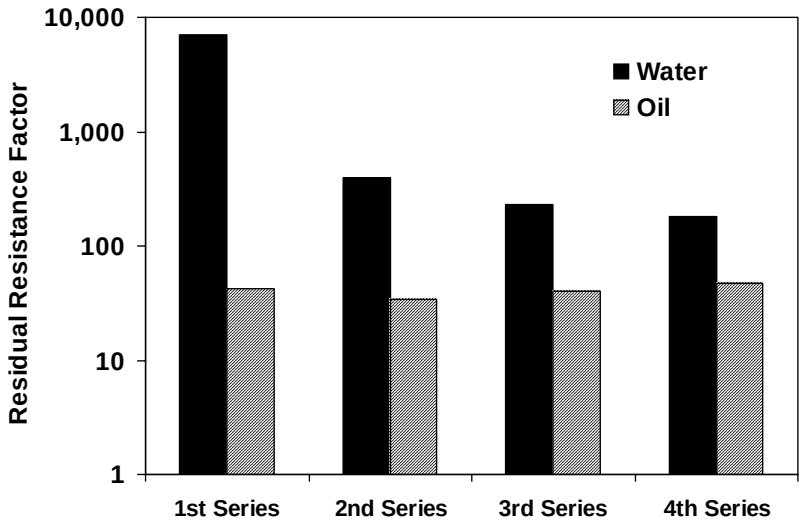

Fig. 73—Four post-gel-placement water/oil floods for the 1X gel.

At the end of the first oil flood, the final fracture permeability to oil was 2,000,000 md, yielding a permeability reduction factor of only 42. *During the next three flooding series, the final permeability to oil remained constant, within experimental error. However, brine F_{rr} values progressively declined from 7,000 to 180 (i.e., by a factor of 38). The final fracture permeability to brine flow progressively increased from 12,000 to 460,000 md.*

3X Gel Exhibits DPR. We conducted an additional experiment to study disproportionate permeability reduction using a relatively strong 3X CC/AP gel in a 1-mm fracture. After the first brine flood, oil was injected at a rate of 500 cm^3/hr. Results of this experiment are summarized in Table 24. "Final permeability" in Table 24 refers to the permeability after injection of 30 FV of brine or oil.

Table 24—Disproportionate permeability reduction by a 3X gel.

Polymer concentration in gel, wt%	1.5
Final brine permeability, md	**3,900**
Final oil permeability, md	**300,000**
Ratio, k_{of}/k_{wf}	**77**
Brine F_{rr}	22,000
Oil F_{rr}	280

The ratio of oil permeability to water permeability (k_{of}/k_{wf}) was 77, about half of the value for the 1X gel (Table 23). As expected, the F_{rr} values for brine and oil for the 3X gel were significantly larger than the F_{rr} values for the 1X gel.

The water/oil flooding sequence was repeated three more times. Fig. 74 plots the brine and oil residual resistance factors (F_{rr}) for the four series of post-gel-placement brine and oil floods. During each cycle, 30 FV of brine and oil were injected.

As was observed with the 1X gel, the oil F_{rr} values and the permeabilities remained fairly constant during the four series of brine and oil floods. However, final brine F_{rr} values progressively declined from 22,000 to 1,000.

A final brine permeability reduction factor of 1,000 should be adequate for many water-shutoff applications in 1-mm- fractures. In very wide fractures, larger residual resistance factors may be needed.

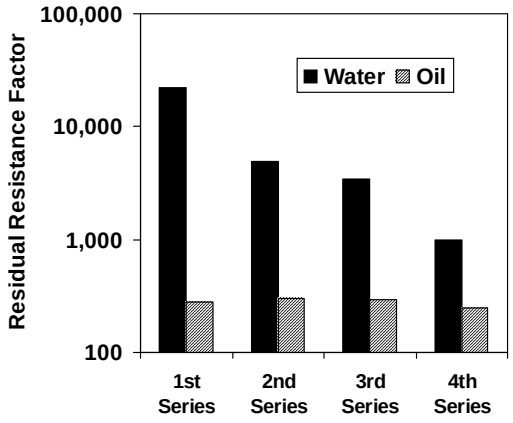

Fig. 74—Four post-gel-placement water/oil floods for the 3X gel.

Additional Discussion

Gel Washout? Terms such as "gel washout" and "gel failure" have been invoked to describe brine breaching gel in fractures. In a sense, these terms can be misleading because the bulk of the fracture volume remains filled with gel that can substantially reduce water flow through the fracture.

Inferior Field Performance and What Is Needed. Why don't we see more reduction in brine production during field applications of polymer-gel water-shutoff treatments? There are a number of possible explanations. First, several fractures (with different flow capacities and different contributions to oil and water flow) can be connected to a given production well, and the vertical and areal distribution of gel within these fractures can differ during a given gel treatment. Second, if a well is not pumped off (even for water being produced from a single fracture), the reduction in water production rate will probably be less than the permeability reduction factor that the gel imparted to the treated fracture. Third, the reservoir fractures may have large apertures such that the applied gel does not have sufficient mechanical strength to withstand the prevailing pressure gradients. Fourth, complete filling of the fracture volume with gel can be more difficult in the field than in our laboratory experiments. For example in large aperture vertical fractures, the gel formulation may gravity-segregate to the bottom of the fracture during placement on the field scale. Since the top part of the fracture remains open, water flow to the well may not be retarded sufficiently. In the field setting, this fourth explanation is probably a *major contributor* to less than optimum performance of polymer-gel water-shutoff treatments in fractured production wells.

This chapter reported large permeability reduction factors for water flow in gel-treated fractures. Our results and discussion imply that ineffective fracture-volume-filling during gel placement is often responsible for attaining smaller water-shutoff values in the field than in the laboratory. Mastering how to more completely fill fractures with a gel may be the key to improving the success rate and the effectiveness of polymer gels in fractures and fracture systems.

Brine Flow Rates. The post-gel-placement flow rates investigated during this study were relatively low. At higher brine flow rates, and associated higher pressure drops, gel erosion or compaction (dehydration) can occur—increasing fracture flow capacity and reducing gel effectiveness (see Chapter 6). However, as will be shown in the next chapter, special gels can be formulated to mitigate this problem.

Wormholing. This study found that brine and oil usually "wormhole" through water-shutoff gels in fractures. This finding is not surprising, since the brine and oil are tremendously more mobile than the gels. "Fingers" (for the case of liquids displacing liquids) and "wormholes" (for the case of fluids destructively penetrating into solids) are well known to occur for displacements involving unfavorable mobility ratios. In previous work,[13,19] we reported a special type of wormholing where a 1-day-old gel was extruded into fractures. During the extrusion process, the gel dehydrated or concentrated, forming an immobile gel within the fracture that became increasingly concentrated with time. Gel of the original concentration was forced to wormhole through the concentrated immobile gel in order to continue propagating down the fracture. Consequently, at the end of the gel placement process, most of the fracture was filled with a

strong, concentrated gel, but the wormholes were filled with less concentrated and less rigid gel. During brine or oil flow after gel placement, the first breach of the gel occurred in these pre-established wormholes. In contrast, when the formulation was placed as a gelant or partially formed gel, these pre-established wormholes were not necessarily present. Thus, during brine or oil flow, *different breach points* occurred within the gels. Nonetheless, for all the experiments to date, the wormhole pathways had a similar appearance, regardless of whether the gels were placed as gelants, partially formed gels, or "fully formed" gels. Also, as pointed out in Tables 17 and 21, the final stabilized pressure gradients and residual resistance factors were not sensitive to the age of the formulation at the time of placement.

Conclusions

The following conclusions are limited to the polymer gels and the experimental conditions of this study.

1. A partially formed (7-hr-old) 1X CC/AP gel propagated more readily through a 1-mm wide fracture than a "fully formed" (1-day-old) gel with the same chemical composition. The effective viscosity of the "fully formed" gel in the fracture was nearly an order of magnitude greater than the effective viscosity of the partially formed gel. The effective viscosity of the partially formed 1X CC/AP gel ranged from 30 to 34 cp (at 16,600 ft/d superficial velocity in the fracture).
2. During first brine injection after gel placement in 1-mm wide fractures, the pressure gradient required to first breach the gel ranged from 5 to 99 psi/ft for gels containing from 0.5% to 1.5% polymer.
3. For the 1X gel, the peak pressure gradient (at which brine first breached the gel) increased with gel aging time (i.e., the time between preparation and injection of the formulation) from 0.25 to 24 hours.
4. During brine flow after gel placement, most (>90%) of the gel remained in the fracture and did not "washout."
5. The stabilized residual resistance factors (permeability reduction factors) for the first brine floods ranged from 6,400 to 12,000, increasing with increased polymer concentration and gel strength.
6. For the 1X gel, these stabilized permeability reduction factors were comparable for formulations injected in the gelant state, the partially formed state, and the "fully formed" state.
7. The CC/AP gels exhibited disproportionate permeability reduction during brine and oil flow through fractures.
8. During one experiment with the 1X gel, brine permeability in the fracture was reduced 166 times more than that for oil. In this case, brine was flooded first, followed by oil.
9. For the 1X and 3X gels, the permeability reduction factor for oil flow remained constant through four cycles of brine and oil injection. In contrast, the permeability reduction factor for brine decreased more than a factor of 10 during these cycles.

9. GELS CONTAINING HIGH- AND LOW- Mw POLYMERS IN FRACTURES

Introduction

The objective of this investigation was to develop and characterize stronger, more durable polymer-gel formulations for water-shutoff applications in fractures or other multi-Darcy flow channels–especially for applications when large drawdown pressures or large aperture (>1.5 mm) fractures are encountered.

This study was part of an investigation of water-shutoff polymer gels that are to be injected in the *partially formed* state into fractures or other high-permeability anomalies that are connected to petroleum production wells.

Experimental

The experimental setup and procedures used in this study were described in the previous chapter. The experiments were conducted in 1.5-in. by 1.5-in. by 2.0-ft long rectangular, 700-md, 19% porosity, unfired Berea sandstone cores, where a 1- to 4-mm (0.04- to 0.16-in.) sawed-surface fracture ran down the middle of the length of the core.

Gel (and other fluids) exiting from the downstream end of the fracture flowed into a chamber in the core's acrylic end cap that was ~4-mm (~0.16-in.) deep and ~26x26-mm (~1.0x1.0-in.) square. The gel then flowed into a stainless-steel effluent port fitting having an ID of 4.5 mm (0.18 in) for the 1-mm wide fracture and having 6.4-mm (0.25-in.) ID for 2- or 4-mm (0.08- or 0.16-in.) aperture fractures.

Two ports for collecting effluent from the matrix rock were placed at the downstream end of the core. The injected fluids were distributed over the majority of the injection face, including the fracture and the matrix sandstone. The matrix rock at the outlet end of the core was sealed so that fluids could only flow out of the fracture at this point. All effluent fluid flow out of the matrix rock occurred at the downstream matrix effluent ports. The Berea sandstone core was cast in epoxy. During each experiment, the rates of fluid production from the fracture and the matrix-rock effluent ports were recorded versus time.

Differential pressures were measured across four equally spaced intervals along the fracture length. A fifth pressure transducer continuously measured the differential pressure across the entire core and fracture length. There was always good agreement between the measured overall differential pressure and the sum of the differential pressures for the four fracture intervals. The final differential-pressure readings during any given fluid flood were corrected for pressure-transducer baseline drift. These values were used to calculate the stabilized and/or final permeability and residual resistance factors.

All flooding experimental work was conducted at 105°F (41°C). The brine and gel formulations contained 1.0 wt% NaCl and 0.1 wt% $CaCl_2$. The oil used was Soltrol 130^{TM} (mixed C10-C13 isoparaffins).

The CC/AP [chromium(III)-carboxylate/acrylamide-polymer or Cr(III)-acetate-HPAM] gels in this study used chromic triacetate as the chemical crosslinking agent. All gels were formulated in

the brine that was described in the previous paragraph. No pH adjustment was made to any of the solutions. The crosslinking agent, chromic triacetate, was obtained from McGean as a 50 wt% active aqueous solution and was added to the polymer solutions in this form. The "high" molecular weight (Mw) polymer was Ciba Alcoflood 935^{TM} commercial HPAM (hydrolyzed polyacrylamide). This acrylamide polymer has a nominal Mw of $5x10^6$ daltons and is 5-10 mole% hydrolyzed. The concentration of active polymer in the as-supplied sample of Alcoflood 935 HPAM was 92%. The low-Mw polymer was Ciba Alcoflood 254-S^{TM} commercial HPAM. This latter acrylamide polymer has a nominal Mw of 500,000 daltons and is 5-10 mole% hydrolyzed. Pertinent information regarding the CC/AP gel employed in this study is provided in Table 25.

Table 25—H&LMW CC/AP gel used in this study.

Gel Designation	H&LMW
As-supplied concentration of "high" MW HPAM, wt%	1.5
As-supplied concentration of low MW HPAM, wt%	2.0
Concentration active Cr(III), ppm	601
Aging time prior to injection, min.	40
Viscosity of the polymer solution without crosslinking agent added (at 28 sec^{-1} and 41 °C), cp	850

The gel aging time (between crosslinker addition to the polymer solution and initiating injection of the gel formulation into the fractured core) was 40 minutes. Superficial velocities for brine or oil flow through gel-treated fractures will be reported in units of ft/d. These superficial velocities were calculated assuming that the fluid flow occurred through the original fracture without any gel present. The actual superficial velocity of brine or oil flow through the gel-treated fractures was probably more than ten times larger than stated because the fluid flow actually occurred through relatively small channels in the gel (see the previous chapter for more on this subject).

Improved Water-Shutoff Performance for Gels

The goal of this study was to improve the performance (especially the strength) of polymer gels that are used to treat fractures and other high-permeability anomalies which are in direct contact with production wells—especially when encountering large drawdown pressures and large apertures in high-permeability channeling anomalies, such as fractures or solution channels.

Strategy of Incorporating High- and Low- Mw Polymers for Improved Performance. The strategy employed in this study was to formulate the gels with a combination of *high*- and *low*-Mw HPAM polymer. The overall performance improvements that we hope to achieve by this approach include 1) mechanical strength, 2) thermal and chemical stability, and 3) durability. However, the present study is limited to gels having improved mechanical strength.

Although presently available polymer gels have sufficient strength for the successful treatment of wells in numerous producing provinces (e.g., the Wyoming Big Horn Basin and the Texas Permian Basin), a need exists for stronger gels when encountering fractures with large apertures (>1.5 mm) and/or large drawdown pressures. For example, large drawdown pressures can be

encountered when a horizontal well is drilled through a low-permeability oil-bearing formation and the well intersects a single highly conductive vertical fracture that extends down into a prolific water aquifer.

The strategy of mixing high- and low-Mw HPAM polymer in gel formulations is based on the following premises. First, there is an upper concentration limit for incorporating relatively high-Mw HPAM into polymer-gel formulations. This upper concentration limit is set by the upper viscosity limit that can be tolerated during pumping and placement of the gel formulations.

The second premise is that any gel formulated for fracture water-shutoff purposes should contain as much high-Mw polymer as possible (up to a limit to be discussed shortly). More gel strength per unit weight or unit cost is attained by incorporating high-Mw polymer rather than low-Mw polymer. However, as the concentration of high-Mw polymer increases above a threshold value, addition of low-Mw polymer imparts improved gel strength and stability that are comparable to addition of the same amount of high-Mw polymer. In this case, this occurs because both polymer chains are long enough to form effective crosslinks within the gel network.

The attractive feature of adding low-Mw polymer to a base gel formulation that contains high-MW polymer is that the low-MW polymer *imparts a minor increase in viscosity* to the gelant solution, while substantially improving the gel strength and stability.

Gel Formulated with 1.5% High-Mw and 2.0% Low-Mw Polymer. The high- and low-molecular weight (H&LMW) CC/AP gel employed in the study was formulated in a 1.0 wt% NaCl and 0.1 wt% $CaCl_2$ brine and contained 1.5 wt% high-Mw Alcoflood 935 HPAM, 2.0 wt% low-Mw Alcoflood 254-S HPAM, and 601 ppm Cr(III) as chromic triacetate.

1-mm Aperture Fracture. During the first evaluation phase of the H&LMW gel, 40 FV of partially formed gel was injected at 8,000 cm^3/hr (16,600 ft/d superficial velocity) into a 1-mm-wide, 2-ft-long fracture. (The gelant solution was aged at room temperature (~24°C [~75°F]) for 40 minutes before injection.) During injection, the effective viscosity in the fracture ranged from 470 to 510 cp. The gel was then allowed to age 48 hours before initiating brine injection. The following post-gel-placement results involved *constant-pressure flooding*.

During the first brine injection, we attempted to inject brine using a total injection pressure of **52 psi** (differential pressure), which provided a pressure gradient of 26 psi/ft. During the **24 hours** that we maintained this brine injection pressure, **no brine flow** through the fracture was detected.

Next, we raised the injection pressure to **75 psi** (pressure gradient of 38 psi/ft) for 7.0 hrs. At this point, the average permeability of the fractured core was measured to be 700 md—yielding a r**esidual resistance factor (permeability reduction factor)** of **120,000**. The similarity of this measurement to the 700-md permeability of the original matrix Berea rock is totally serendipitous.

Subsequently, we conducted six additional brine floods (in the same fractured core) where the injection pressure was increased in increments and then decreased in increments. The pressure responses of four floods of this series are shown in Fig. 75. In this figure, permeability of the gel-

treated fractured core is plotted against the brine pressure gradient. The order of the sequence of floods was: Flood A, Flood B, Flood C, and Flood D. The data is based on the average pressure of the two internal pressure taps along the length of the fracture.

In general, the curves for these four floods were qualitatively similar, and all the pressure-cycle curves originated from the same abscissa point on the plot. That is, below roughly 12 psi/ft injection pressure gradient (or 24 psi injection differential pressure), there was no measurable brine flow through the gel-filled fracture for any of the flooding pressure cycles, and thus no measurable fracture permeability below this "critical" pressure gradient. With increasing number of flood cycles and/or increasing applied injection pressure, there may be a downward trend in the slopes of the curves.

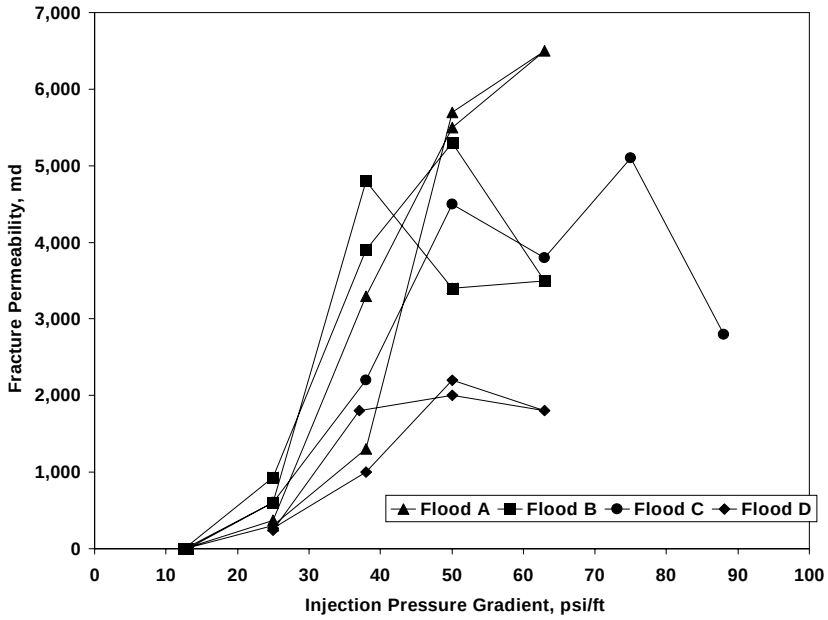

Fig. 75—Constant-pressure brine floods in a 1-mm fracture containing the H&LMW gel.

F_{rr} was 13,000 for the maximum pressure gradient point (63 psi/ft) of Flood A in the above plot. F_{rr} (permeability reduction factor) was 30,000 for the maximum pressure gradient point (88 psi/ft) of Flood C.

As the injection pressure was increased up to about 150 psi (75 psi/ft pressure gradient), proportionally more of the differential pressure occurred over the final downstream section of the fracture. In contrast, at significantly lower injection pressures, the differential pressures measured over all four fracture sections were quite comparable. This trend appeared to be reversible with increasing and decreasing pressure cycles and during multiple floods. At present, we don't completely understand why this occurred. The phenomenon is demonstrated in Table 26 for Flood A.

Perhaps the most significant finding of this experiment can be discerned from close inspection of the curve for Flood C in Fig. 75. That is, the gel **successfully withstood 175 psi of total injection pressure (88 psi/ft pressure gradient) within the 1-mm-wide fracture**. Due to pressure limitations of the core/fracture system and safety considerations, we did not raise the injection pressure above 175 psi.

Table 26—Injection pressure gradient cycle for Flood A.

Injection ΔP total, psi	25	50	75	100	125	100	75	50	25
Injection pressure gradient, psi/ft	13	25	38	50	63	50	38	25	13
Tap 1 Pressure gradient, psi/ft	10	12	12	17	23	16	11	8	13
Tap 2 pressure gradient, psi/ft	15	11	12	16	28	22	12	7	14
Tap 3 pressure gradient, psi/ft	12	14	30	12	13	13	10	7	4*
Tap 4 pressure gradient, psi/ft	14	68	97	157	189	150	120	78	20*
* Due to experimental problems, the exact values of these 2 data points are uncertain.									

2-mm Aperture Fracture. As the next step in evaluating the H&LMW gel formulation, a series of experiments were conducted using the same procedures as in the previous section, except that the fracture aperture was 2 mm and all floods were conducted using a *constant-rate*. During injection of the partially formed gel, the effective viscosity ranged from 550 to 630 cp.

The stabilized F_{rr} for the **first post-gel-placement brine flood was 260,000**. After two cycles of flooding with 15 FV each of brine and oil, the **stabilized F_{rr} to brine was 53,000** and the **stabilized F_{rr} to oil was 11,000**. Thus, the k_{of}/k_{wf} ratio was 4.8 during this second cycle of brine and oil flooding. The permeability of the original 2-mm-wide fracture was 340,000 darcies. During first brine flooding at 100 cm^3/hr (100 ft/d superficial velocity in fracture), the **critical differential pressure** gradient (averaged from the four pressure taps) required to first breach the gel was **37 psi/ft**, a very encouraging value.

Next, a series of brine and oil floods were conducted to investigate the effectiveness the H&LMW gel as the flow rates and differential pressures increased in the 2-mm fracture. During this series, all the brine floods were conducted first, and flooding proceeded from low to high flow rates. Next, the oil floods were conducted from low to high flow rates. The results of these experiments are summarized in Table 27.

The brine permeability reduction factor decreased from 52,000 to 14,000 as superficial velocity in the fracture increased from 515 to 8,240 ft/d (Table 27). It is noteworthy that the residual resistance factor (F_{rr}) was 14,000 to brine flow after injecting 21 FV of brine at a 8,000 cm^3/hr

and at a superficial velocity in the fracture of 8,240 ft/d. Permeability to brine flow in the gel-filled fracture slowly increased with brine throughput volume at the 8,000 cm^3/hr injection rate.

Table 27—Effect of rate on oil and water F_{rr} values for the H&LMW gel in a 2-mm fracture.

Rate, cm^3/hr	Superficial velocity, ft/d	Brine F_{rr}	Incremental FV of brine	Total FV brine	Oil F_{rr}	Incremental FV of Soltrol	Total FV Soltrol
500	515	**52,000**	2.7	2.7	**15,000**	3.4	3.4
1,000	1,030	**39,000**	5.5	8.2	**7,100**	5.5	8.9
2,000	2,060	**21,000**	10.9	19.1	**4,200**	11.0	19.9
4,000	4,120	**16,000**	21.1	40.2	**2,400**	21.2	41.1
8,000	8,240	**14,000**	21.4	61.6	**1,500**	21.4	62.5

Table 27 also shows that oil residual resistance factors decreased with increased rate and throughput. A summary of the results of Table 27 are depicted graphically in Fig. 76. The reader should be cautioned against making judgments concerning disproportionate permeability reduction based on this data (because the entire water rate sequence was completed before the oil rate sequence).

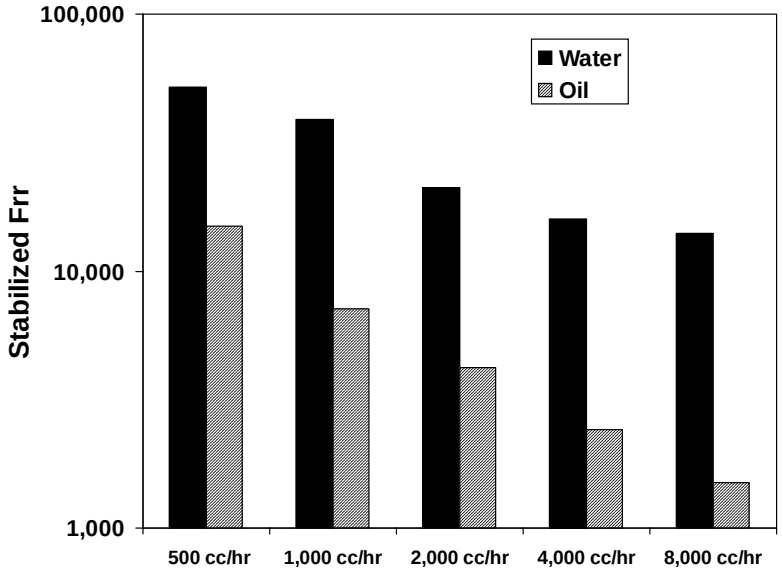

Fig. 76—Summary of variable-rate floods for a H&LMW gel in a 2-mm fracture.

In summary, concerning the H&LMW gel in a 2-mm-wide fracture, possibly **the most significant finding was that the gel was not breached by brine flow until 37 psi/ft pressure gradient was exceeded.**

4-mm Aperture Fracture. In the final studies of this series on the H&LMW gel in fractures, we used a 4-mm-wide fracture. During this experiment, 10 FV of the partially formed gel were injected into the 2.0-ft-long fracture at 8,000 cm^3/hr (4,100 ft/d superficial velocity in the fracture), and then the core was shut in for 48 hours. During injection, the effective viscosity of the gel in the fracture ranged from 1,400 to 1,500 cp.

During first brine flooding at 100 cm^3/hr injection rate (52 ft/d superficial velocity in the fracture), the **critical pressure gradient** (average of the four pressure taps) required to first breach the gel was **25 psi/ft**—the highest pressure gradient that we have seen for any of our studies to date in 4-mm-wide fractures.

At the end of the first post-gel-placement brine flood (after 10 FV of brine had been injected), the **stabilized permeability reduction factor** for brine flow was again **260,000**. The permeability of the original (untreated) 4-mm-wide fracture was 1.4 million darcies.

Next, an oil flood was conducted, followed by three cycles of brine and oil flooding. During all of these floods, 10 FV of fluid was injected at a rate of 500 cm^3/hr (259 ft/d superficial velocity in the fracture). At the end of the fourth brine injection, the **permeability reduction factor** for brine flow was **84,000.** At this point, the ratio, k_{of}/k_{wf}, was 2.5. The disproportionate permeability reduction was modest (2.5 to 6) for all four cycles (see Fig. 77). The magnitude of the disproportionate permeability reduction (as measured by the ratio, k_{of}/k_{wf}) decreased with increasing cycles of brine and oil.

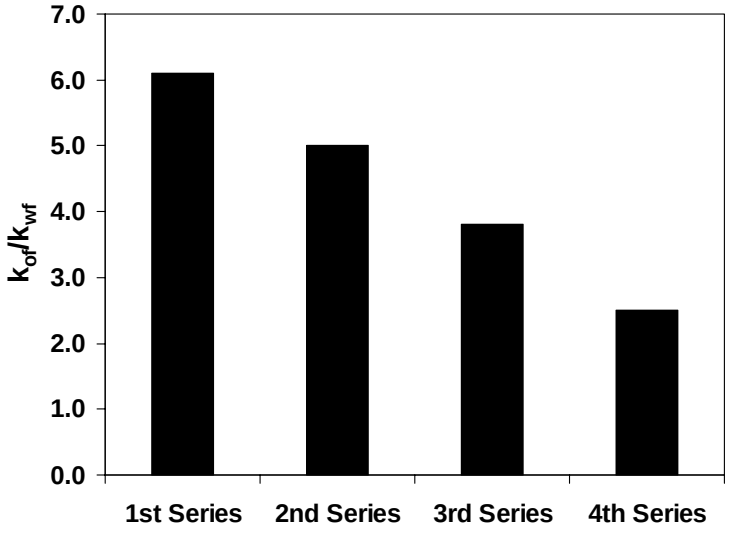

Fig. 77—Disproportionate permeability reduction for a H&LMW gel in a 4-mm fracture.

Finally, using the same 4-mm-wide fracture, we carried out a series of brine floods using increasing flow rates, followed by a single oil flood. During this flooding sequence, the five brine floods were completed first, followed by the oil flood. Results of this sequence of experiments are summarized in Table 28.

The final residual resistance factors imparted by the gel in the 4-mm fracture were substantial for both brine and oil flow (Table 28). The **final brine and oil permeability reduction factors were 39,000 and 18,000, respectively.** In total, more than 100 FV of water and 84 FV of oil were injected. Roughly 40 FV each of water and oil were injected during the studies associated with Fig. 77, and in generating Table 28, an additional 64.6 FV of water and 44 FV of oil were injected. During the brine injection at 8,000 cm^3/hr, we noted a small but steady increase in brine fracture permeability with time and volume of brine injected.

Table 28—Effect of rate on water and oil F_{rr} values for the H&LMW gel in a 4-mm fracture.

Rate, cm^3/hr	Superficial velocity, ft/d	Brine final F_{rr}	Incremental FV brine	Total FV brine	Oil final F_{rr}	Total FV Soltrol
500	259	**100,000**	1.4	1.4	---	---
1,000	518	**67,000**	2.8	4.2	---	---
2,000	1,040	**53,000**	5.6	9.8	---	---
4,000	2,070	**45,000**	10.8	20.6	---	---
8,000	4,140	**39,000**	44.0	64.6	**18,000**	44.0

As expected, when the gel was subjected to higher brine flow rates and differential pressures, the water-blocking performance of the gel deteriorated somewhat. However, the gel exhibited substantial permeability reduction factors, even after experiencing high rates and large throughput volumes of brine and oil.

Additional Discussion

Versatility and Optimization of High- and Low-Mw Polymer Gels. Formulating water-shutoff gels with a combination of high- and low-Mw polymers should prove to be a robust and powerful strategy. By varying the concentrations and Mw of the two polymers, gels with a broad range of costs and properties (especially gel strengths and gelant viscosities) can be readily formulated.

Use of high- and low-Mw polymer gels may be more expensive than conventional oilfield water-shutoff polymer gels. Field applications of high- and low-Mw polymer water-shutoff gels are envisioned to be most attractive if applied in one of the following two modes. First, these gels could be applied as relatively small volume (near-wellbore) water-shutoff jobs when large aperture fractures or large drawdown pressures are encountered. Second, these gels could be applied in conjunction with larger volume water-shutoff treatments (i.e., that employ weaker and less costly polymer gels) when large aperture fractures or large drawdown pressures are encountered. In this case, the high- and low-Mw polymer gels could be injected last (into the near-wellbore high-differential-pressure region) in order to prevent the conventional (weaker) water-shutoff gel from being back-produced.

A complementary strategy can be employed when the exact nature of highly conductive water-producing fractures is unknown at the onset of a water-shutoff gel treatment (often the case).

First, a more conventional high-Mw polymer gel is pumped. Depending on the pumping pressure response during this gel injection, the concentration of high-Mw polymer in the gel formulation is gradually increased to the maximum tolerable value. If warranted near the end of the planned injection volume of the gel treatment, low-Mw polymer is added in increasing concentrations to the high-Mw gel formulation, as dictated by the injection-pressure responses and good engineering judgment.

The high- and low-Mw polymer gel formulation used in this study may not be the optimum composition. On the other hand, there may not be a single optimum formulation when treating fractured production wells for water-shutoff purposes. The optimum composition may vary with 1) the exact nature of the excessive water-production problem to be treated and 2) the business objectives and cost constraints of the oilfield operator.

Putting Results in Perspective. The primary focus of this study was creating and characterizing the permeability reduction (plugging power) imparted by water-shutoff polymer gels that are placed in reservoir fractures. In particular, we studied gel placement in fractures within Berea sandstone. However, the following two points should be noted to put our findings in proper perspective.

First, if an oilfield operator desires to essentially eliminate water production from a highly conductive water-producing fracture, the required level of permeability reduction will increase with increasing fracture width. Thus, depending on the treatment objectives, larger residual resistance factors may be needed for wider fractures.

Second, during the present study, experiments were not designed to quantify permeability damage to the matrix sandstone that resides adjacent to the gel-treated fracture (resulting from gel leakoff during placement). The primary intent of the present study was to characterize the permeability reduction (to both water and oil) that polymer gels impart within fractures. The study of gel-induced matrix-rock damage may be a fruitful area for future work. Matrix-rock permeability damage may not be a concern if it occurs in the intermediate or far-wellbore region and it does not inhibit oil from reaching the production well. However, this matrix damage is of concern if the oil flow path to the wellbore is significantly impaired.

Effective Viscosity Versus Fracture Aperture. For the H&LMW gel, Table 29 lists effective viscosities in 1- to 4-mm-wide fractures, at the fixed injection rate of 8,000 cm^3/hr. This viscosity trend probably resulted because the formulation is shear-thinning. When injecting a shear-thinning fluid at a fixed rate into fractures of increasing apertures, the fluid will experience reduced shear rates.

Table 29—Effective viscosity of the H&LMW gel during placement.

Fracture aperture, cm	Effective viscosity range of gel formulation, cp
1.0	470-510
2.0	550-630
4.0	1,400-1,500

Pressure Gradient Along the Fracture Length. During injection of the H&LMW gel and the 2X and 3X gels, we often observed that pressure gradients became progressively larger along the length of the fracture during post-gel-placement brine and oil flooding (from injection to effluent end). At present, we do not completely understand this behavior. This phenomenon was not apparent for relatively weak gels (e.g., 1X gels of the previous chapters) in fractures. This behavior became much more significant as gel strength increased and/or the overall differential pressure became larger. The larger downstream pressure gradients occurred despite 1) the ID of the effluent port (from the fracture) was large relative to the fracture aperture, 2) the effluent flow line from the fracture was cleared of gel before brine injection, and 3) all the other effluent lines and pressure taps were maintained gel-free. Additional work will be required to fully understand this phenomenon.

Conclusions

The following conclusions are limited to the polymer gel and the experimental conditions of this study.

1. The CC/AP gel formulation of this study (which contained a combination of high- and low-Mw polymers) exhibited an effective viscosity of roughly 500 cp during placement at 16,600 ft/d superficial velocity in a 1-mm-wide fracture. After placement, it provided exceptionally good fracture plugging characteristics. The gel withstood 52 psi differential pressure (26 psi/ft pressure gradient) for 24 hrs while permitting no detectable brine flow through the fracture. Subsequently when the differential pressure was increased to 175 psi (88 psi/ft pressure gradient), the gel imparted a brine residual resistance factor (permeability reduction factor) of 30,000.
2. When placed in a 2-mm-wide fracture, the same gel required 37 psi/ft pressure gradient for brine to breach the gel. After exceeding this critical pressure gradient, the stabilized brine residual resistance factor in the fracture was 260,000.
3. When placed in a 4-mm-wide fracture, the same gel required 25 psi/ft pressure gradient for brine to breach the gel. After exceeding this critical pressure gradient, the stabilized brine residual resistance factor in the fracture was again 260,000.
4. At a fixed injection rate, the effective viscosity within the fracture of the gel solution increased with fracture aperture. The shear-thinning nature of the formulation explains this behavior.
5. During this study, the high- and low-Mw CC/AP (H&LMW) gel exhibited modest disproportionate permeability reduction in fractures (by factors from 2 to 6).
6. After placement of the H&LMW gel in a 4-mm-wide fracture, stabilized residual resistance factors decreased by a factor of 2.6 when the brine superficial velocity was increased by a factor of 16 (i.e., from 259 to 4,140 ft/d in the fracture). Similar results were obtained during an analogous experiment in a 2-mm fracture.
7. After placement of the H&LMW gel in a fracture, the magnitude of the disproportionate permeability reduction decreased with increasing cycles of water/oil flooding.

NOMENCLATURE

A_f = fracture area, ft^2 [m^2]
F_{rr} = residual resistance factor (mobility before gel divided by mobility after gel)
F_{rro} = oil residual resistance factor
F_{rrw} = water residual resistance factor
G' = elastic modulus, psi [Pa]
h = height, ft [m]
h_f = fracture height, ft [m]
J_{oil} = oil injectivity after gel placement, BPD/psi [m^3/Pa-s]
J_{oil0} = oil injectivity before gel placement, BPD/psi [m^3/ Pa-s]
J_{w0} = water injectivity before gel placement, BPD/psi [m^3/ Pa-s]
J_{water} = water injectivity after gel placement, BPD/psi [m^3/ Pa-s]
k = permeability, darcys [μm^2]
k_f = fracture permeability, darcys [μm^2]
k_{final} = final permeability, darcys [μm^2]
k_{gel} = gel permeability to water, darcys [μm^2]
k_m = matrix permeability, darcys [μm^2]
k_o = permeability to oil, darcys [μm^2]
k_{of} = permeability to oil in a fracture, darcys [μm^2]
k_{ro} = endpoint relative permeability to oil, darcys [μm^2]
k_{rw} = endpoint relative permeability to water, darcys [μm^2]
k_w = permeability to water, darcys [μm^2]
k_{wf} = permeability to water in a fracture, darcys [μm^2]
L = distance along a fracture, ft [m]
L_f = fracture length, ft [m]
L_p = distance of gelant penetration, ft [m]
Δp = pressure drop, psi [Pa]
dp/dl = pressure gradient, psi/ft [Pa/m]
q = injection or production rate, BPD [m^3/d]
r = correlation coefficient
r_e = external drainage radius, ft [m]
r_w = wellbore radius, ft [m]
S_{or} = residual oil saturation
S_w = water saturation
S_{wr} = residual water saturation
t = time, s
u = leakoff rate or flux, ft/d [cm/s]
V_{gelant} = volume of gelant injected, ft^3 [m^3]
w_f = fracture width, in. [mm]
ϕ = porosity
μ = viscosity, cp [mPa-s]
μ_{gelant} = gelant viscosity, cp [mPa-s]
μ_o = oil viscosity, cp [mPa-s]
μ_w = water viscosity, cp [mPa-s]

REFERENCES

1. Seright, R.S.: “Conformance Improvement Using Gels,” Annual Technical Progress Report (U.S. DOE Report DOE/BC/15316-2), U.S. DOE Contract DE-FC26-01BC15316 (Sept. 2002).
2. Seright, R.S, Liang J., Lindquist, B.W., and Dunsmuir, J.H.: “Characterizing Disproportionate Permeability Reduction Using Synchrotron X-Ray Computed Microtomography,” *SPE Reservoir Engineering & Evaluation* (Oct. 2002) 355-364.
3. Seright, R.S, Liang J., Lindquist, B.W., and Dunsmuir, J.H.: “Use of X-Ray Computed Microtomography to Understand Why Gels Reduce Permeabilty to Water More Than That to Oil,” *J. Petroleum Science and Engineering*, **Vol. 39,** Nos. 3-4 (Sept. 2003) 217-230.
4. Seright, R.S.: “Using Chemicals to Optimize Conformance Control in Fractured Reservoirs,” Annual Technical Progress Report (U.S. DOE Report DOE/BC/15110-6), U.S. DOE Contract DE-AC26-98BC15110 (Sept. 2001).
5. Seright, R.S.: "Using Chemicals to Optimize Conformance Control in Fractured Reservoirs," Annual Technical Progress Report (U.S. DOE Report DOE/BC/15110-2), U.S. DOE Contract DE-AC26-98BC15110, (Sept. 1999) 21-28.
6. Seright, R.S.: "Effect of Rock Permeability on Gel Performance in Fluid-Diversion Applications," *In Situ* (1993) **17**, No.4, 363-386.
7. Chatzis, I., Morrow, N.R., and Lim, H.T.: “Magnitude and Detailed Structure of Residual Oil Saturation,” *SPEJ* (April 1983) 311-326.
8. Wang, D. *et al*: “Study of the Mechanism of Polymer Solution with Visco-Elastic Behavior Increasing Microscopic Oil Displacement Efficiency and the Forming of Steady Oil Thread Flow Channels,” paper SPE 68723 presented at the 2001 SPE Asia Pacific Oil and Gas Conference and Exhibition, Jakarta, Indonesia, April 17-19.
9. Al-Sharji, H.H., *et al*.: “Pore-Scale Study of the Flow of Oil and Water through Polymer Gels,” paper SPE 56738 presented at the 1999 SPE Annual Technical Conference and Exhibition, Houston, TX, Oct. 3-6.
10. Willhite, G.P., *et al*.: “Mechanisms Causing Disproportionate Permeability in Porous Media Treated With Chromium Acetate/HPAAM Gels,” *SPEJ* (March 2002) 100-108.
11. Ganguly, S., *et al*.: “Effect of Flow Rate on Disproportionate Permeability Reduction,” paper SPE 80205 presented at the 2003 SPE International Symposium on Oilfield Chemistry, Houston, TX, Feb. 5-7.
12. Liu, Jin, and Seright, R.S.: "Rheology of Gels Used For Conformance Control in Fractures," paper SPE 59318 presented at the 2000 SPE/DOE Improved Oil Recovery Symposium, Tulsa, OK, April 3-5.
13. Seright, R.S.: “Washout of Cr(III)-Acetate-HPAM Gels from Fractures,” paper SPE 80200 presented at the 2003 SPE International Symposium on Oilfield Chemistry, Houston, TX, Feb. 5-7.
14. Seright, R.S., Liang, J., and Sun, H.: “Gel Treatments in Production Wells with Water Coning Problems,” *In Situ* (1993) **17**, No.3, 243-272.
15. Seright, R.S., Liang, J., and Seldal, M.: “Sizing Gelant Treatments in Hydraulically Fractured Production Wells,” *SPE Production & Facilities* (Nov. 1998) 223-229.
16. Marin, A., Seright, R., Hernandez, M., Espinoza, M., Mejias, F.: “Connecting Laboratory and Field Results for Gelant Treatments in Naturally Fractured Production Wells,” paper SPE

77411 presented at the 2002 SPE Annual Technical Conference and Exhibition, San Antonio, TX, Sept. 29-Oct. 2.
17. Moffitt, P.D.: "Long-Term Production Results of Polymer Treatments on Producing Wells in Western Kansas," *JPT* (April 1993) 356-362.
18. Bird, R.B., Stewart, W.E., and Lightfoot, E.N.: *Transport Phenomena*, John Wiley & Sons, New York (1960) 46-62.
19. Seright, R.S.: "An Alternative View of Filter Cake Formation in Fractures Inspired by Cr(III)-Acetate-HPAM Gel Extrusion," *SPE Production and Facilities* (Feb. 2003) 65-72.
20. Seright, R.S.: "Gel Placement in Fractured Systems," *SPE Production & Facilities* (Nov. 1995), 241-248.
21. Seright, R.S.: "Use of Preformed Gels for Conformance Control in Fractured Systems," *SPE Production & Facilities* (Feb. 1997) 59-65.
22. Seright, R.S: "Mechanism for Gel Propagation Through Fractures," paper SPE 55628 presented at the 1999 SPE Rocky Mountain Regional Meeting, Gillette, WY, May 15-19.
23. Seright, R.S: "Polymer Gel Dehydration During Extrusion Through Fractures," *SPE Production & Facilities* (May 1999) 110-116.
24. Seright, R.S.: "Gel Propagation Through Fractures," *SPE Production & Facilities* (Nov. 2001) 225-232.
25. Green, C., Creel, P., McDonald, S., Ryan, T.: "Utilization of a Crystallized Hydrating Copolymer to Modify an Injectivity Problem in a Horizontal co, WAG Injector in the South Cowden Unit, Ector County, Texas—Post treatment Coil Tubing Acidizing Stimulation—Case History," Southwestern Petroleum Short Course, Lubbock, TX (2003).
26. Sydansk, R.D., "Acrylamide-Polymer/Chromium(III)-Carboxylate Gels for Near Wellbore Matrix Treatments," *SPE Advanced Technology Series*, Vol. 1, No. 1 (April 1993) 146-152.
27. Bass, D.M.: *Petroleum Engineering Handbook*, H.B. Bradley (ed.), Society of Petroleum Engineers, Richardson, TX (1987) 26-16.
28. Ganguly, S., Willhite, G.P., Green, D.W., and McCool, C.S.: "The Effect of Fluid Leakoff on Gel Placement and Gel Stability in Fractures," *SPE Journal* (Sept. 2002) 309-315.

APPENDIX A: Technology Transfer

Presentations

On October 21, 2003, we (Robert Sydansk) presented the talk, "Polymer Gels for Water Shutoff and for Use during CO_2 Flooding" for the SPE Gulf Coast Study Group in Houston, TX.

On October 18, 2003, we presented the short course, "Water Shutoff", at the 2003 SPE International IOR Conference in Kuala Lumpur, Malaysia.

On July 31, 2003, we (Robert Sydansk) made a presentation "Water Shutoff Using CC/AP Gels in Fractured Producers" at the North Midcontinent PPTC workshop, "Reducing Water Production Using Gelled Polymers," that was held in Wichita, KS.

On February 27, 2003, we (Robert Sydansk) participated in the Oxy Permian Conformance Workshop that was held at Oxy's Midland, TX office.

On February 6, 2003, we presented SPE paper 80200, "Washout of Cr(III)-Acetate-HPAM Gels from Fractures," at the 2003 SPE International Symposium on Oilfield Chemistry in Houston, TX.

On January 23, 2003, we made a presentation "Causes and Treatments of Excessive Water Production – Science and Technology of Polymer Gel Treatments" at the West Coast PTTC workshop, "Water Reduction Through Polymer Treatments in Injection and Production Wells," that was held in Valencia, CA.

On December 5, 2002, we presented the talk, "A Strategy for Attacking Excess Water Production," at the PRRC/PTTC Produced Water Workshop in Farmington, NM.

On December 5, 2002, we (Robert Sydansk) presented the talk, "Water Shutoff Using Polymer Gels in Fractured Producers," at the PRRC/PTTC Produced Water Workshop in Farmington, NM.

On October 10, 2002, we held a project review at Shell's offices in Rijswijk, Netherlands.

On October 8, 2002, we presented "Treatment of Fracture Problems Using Gels," at the SPE Applied Technology Workshop, "Emerging Chemical Solutions for Water Control," in Copenhagen, Denmark.

On September 30, 2002, we presented SPE paper 77411, "Connecting Laboratory and Field Results for Gelant Treatments in Naturally Fractured Production Wells," at the 2002 SPE Annual Technical Conference and Exhibition, in San Antonio, TX.

On August 5, 2002, we presented "Permeability Reduction Mechanisms using Microtomography," at the Gordon Research Conference, "Flow & Transport In Permeable Media," at the Proctor Academy in Andover, NH.

On June 12, 2002, we held a project review at BP's offices in Houston, TX.

On April 16, 2002, we presented SPE paper 75158, "An Alternative View of Filter Cake Formation in Fractures," at the 2002 SPE/DOE Symposium on Improved Oil Recovery, in Tulsa, OK.

On April 14, 2002, we presented the Short Course, "Water Shutoff," at the 2002 SPE/DOE Improved Oil Recovery Symposium in Tulsa, OK.

On March 11, 2002, we presented "Use of X-Ray Computed Microtomography to Understand Why Gels Reduce Permeabilty to Water More Than That to Oil," at the 7th International Symposium on Reservoir Wettability in Freycinet, Tasmania, Australia.

On March 8, 2002, we presented "A New Model for Filter Cake Formation in Fractures" at the University of Tulsa, Department of Petroleum Engineering graduate seminar.

On December 19, 2001, we held a project review at Shell's offices in Rijswijk, Netherlands.

On October 1, 2001, we presented the talk, "Characterizing Disproportionate Permeability Reduction Using Synchrotron X-Ray Computed Microtomography," at the 2001 SPE Annual Technical Conference and Exhibition in New Orleans, Louisiana.

Internet Postings on the Project and Software to Download

A description of our research group can be found at the following New Mexico PRRC web site: http://baervan.nmt.edu/randy. The site lists the publications of our group and allows downloads of several papers, reports, and presentations.

This web site also allows downloading of software, Version 2.0 of "Gel Design," for sizing gelant treatments in hydraulically fractured production wells.

Papers and Publications

Seright, R.S, Liang J., Lindquist, B.W., and Dunsmuir, J.H.: "Use of X-Ray Computed Microtomography to Understand Why Gels Reduce Permeabilty to Water More Than That to Oil," *J. Petroleum Science and Engineering*, **Vol. 39,** Nos. 3-4 (Sept. 2003) 217-230.

Seright, R.S., Lane, R.H., and Sydansk, R.D.: "A Strategy for Attacking Excess Water Production," *SPE Production and Facilities* (Aug. 2003) 158-169.

Seright, R.S.: "An Alternative View of Filter Cake Formation in Fractures Inspired by Cr(III)-Acetate-HPAM Gel Extrusion," *SPE Production and Facilities* (Feb. 2003) 65-72.

Seright, R.S.: "Washout of Cr(III)-Acetate-HPAM Gels from Fractures," paper SPE 80200 presented at the 2003 SPE International Symposium on Oilfield Chemistry, Houston, TX, Feb. 5-7.

Seright, R.S, Liang J., Lindquist, B.W., and Dunsmuir, J.H.: "Characterizing Disproportionate Permeability Reduction Using Synchrotron X-Ray Computed Microtomography," *SPE Reservoir Evaluation & Engineering*, **5**(5), (Oct. 2002) 355-364.

Marin, A., Seright, R., Hernandez, M., Espinoza, M., Mejias, F.: "Connecting Laboratory and Field Results for Gelant Treatments in Naturally Fractured Production Wells," paper SPE 77411 presented at the 2002 SPE Annual Technical Conference and Exhibition, San Antonio, TX, Sept. 29-Oct. 2.

Seright, R.S.: "Conformance Improvement Using Gels," Annual Technical Progress Report (U.S. DOE Report DOE/BC/15316-2), U.S. DOE Contract DE-FC26-01BC15316 (Sept. 2002).

Seright, R.S.: "An Alternative View of Filter Cake Formation in Fractures," paper SPE 75158 presented at the 2002 SPE/DOE Symposium on Improved Oil Recovery, Tulsa, OK, April 13-17.

Seright, R.S, Liang J., Lindquist, B.W., and Dunsmuir, J.H.: "Use of X-Ray Computed Microtomography to Understand Why Gels Reduce Permeabilty to Water More Than That to Oil," 7th International Symposium on Reservoir Wettability in Freycinet, Tasmania, Australia, March 12-15, 2002.

Seright, R.S.: "Gel Propagation Through Fractures," *SPE Production & Facilities* (Nov. 2001) 225-232.

Seright, R.S, Liang J., Lindquist, B.W., and Dunsmuir, J.H.: "Characterizing Disproportionate Permeability Reduction Using Synchrotron X-Ray Computed Microtomography," paper SPE 71508 presented at the 2001 SPE Annual Technical Conference and Exhibition, New Orleans, LA, Sept. 30- Oct. 3.

Liang, J., and Seright, R.S.: "Wall-Effect/Gel Droplet Model of Disproportionate Permeability Reduction," *SPE Journal* (September 2001) 268-272.